

ABSTRACT

Title of Document: Synthesis, Stability, and Reactivity of High Oxidation State Pentamethylcyclopentadienyl Acetamidinate β -Hydride- or β -Methide-Bearing Alkyl Complexes of Zirconium, Titanium, and Tantalum

Albert Epshteyn, Doctor of Philosophy, 2006

Directed By: Professor Lawrence R. Sita
Department of Chemistry and Biochemistry
University of Maryland, College Park, MD 20740

In the course of study into the stability and reactivity of early transition metal (TM) complexes, it has been further confirmed that the pentamethylcyclopentadienyl acetamidinate ligand set is particularly apt for the stabilization of early TM-alkyl species.

The first examples of a solid state structure of cyclobutylmethyl complexes were obtained, after pentamethylcyclopentadienylacetamidinatezirconium (Cp^*ZA) cyclobutylmethyl compounds were prepared via hydrozirconation of methylenecyclobutane. The ring opening of neutral and cationic cyclobutylmethyl Cp^*ZAs and the conformation of the product pendant olefin pentenyl cation were studied via selective nuclear Overhauser effect (nOe) confirming that the pendant olefin was coordinated to the cationic Zr center. To further study the properties of pendant olefin complexes, a methyl butenyl Cp^*ZA complex was prepared, and was observed to convert to a Cp^*ZA butadiene complex, presumably via a β -H abstraction by the metal-based methyl group.

The reactivity of the first known non-base stabilized η^2 -styrene zirconium complex, supported by the Cp* acetamidinate ligands, was studied with olefins, 1,3-butadienes, and 2-butyne. It was shown that the initial products of α -olefin insertion into the η^2 -styrene complex are saturated zirconacyclopentanes that can then undergo a dehydrogenation producing H₂ and a Cp*ZA butadiene complex. The reaction of the η^2 -styrene Cp*ZA with 2-butyne was shown to produce a Cp*ZA butadiene complex via a sequential butyne insertion followed by a formal 1,3-hydride shift, and the reaction with 1,3-butadienes yielded Cp*ZA butadiene complexes with loss of styrene.

The chemistry of pentamethylcyclopentadienyl acetamidinate titanium (Cp*TiA) was pursued, and the reaction of the Cp*TiA dichloride with 2 equiv. of MeLi yielded the dimethyl Ti(IV) complex, while the reaction with 2 equiv. of EtLi yielded the Ti(III) ethyl complex.

Studies were carried out with Cp* acetamidinate compounds of Ta (Cp*TaAs). The reactions of Cp*TaA trichloride with EtLi, ⁿBuLi, ⁱBuLi, NpLi produced a series of new Ta(V), Ta(IV), and Ta(III) complexes. The Ta(IV) dichloride was also accessed via a Na/Hg reduction allowing further access to Ta(IV) alkyl compounds. The thermal decomposition of the Ta(IV) diisobutyl yielded a Ta(IV) TMM complex and a diamagnetic Ta(IV) dimeric dihydride.

**Synthesis, Stability, and Reactivity of High-Oxidation-
State Pentamethylcyclopentadienyl Acetamidinate
 β -Hydride- or β -Methide-Bearing Alkyl Complexes of
Zirconium, Titanium, and Tantalum**

By

Albert Epshteyn

Dissertation submitted to the Faculty of the Graduate School of the
University of Maryland, College Park, in partial fulfillment
of the requirements for the degree of
Doctor of Philosophy
2006

Advisory Committee:

Professor Lawrence R. Sita (Chair)
Professor Kyu-Yong Choi
Professor Michael P. Doyle
Professor Brian W. Eichhorn
Assistant Professor Andrei N. Vedernikov

© 2006
Albert Epshteyn

This is dedicated to my family.

Acknowledgements

I would like to thank my advisor, Professor Lawrence R. Sita, for all his guidance and help during the four years of graduate research that I have enjoyed at the University of Maryland. His tutelage, foresight and spirit of exploration reassured and inspired me throughout this endeavor. Thank you for helping me to grow and improve both as a scientist and a person.

I would also like to thank my thesis committee: Dr. Michael P. Doyle, Dr. Brian W. Eichhorn, and Dr. Andrei N. Vedernikov for their mentorship. I have been greatly privileged to have had a complete educational experience having received guidance in professional and scientific matters from them. I thank Dr. Kyu-Yong Choi for graciously accepting the role of Dean's Representative.

Also, I would very much like to thank Dr. Yiu-fai Lam, Dr. Yinde Wang, Dr. James C. Fettinger, and particularly Dr. Peter Zavalij, without whose excellent NMR and crystallographic support none of this work would have been possible.

I would also like to thank Dr. Richard L. Karpel, Dr. Dorothy Beckett, Dr. Don Berkowitz, Dr. Jason Kahn, Dr. John Moore, Dr. Jeffrey Davis, Dr. Marco Colombini and Dr. Andrew Morehead, for outstanding educational experiences that captured my imagination both in the classroom and in the laboratory, providing the impetus for my pursuit of graduate studies in chemistry.

I would like to thank all of the Sita group members past and present including: Dr. Denis A. Kissounko, Dr. Yonghui (Felix) Zhang, Lixin Wang, Andrea Young, Dr. Laura Picraux, Dr. Matthew B. Harney, Wei Zhang, Dr. Phillip Fontaine, Dr. Masakazu Hirotsu and Samuel Hundert, for making working in the group a truly enjoyable experience.

Finally, I would also like to thank my great friends Oktay Demircan, Arthur Winter, Dr. Chad Stoltz, Aprilgrace A. Aytona and my family. Thank you for your support. I could not have done it without you.

Table of Contents

Dedication.....	ii
Acknowledgements.....	iii
List of Tables.....	vii
List of Figures.....	viii
List of Schemes.....	xi
List of Abbreviations.....	xiv
Chapter 1: Introduction.....	1
1.1 Pentamethylcyclopentadienyl Acetamidinate Cationic Zirconium Living Stereospecific Ziegler Natta Polymerization of α -Olefins.....	1
1.2 Overview of Pertinent Early Transition Metal Organometallic Chemistry ..	2
1.2.1 A Brief Historical Perspective	2
1.2.2 Ziegler-Natta Olefin Polymerization	4
1.2.3 Hydrozirconation of Alkene and Alkynes with Schwartz' Reagent.....	6
1.2.4 Alkene or Alkyne "Oxidative" Coupling With Negishi Reagent	8
1.2.5 Olefin Oligomerization	11
Chapter 2: Cyclobutylmethyl Cp*ZAs and Related Chemistry	14
2.1 Introduction and Background	14
2.2 Hydrozirconation of Methylene cyclobutane and Related Transformations	16
2.2.1 Hydrozirconation of Methylene cyclobutane.....	16
2.2.2 Hydrozirconation of Methylene cyclopropane	19
2.2.3 Methylation of Cyclobutylmethyl Chloro Cp*ZA.....	19
2.3 Ring Opening of Neutral Chloro Cyclobutylmethyl Cp*ZA.....	22
2.3.1 NMR Confirmation of Transformation.....	22
2.2.4 Deuterium Labeling Experiment.....	23
2.3.3 Kinetic Study of the Ring Opening.....	24
2.4 Cation Studies	26
2.4.1 Generation of Cation from Cyclobutylmethyl Methyl CpZA.....	26
2.4.2 Generation of Cation from Pentenyl Methyl Cp*ZA	27
2.4.3 Conformational Analysis of Pentenyl Cp*ZA Cation by Selective nOe	28
2.4.4 1-Hexene Polymerization Studies With Pentenyl Cp*ZA Cation	31
2.5 Study of the Methyl Butenyl Cp*ZA.....	32
2.5.1 Synthesis of Methyl Butenyl Cp*ZA.....	32
2.5.2 Decomposition of Methyl Butenyl Cp*ZA.....	35
2.5.3 Study Of Butenyl Cp*ZA Cation.....	39
Chapter 3: Reactivity of a Non-Base Stabilized Styrene Complex of Zirconium	41
3.1 Oxidative Coupling of Alkenes and Alkynes With The Styrene Cp*ZA...	41
3.1.1 Background.....	41
3.1.2 Synthesis of an Unsubstituted Zirconacyclopentane	42

3.1.3	Ethene Insertion	43
3.1.4	Propene Insertion	44
3.1.5	Styrene Insertion	48
3.1.6	Vinyl-TMS Insertion.....	51
3.1.7	2-Butyne Insertion	53
3.2	Oxidative Addition To The η^2 -Styrene Cp*ZA	56
3.4.1	Oxidative Addition of 1,3-Butadienes	56
3.4.2	Vinyl Bromide Oxidative Addition	56
3.5	Mechanistic Discussion of Alkene and Alkyne Coupling with the η^2 -Styrene Cp*ZA.....	59
3.5.1	Unified Explanation For The Styrene Cp*ZA Complex Reactivity With Alkenes	59
3.5.2	Mechanistic Discussion of Insertion of Ethene	60
3.5.3	Mechanistic Discussion of Insertion of Propene	62
3.5.4	Mechanistic Discussion of Insertion of Styrene	63
3.5.5	Mechanistic Discussion of Insertion of Vinyl-TMS.....	63
3.5.6	Mechanistic Discussion of Decomposition of 15 to 16	64
3.5.7	2-Butyne Insertion and Rearrangement	65
3.6	Conclusions About The Chemistry Of The Styrene Cp*ZA	68

Chapter 4: Pentamethylcyclopentadienyl Acetamidinate Titanium Chemistry

4.1	Titanium In Ziegler-Natta Polymerization and Olefin Oligomerization	71
4.2	Exploration of Titanium Synthesis and Reactivity	72
4.2.1	Synthesis of Cp*TiCl ₂ [ⁱ PrNC(Me)N ⁱ Pr].....	72
4.2.2	Alkylation of Cp*[ⁱ PrN(Me)N ⁱ Pr]TiCl ₂ With MeLi.....	72
4.2.3	Alkylation of Cp*[ⁱ PrNC(Me)N ⁱ Pr]TiCl ₂ With EtLi	73
4.2.4	Insertion Of ^t BuNC Into Cp*[ⁱ PrNC(Me)N ⁱ Pr]Ti(III)Et.....	75
4.2.5	Generation Of Cp*[ⁱ PrNC(Me)N ⁱ Pr]Ti(IV)Me Cation.....	76
4.3	Conclusions About Cp* Acetamidinate Titanium Chemistry	78

Chapter 5: Exploration of Cp*TaXn[ⁱPrNC(Me)NⁱPr] Chemistry (X= Cl, H, Alkyl, Alkylidene)

5.1	Brief Overview of Pertinent Tantalum Chemistry	79
5.2	Reactions of Cp*TaCl ₃ [ⁱ PrNC(Me)N ⁱ Pr] with Alkyl Lithiums	82
5.2.1	Reaction with 3 Equivalents of MeLi	82
5.2.2	Reaction with 3 Equivalents of EtLi.....	82
5.2.2	Reaction with 3 Equivalents of ⁿ BuLi	85
5.2.3a	Cp*Ta ⁿ Bu ₂ [ⁱ PrNC(Me)N ⁱ Pr].....	86
5.2.3b	Cp*Ta ⁿ Bu(η^2 -CH ₂ =CHCH ₂ CH ₃)[ⁱ PrNC(Me)N ⁱ Pr]	88
5.2.3	Reaction with 3 Equivalents of ⁱ BuLi.....	91
5.2.4	Reaction with 3 Equivalents of NpLi.....	93
5.2.5	Conclusions Regarding Reactivity of Cp*TaA Trichloride with Alkyl Lithiums.....	96
5.3	Reduction Chemistry of Cp*TaCl ₃ [ⁱ PrNC(Me)N ⁱ Pr]	98
5.3.1	Synthesis of Cp*TaCl ₂ [ⁱ PrNC(Me)N ⁱ Pr]	98

5.3.2	Synthesis of $\{\text{Cp}^*\text{TaCl}[\text{iPrNC}(\text{Me})\text{N}^i\text{Pr}]\}_2(\mu\text{-}\eta^1, \eta^1\text{-N}_2)$	100
5.3.3	Alkylation Reactions of $\text{Cp}^*\text{TaCl}_2[\text{iPrNC}(\text{Me})\text{N}^i\text{Pr}]$	102
5.4	Alkylations of $\text{Cp}^*\text{TaCl}_2[\text{iPrNC}(\text{Me})\text{N}^i\text{Pr}]$	103
5.4.1	Synthesis of $\text{Cp}^*\text{TaEt}_2[\text{iPrNC}(\text{Me})\text{N}^i\text{Pr}]$	103
5.4.2	Synthesis of $\text{Cp}^*\text{TaCl}(\text{CH}_2\text{CRMe}_2)[\text{iPrNC}(\text{Me})\text{N}^i\text{Pr}]$ for R = H or Me	104
5.4.3	Synthesis of $\text{Cp}^*\text{TaMe}(\text{CH}_2\text{CRMe}_2)[\text{iPrNC}(\text{Me})\text{N}^i\text{Pr}]$ for R = H or Me	107
5.5	Generation of Ta(IV) and Ta(V) Cations.....	109
5.5.1	Introduction to Generating Early Transition Metal Cations	109
5.5.2	Generation of $\{\text{Cp}^*\text{TaNP}[\text{iPrNC}(\text{Me})\text{NiPr}]\}[\text{B}(\text{C}_6\text{F}_5)_4]$: The First Stable Ta(IV) Alkyl Cation.....	110
5.5.2a	Protonation of Amidenaminate Ta(IV).....	110
5.5.2b	Protonation of Methyl Neopentyl Ta(IV)	113
5.5.3	Generation of $\{\text{Cp}^*\text{Ta}^i\text{Bu}[\text{iPrNC}(\text{Me})\text{N}^i\text{Pr}]\}[\text{B}(\text{C}_6\text{F}_5)_4]$	113
5.5.3a	Attempts in PhCl.....	113
5.5.3b	Attempts in Toluene.....	115
5.5.4	Generation of Ta(V) Dimethyl Cation.....	116
5.6	Thermolysis of Ta(V) and Ta(IV) Alkyls.....	117
5.6.1	Thermolysis of Ta(V) Ethyl, Ethylidene	117
5.6.2	Thermolysis of Ta(IV) Dialkyls.....	117
5.6.2	Generation of a Ditantalum Monocationic μ -Trihydride Complex ..	122
5.4	Discussion of Cp^* Acetamidinate Ta(V) and Ta(IV) Alkyl Complexes..	125
5.4.1	General Trends in Electron Affinity of Ta Species	125
5.4.2	Comparison of Ta(IV) Alkyls to Hf(IV) Alkyls.....	126
	Experimental	128
	References.....	141

List of Tables

Table 1 Selected bond distances for 9 in angstroms (Å).....	33
Table 2 Selected bond distances for 10a in angstroms (Å).....	35
Table 3 Selected bond distances for 14 in angstroms (Å).....	44
Table 4 Selected bond distances for 15a in angstroms (Å).....	45
Table 5 Selected bond distances for 16a in angstroms (Å).....	48
Table 6 Selected bond distances for 16a in angstroms (Å).....	49
Table 7 Selected bond distances for 16c in angstroms (Å).....	53
Table 8 Selected bond distances for 18 in angstroms (Å).....	54
Table 9 Selected bond distances and bond angles for solid state structure of 28	84
Table 10 Selected bond distances for 29 and its isostructural Zr(IV) analog	87
Table 11 Selected bond distances for 31 and its Zr(IV) and Hf(IV) isostructural analogs	92
Table 12 Selected bond distances for 33 and the isostructural Hf(IV) analog.....	99
Table 13 Selected bond distances for 11 and the isostructural Hf(IV) analog.....	107
Table 14 Selected bond distances for 32 and 40	112
Table 15 Selected bond distances for 42	116
Table 16 Selected bond distances for 44 and 45	123
Table 17 Atomic and covalent radii of Hf and Ta ¹⁴¹	126

List of Figures

Figure 1 2D-COSY spectrum of 3	17
Figure 2 Solid state structure of 3 with 30% probability ellipsoids; hydrogens omitted for clarity.....	18
Figure 3 Solid state structure of 5 with 30% ellipsoids; hydrogens omitted for clarity	20
Figure 4 Eyring plot for 321 K to 363 K temperature range for the ring opening of neutral cyclobutylmethyl chloro Cp*ZA 3	24
Figure 5 Diagram depicting the solution structure of 7 and also showing the nOe interactions found in 7	30
Figure 6 Solid state structure of 9 depicting possible secondary interactions drawn with 30% probability ellipsoids; some hydrogens have been omitted for clarity... ..	33
Figure 7 Solid state structure of 10a with 30% ellipsoids; hydrogens omitted for clarity	35
Figure 8 Solid state structure of 14 with 30% probability ellipsoids; Cp* and amidinate hydrogens have been omitted for clarity	43
Figure 9 Solid state structure of 15a with 30% probability ellipsoids; all but the metallocycle hydrogens have been omitted for clarity.	45
Figure 10 ¹ H-NMR spectrum of crystals of 15a at RT in C ₆ D ₆	46
Figure 11 ¹ H-NMR in C ₆ D ₆ of the product of decomposition of 15a after overnight at RT to produce 16a and 17	46
Figure 12 Solid state structure of 16a with 30% probability ellipsoids; all but the metallocycle hydrogens have been omitted for clarity	47
Figure 13 Styrene insertion into 12 yields 15'b	48
Figure 14 Solid state structure of 15'b with 30% probability ellipsoids; hydrogens omitted for clarity	49
Figure 15 ¹ H-NMR of 15'b at RT in C ₆ D ₆	50
Figure 16 ¹ H-NMR of 15'b after 1 h at RT in C ₆ D ₆	51
Figure 17 ¹ H-NMR spectrum of 16c in C ₆ D ₆	52

Figure 18 Solid state structure of 16c with 30% probability ellipsoids; hydrogens omitted for clarity	53
Figure 19 Solid state structure of 18 with 30% probability ellipsoids; hydrogens omitted for clarity	54
Figure 20 ¹ H-NMR of 18 at RT in C ₆ D ₆	55
Figure 21 EXSY (800ms mixing time) of 18 ; Bruker 500MHz spectrometer at RT in C ₆ D ₆	55
Figure 22 Solid state structure of 20	57
Figure 23 Solid state structures of 13 , 15a , 15'b	60
Figure 24 Solid state structure of 23 with 30% ellipsoids; all but ethyl hydrogens have been omitted for clarity	74
Figure 25 Solid state structure of 4 with 30% ellipsoids; hydrogens omitted for clarity	76
Figure 26 Solid state structure of 28 with 30% ellipsoids; Cp* and amidinate hydrogens have been omitted for clarity.....	84
Figure 27 Solid state structure of 29 with 30% probability ellipsoids; hydrogens omitted from clarity	86
Figure 28 Solid state structure of 30 with 30% probability ellipsoids; all but the C10B and C11B hydrogens have been omitted for clarity	89
Figure 29 Solid state structure of 31 with 30% ellipsoids; hydrogens omitted for clarity.	92
Figure 30 Solid state structure of 32 with 30% probability ellipsoids; all but the C(1) and C(11) hydrogens have been omitted for clarity.....	94
Figure 31 Solid state structure of 33 with 30% probability ellipsoids; hydrogens omitted for clarity	98
Figure 32 Solid state structure of 34 with 30% probability ellipsoids; hydrogens omitted for clarity	101
Figure 33 Solid state structure of 35 with 30% probability ellipsoids; all except ethyl group hydrogens have been omitted for clarity	103

Figure 34 Solid state structures of 36 and 37 , respectively, with 30% probability ellipsoids; hydrogens have been omitted for clarity	106
Figure 35 Solid state structures of 38 and 39 , respectively, with 30% probability ellipsoids; hydrogens have been omitted for clarity	108
Figure 36 Solid state structure of 40 with 30% probability ellipsoids; all but C(2) and C(9) hydrogens have been omitted for clarity.....	111
Figure 37 Solid state structure of 41 with 30% probability ellipsoids; hydrogens omitted for clarity	114
Figure 38 Solid state structure of 42 with 30% probability ellipsoids; hydrogens omitted for clarity	116
Figure 39 Solid state structures of 43 and 44 , respectively, with 30% probability ellipsoids; Cp* and amidinate hydrogens have been omitted for clarity	118
Figure 40 Solid state structure of 45 with 30% probability ellipsoids; all except for metal-bound hydrogens have been omitted for clarity.	123
Figure 41 Trend of electrophilicity of Ta species in increasing order	126

List of Schemes

Scheme 1	The Cossee-Arlman mechanism for Ziegler-Natta propagation.....	5
Scheme 2	Hydrozirconation of alkenes and alkynes with Cp ₂ ZrHCl (Schwartz' Reagent)	7
Scheme 3	Chain walking behavior of Schwartz' reagent.....	7
Scheme 4	Proposed <i>in situ</i> synthesis of Negishi reagent	9
Scheme 5	Sample of possible synthetic utility of Negishi reagent	10
Scheme 6	Olefin dimerization mechanism.....	11
Scheme 7	Proposed olefin trimerization mechanism	12
Scheme 8	Hydrozirconation of methylenecyclobutane	16
Scheme 9	Hydrozirconation of methylenecyclopropane.....	19
Scheme 10	Methylation of 3 to generate 5	19
Scheme 11	Ring opening rearrangement of 3 to pendant olefin complex 6 with mechanism	22
Scheme 12	Synthesis of 3' and its ring opening rearrangement to 6'	23
Scheme 13	Protonation of 5 generates pentenyl cation 7	26
Scheme 14	Another route to generate cation 7	27
Scheme 15	Proposed mechanism of disappearance of end-group olefinic groups during polymerization of 1-hexene by cation 7	31
Scheme 16	Synthesis of methyl butenyl Cp*ZA 9	32
Scheme 17	Decomposition of 9 to 10a	36
Scheme 18	Proposed stepwise mechanism for the decomposition of 9 to 10a	36
Scheme 19	Pathway originally proposed for thermolysis of [Zr] ⁿ Bu ₂ to make 10b	37
Scheme 20	New proposed mechanism for decomposition of [Zr] ⁿ Bu ₂ to 10b based on decomposition of 9 to 10a	38

Scheme 21	Protonation of 9 or 10a gives the same allyl cation 11	40
Scheme 22	Two different syntheses of 13	42
Scheme 23	Reaction of 12 with ethene to form 14	43
Scheme 24	The isolated product of propene reaction with 12 is 15a	44
Scheme 25	Decomposition of 15a yields 16a	47
Scheme 26	The only pure product isolated from reaction of 12 with vinyl-TMS is 16c	51
Scheme 27	The product of reaction of 12 with 2-butyne is Cp*ZA butadiene complex 18	53
Scheme 28	Oxidative addition of butadienes to a formal Zr(II) to form 19b,c	56
Scheme 29	Vinyl bromide reaction with 12 to produce 20	57
Scheme 30	Proposed reaction scheme for observed reactivity of 12 with α -olefins.	59
Scheme 31	Proposed mechanism of decomposition of 15 to 16	64
Scheme 32	Stepwise mechanism for formation of 18	66
Scheme 33	Proposed concerted mechanism for formation of 18	66
Scheme 34	Synthesis of 16b from insertion of PhCCH into 12	67
Scheme 35	The synthesis of 21	72
Scheme 36	Synthesis of 22 via methylation of 21	72
Scheme 37	Synthesis of 23 from 21	73
Scheme 38	The possible e- transfer pathways for the formation of 23	75
Scheme 39	Synthesis of 24 via insertion of ^t BuNC into T-C bond of 23	75
Scheme 40	Protonation of 22 to make cationic 25	77
Scheme 41	Synthesis of 28	83
Scheme 42	Reaction of 26 with ⁿ BuLi under varying conditions producing 29 and 30	85

Scheme 43 Reaction of 26 with $i\text{BuLi}$ to produce 31	91
Scheme 44 Polarization of the TS^\ddagger during a $\beta\text{-H}$ elimination	91
Scheme 45 Synthesis of 32 via reaction of NpLi with 26	94
Scheme 46 Possible intermediates for the reactivity pathways in the reactions of 26 with three equivalents of various alkyl lithium reagents.	97
Scheme 47 Synthesis of 33 via Na/Hg reduction of 26	99
Scheme 48 Synthesis of 35	103
Scheme 49 Synthesis of 36 and 37	105
Scheme 50 Synthesis of 38 and 39	107
Scheme 51 Protonation of 32 to make cation 40	110
Scheme 52 Thermolysis of 31 to produce 43 and 44	118
Scheme 53 Proposed mechanism for the formation of TMM complexes via thermolysis of diisobutyl complexes of Cp^* acetamidinate Zr(IV) and Ta(IV)	119
Scheme 54 Zwitterionic η^3 -allyl resonances form of the TMM moiety on 43 and is found in the solid state structure of 43 and is different from the structure found for the Cp^*ZA analog.	120
Scheme 55 Synthesis of $\{\text{Cp}^*\text{ZrH}_2[\text{iPrNC}(\text{Me})\text{N}^i\text{Pr}]\}_2^{73}$	121
Scheme 56 Direct hydrogenation of 31 to produce 44	122
Scheme 57 Generation of the cationic complex 45 from 44	123

List of Abbreviations

ⁱ Bu	<i>iso</i> -butyl
ⁿ Bu	<i>n</i> -butyl
^t Bu	<i>tert</i> -butyl
COSY	correlation spectroscopy
Cp	cyclopentadienyl (η^5 -C ₅ H ₅)
Cp'	Cp-derived ligand
Cp*	pentamethylcyclopentadienyl (η^5 -C ₅ Me ₅)
Cp*MA	pentamethylcyclopentadienylmetal amidinate
Cp*TaA	pentamethylcyclopentadienyltantalum amidinate
Cp*TiA	pentamethylcyclopentadienyltitanium amidinate
CpZA	cyclopentadienylzirconium amidinate
Cp*ZA	pentamethylcyclopentadienylzirconium amidinate
Cy	cyclohexyl
D	deuterium
eq	equivalents
Et	ethyl
EXSY	exchange spectroscopy
HSQC	heteronuclear single quantum correlation
L	neutral η^1 ligand
Me	methyl
nOe	nuclear Overhauser effect
NMR	nuclear magnetic resonance
Np	neopentyl
PDI	polydispersity
PE	polyethylene
PH	poly-1-hexene
PP	polypropylene
Ph	phenyl
ⁱ Pr	<i>iso</i> -propyl
ⁿ Pr	<i>n</i> -propyl
R	alkyl group
RT	room temperature
TMS	trimethylsilyl group
TIPS	triisopropylsilyl group
TM	transition metal
TS [‡]	transition state
X	-1 η^1 ligand

Chapter 1: Introduction

1.1 Pentamethylcyclopentadienyl Acetamidinate Cationic Zirconium Living Stereospecific Ziegler Natta Polymerization of α -Olefins

In 2000 Jayaratne and Sita¹ reported the first living stereospecific polymerization of α -olefins by a pentamethylcyclopentadienylacetamidinate zirconium (Cp*ZA) alkylation. This was an important milestone for the field of homogeneous Ziegler-Natta polymerization allowing a high degree of stereocontrol and at the same time retaining all the characteristics of a living polymerization system. Metallocene-based Ziegler-Natta catalysts have been extensively investigated for important structure-property relationships that can produce varying degrees of polymerization activity and give rise to different polymer microstructures.² To a large extent, the Cp* acetamidinate zirconium Ziegler-Natta system has already been studied regarding the origins of its olefin insertion stereoselectivity, as well as the dynamic processes that are occurring within the polymerization reaction that were harnessed to produce a large variety of polymer microstructures using a single catalyst.^{1,3-12}

The remarkable β -H stability of the Cp*ZA system made it an ideal candidate for attempting to isolate and study early TM-alkyl species that are known to be unstable due to β -H elimination, as well as any other decomposition process that involves an important metallocyclic intermediate. The important systems that were identified as targets for study were models of the Ziegler-Natta cationic intermediates, the Negishi chemistry metallocyclopentanes, and olefin oligomerization catalytic processes also involving metallocyclopentanes.¹³⁻²¹

1.2 Overview of Pertinent Early Transition Metal Organometallic Chemistry

1.2.1 A Brief Historical Perspective

Highly lucrative and industrially important processes of Ziegler-Natta polymerization, olefin oligomerization, and important organic synthetic applications of early transition metal (TM) complexes as reagents/catalysts, have one important aspect in common: they all involve early TM alkyl complexes. In each of the above-mentioned application of early TMs, the stability and reactivity of the active early TM alkyl species is intimately responsible for the utility of each particular process. Therefore, the fundamental understanding of the stability and reactivity of early TM alkyl complexes is of paramount importance for the improvement of their existing applications, as well as the development of new processes, with the possibility of branching out into the areas of C-H and small molecule activation.

Unlike the relatively air and moisture stable complexes of late TMs, such as the platinum olefin complex $\text{Na}[\text{PtCl}_3\text{C}_2\text{H}_4]$ isolated by Zeise in 1827, organometallic compounds of early TMs proved elusive until the advent of metallocene chemistry.²² The major advances in the field of early TM organometallic chemistry have all been achieved beginning in the latter half of the 20th century, following the discovery of $(\text{C}_5\text{H}_5)_2\text{Fe}$ (Cp_2Fe , ferrocene) by Pauson and Miller in 1951.²² The first synthesis of Cp_2ZrBr_2 , Cp_2TiBr_2 , and Cp_2VCl_2 followed in 1953 by Wilkinson and coworkers;²³ however, it was not until the development of Cp_2ZrHCl (Schwartz' reagent) in 1976 for hydrozirconation of alkenes and alkynes, which is still regarded as one of the most successful applications for TM complexes to organic synthesis, that early TM organometallic compounds acquired their current role as important tools for synthetic applications.^{24,25}

Parallel to the discovery of metallocenes, in 1955 Karl Ziegler and Giulio Natta, discovered heterogeneous processes utilizing titanium chlorides on MgCl_2 solid support for the polymerization of olefins.²⁶⁻²⁹ Due to the immense impact of their work on the field of plastics, affecting so many facets of product manufacturing and material science, their efforts were rewarded shortly thereafter by a shared Nobel Prize in chemistry in 1963. To this day their discovery affects the lives of every person, with the total production of polyethylene (PE) and (PP) via the Ziegler-Natta process in 2005 totaling roughly 110 million metric tons worldwide.³⁰

One of the problems with studying the highly active heterogeneous Ziegler-Natta process is its lack of amenability to standard available analytical techniques due to its heterogeneous nature. To this day, the identity of the actual active species for the heterogeneous process has not been unequivocally proven, although the Cossee-Arlman mechanism proposed in the early 1960s is widely accepted as correct (*vide infra*).³¹⁻³³ Due to their ability to stabilize early TMs, metallocenes were used as the basis for stable and well defined homogeneous Ziegler-Natta systems, with initial attempts by Natta³⁴ and Breslow³⁵ having limited success, but finally producing active systems with the development of MAO by Kaminsky,³⁶ and further exploration by Brintzinger,³⁷ which heralded in a new era of homogeneous, well defined, Ziegler-Natta polymerization that is now so well studied and still growing.

It is clear from the above examples that the advent of early TM metallocenes has greatly affected the development of the field of early TM organometallic chemistry, shaping the very face of early TM organometallics. Metallocenes became popular due to their stability and ease of synthesis, and now much of the knowledge of early TM-alkyl

chemistry can be attributed to investigations into metallocenes. The steric and electronic environment of the two Cp ligands in a bent metallocene imparts a special stability on the metal complex dictating the reactivity of the metal; therefore, it is possible to envision that the same metal would behave differently under the influence of a different ligand set.

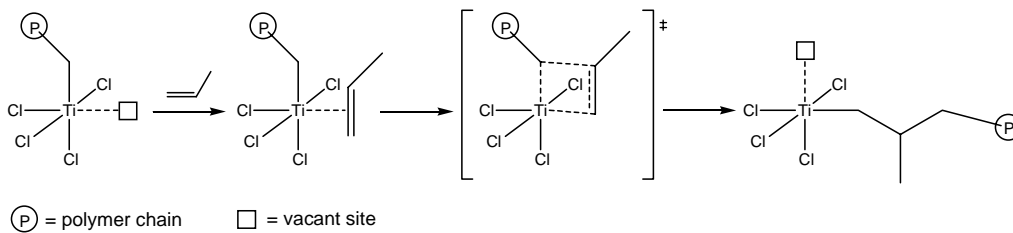
Herein are presented investigations into a new class of group 4 and group 5 alkyl complexes stabilized by a combination of a pentamethylcyclopentadienyl (Cp*) and an acetamidinate ([R-N=C(Me)=N-R']], where R = Alkyl) ligands to produce half-sandwich Cp* Metal Amidinate (Cp*MA) alkyl neutral and cationic species of unprecedented stability, with most of the alkyl complexes reported bearing β -H and/or β -Me substituents on the alkyl ligands. This makes the Cp*MA system extremely versatile, and has allowed the isolation and characterization of a large variety of compounds that, *a priori*, one would have thought to be unstable based on the previously known chemistry of metallocenes.

This chapter was designed to give a brief overview of the chemistry that is affected by the work conducted with Cp*MA. Each section will present and summarize an important early TM process and conclude by highlighting the relevance of new Cp*MA chemistry to each respective system.

1.2.2 Ziegler-Natta Olefin Polymerization

The process that Ziegler and Natta discovered proved itself highly useful within a short period and their discovery quickly transformed production of plastics and polymers from the WWII era Bakelite into the modern industrial age of polyolefins. Ziegler²⁶ was first to discover the heterogeneous catalyst system of TiCl₄/AlEt₃ that polymerizes

ethylene at low pressure to make linear high density polyethylene (HDPE). Soon to follow was Natta's discovery of the $\text{TiCl}_3/\text{AlEt}_3$ catalyst's ability to control the stereoselectivity of the polymerization process to produce stereoregular (isotactic) polypropylene (PP), which is a highly desirable material for manufacturing of consumer goods.²⁷⁻²⁹



Scheme 1 The Cossee-Arlman mechanism for Ziegler-Natta propagation

In order to design better catalysts, and to better understand the source of stereocontrol in the heterogeneous system many studies were conducted, and to this day, the most widely accepted mechanism for the Ziegler-Natta process was proposed by Cossee and Arlman.^{31-33,38,39} As shown in Scheme 1, the process necessitates the availability of a vacant coordination site on the metal. In the coordination step, the olefin donates its π electrons to the Lewis acidic metal making an intermediate metal- π -olefin complex. The next step is a migratory insertion of the π -bound olefin into the σ -bound alkyl polymer chain via a four-membered transition state (TS^\ddagger). After the insertion the polymer chain, which has been extended by one unit of monomer, now occupies the previously vacant coordination site, and *vice versa*, the site that was previously occupied by the polymer chain has now been vacated.

The propagating polymer chain, at least for our purposes, can be viewed as just an alkyl group on the metal. From the Cossee-Arlman mechanism it is possible to infer that

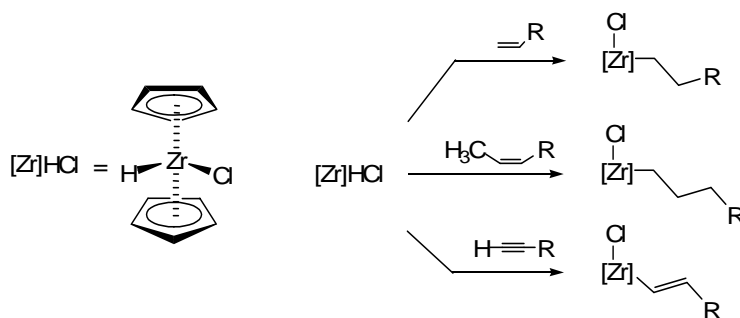
the reactivity and stability of early TM alkyl species is not only important for the ability of Ziegler-Natta systems to propagate, but also in controlling the molecular weight and molecular weight distribution of the product polymer. With a better understanding of the termination processes for the active Ziegler-Natta species it should be possible to control the length of the product polymer chains and increase the effectiveness of the catalyst for producing viable polymer product.

Since the initial discovery of the heterogeneous Ziegler-Natta system there have been many advances in the field. These advances have mainly stemmed from the development of homogeneous metallocene polymerization systems, which have allowed the elucidation of the mechanism of this process, as well as affording new levels of control over polymer microstructure, and control over polydispersity of the the polymer product, all of which have great effect on the physical properties of the polymeric material.¹⁶ The Cp*MA ligand system has been shown to be highly useful for the study of the mechanistic details involved in a single-site Ziegler-Natta polymerization system, but new investigations into the stability and reactivity of cationic Cp*MA's may bring new insights producing new catalytic systems or improving the existing ones.^{11,12,40,41}

1.2.3 Hydrozirconation of Alkene and Alkynes with Schwartz' Reagent

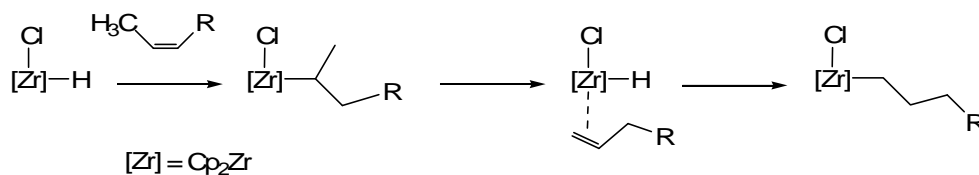
As already mentioned, another application of TM alkyl chemistry is exemplified in Schwartz's Reagent. Though bis-cyclopentadienylzirconium dibromide (Cp_2ZrBr_2 , zirconocene dibromide) was discovered in 1953, it was not until 1976 that Cp_2ZrHCl was

popularized by Schwartz and coworkers^{23,24} as a hydrozirconation reagent for alkenes and alkynes, which was the first useful application for the chemistry of Group 4 metallocenes (Scheme 2).



Scheme 2 Hydrozirconation of alkenes and alkynes with Cp_2ZrHCl (Schwartz' Reagent)

The reaction that has made this reagent popular, the hydrozirconation, involves a formal insertion of an alkene or alkyne into the Zr-H bond of Cp_2ZrHCl (Scheme 2). The product of this reaction is a zirconium alkyl species, which depending on the type of workup chosen can produce various functionalities in the position where the Zr resides, such as an alcohol or a halide. As shown in Scheme 2, when the hydrozirconation is performed upon a substrate containing a non-primary olefin, the Zr species exhibits a chain-walking behavior and can produce the least substituted Zr-alkyl product.

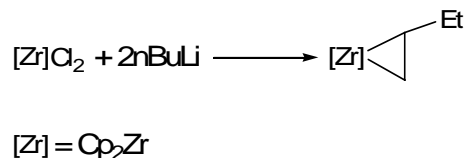


Scheme 3 Chain walking behavior of Schwartz' reagent

The mechanism of this rearrangement has been well studied and is described as a series of β -H eliminations, each followed by a reinsertion of the coordinated olefin into the Zr-H bond, effectively transforming into the primary Zr-alkyl product that is lower in energy due to fewer steric interactions (Scheme 3). This is believed to occur due to the low energy barrier for β -H eliminations in the zirconocene chloro alkyl complexes.²⁵ There have been many modifications and novel methods devised to utilize hydrozirconation in organic synthesis, but the chain walking rearrangement is the accepted mode of reactivity for Schwartz' Reagent.⁴² If it were possible to control the stability of the product Zr-alkyl and prevent the chain walking rearrangement behavior, then it would be possible to synthesize a variety of secondary and tertiary functionalized products making hydrozirconation an even more powerful tool. The process for the hydrozirconation of alkenes using the Cp* zirconium acetamidates (Cp*ZAs) has been recently reported, and in tandem with studies into the stability of Cp*ZA secondary and even tertiary alkyl derivatives has yielded a new system that may provide entry for Cp*ZAs into use as reagents in organic synthesis.^{43,44}

1.2.4 Alkene or Alkyne “Oxidative” Coupling With Negishi Reagent

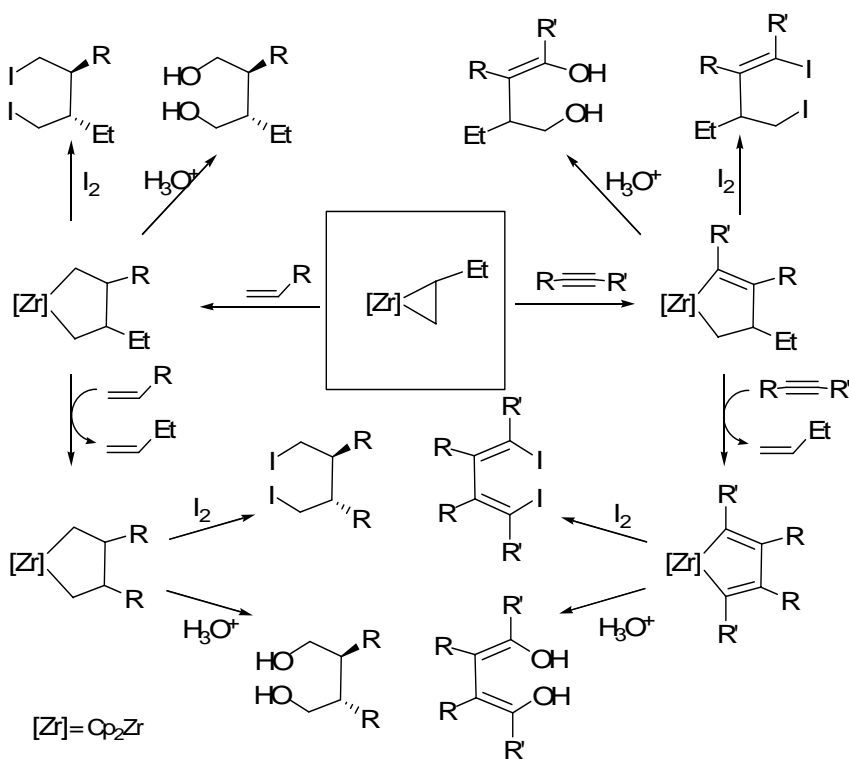
Ei-ichi Negishi⁴⁵ is the pioneer of organozirconium chemistry for synthetic applications and to this day remains a key contributor to the field. The first report of the use of a “Cp₂Zr(II)” equivalent, now dubbed the Negishi Reagent, was in 1986.¹⁹ A sophisticated NMR study by Dioumaev and Harrod⁴⁶ published in 1997 elucidated the mechanistic aspects of the reaction mixture and the mode of action of the Negishi Reagent.



Scheme 4 Proposed *in situ* synthesis of Negishi reagent

The original Negishi procedure to generate the “Cp₂Zr(II)” equivalent *in situ* involves the reaction of a Cp₂ZrCl₂ with 2 equivalents of ⁿBuLi (Scheme 4). Although Harrod and coworkers⁴⁶ showed that the mechanism of formation of the Negishi reagent is very complex,¹⁹ after the reaction of the first equivalent of ⁿBuLi with the dichloride and the formation of the Zr-alkyl chloro species, the second equivalent was originally thought to abstract a β-H, leaving as butane and forming a zirconacyclopropane complex.

The Negishi reagent can insert other olefins to make zirconacyclopentanes, or the butene can be replaced by a stronger binding alkene, such as styrene, or an alkyne. Scheme 5 shows the basic synthetic route for the use of Negishi reagent in coupling alkenes and alkynes to produce a variety of valuable homo- and hetero-coupled diol or dihalide products that can be made using the inexpensive alkenes and alkynes. Many other useful modes of reactivity have been devised for Negishi reagent, including ene-yne and di-ene bis-cyclizations, metallocyclopentane isomerizations, and various transmetallations, just to name a few.⁴⁵

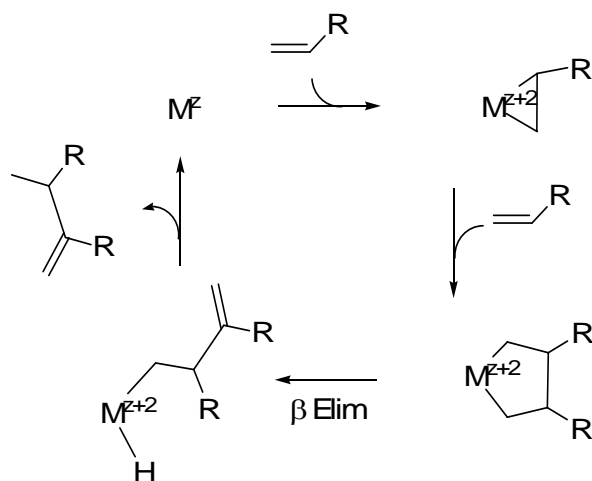


Scheme 5 Sample of possible synthetic utility of Negishi reagent

There is no doubt as to the synthetic utility or the versatility of the Negishi Reagent, making it an important synthetic tool; however, much of this chemistry was developed using organic chemistry methods via isolation and characterization of the organic products. It is possible that a better understanding of the Zr-alkyl reactivity would provide some novel possibilities to further tune the reactivity of the zirconacyclopentane intermediates and therefore allow greater control over regioselectivity and side reactions possibly leading to higher yields or new types of products, which could be achieved by isolating and studying the relatively unstable metallocyclopentane intermediates for the process. The Cp*MA ligand set's ability to stabilize alkyl ligands could be used to produce a series of stable zirconacyclopentanes to study their stability and reactivity.

1.2.5 Olefin Oligomerization

Oligomerization of α -olefins into higher olefins is an important industrial process. In 1978 Richard R. Schrock¹³ produced the first report regarding the dimerization of α -olefins using a Ta(V) alkylidene catalyst initiator. Further investigations into the mechanism of this catalytic oligomerization showed that a metallocyclopentane intermediate is the most likely route through which this process proceeds (Scheme 6).^{14,47}



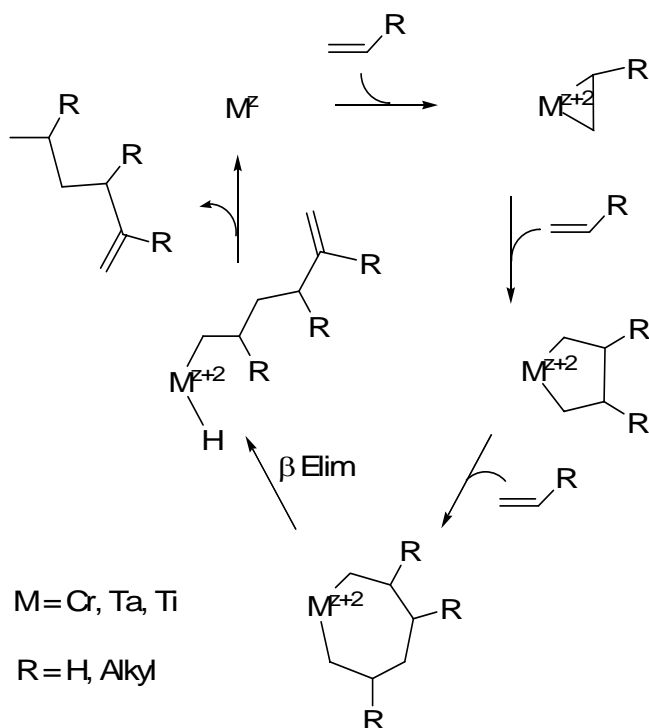
Scheme 6 Olefin dimerization mechanism

Both the olefin oligomerization process developed by Schrock and the Negishi olefin coupling processes proceed through a metallocyclopentane intermediate, which suggests that they are related to each other. The major difference between them is the stability of the metallocycle, and the preferred mode of decomposition that it undergoes. Though the dimerization catalyst is efficient at producing coupled olefin products, it is limited to two units of olefin monomer per product olefin.

Although the olefin oligomerization system discovered by Schrock¹³ was only capable of dimerization of ethylene, there has been much innovation since with ethylene and other olefin oligomerization and trimerization systems developed.⁴⁸⁻⁵⁹

Trimerization of ethylene to produce 1-hexene is a commercial process that uses a heterogeneous Cr catalyst, although well defined homogeneous catalysts of Cr, Ti and Ta are also known to effect trimerization of ethylene.

It has been proposed that for both, the dimerization and the controlled trimerization of olefins, the same catalytic cycle occurs. The difference lies in that instead of elimination after the formation of the metallocyclopentane, another olefin insertion occurs to make a metallocycloheptane ring, which then undergoes the β -elimination/reductive elimination final steps to make the trimer (Scheme 7).



Scheme 7 Proposed olefin trimerization mechanism

Some systems have been reported in the literature that rather than producing well defined dimeric or trimeric products, instead, produce a product mixture with a distribution of products, which suggests that these systems undergo a Cossee-Arlman^{31-33,38,39} insertion process, and simultaneously they are also unstable to β -H elimination,

which is in competition with the insertion of new monomer. This in turn produces a mixture of product olefin oligomers with varying olefin size.

Whether the systems discussed are operating via a metallocycle intermediate or via a Cossee-Arlman mechanism, they both involve early TM-alkyl complexes, and the β -elimination stability of these species dictates the dominant reaction pathway. Therefore it is important for determination of the major products of the reaction. If the factors involved in the decomposition pathway for these metal-alkyl complexes were well understood, it would be possible to design better catalysts with precise control over the product olefin size.

Chapter 2: Cyclobutylmethyl Cp*ZAs and Related Chemistry

2.1 Introduction and Background

In the monoalkyl cationic state, the Cp* zirconium amidinate (Cp*ZA) ligand scaffold has shown evidence of great stability and resistance against β -H elimination. In general, Ziegler-Natta polymerization of α -olefins using various zirconocene and non-zirconocene based catalysts suffer from side reactions such as β -H elimination and β -H transfer to monomer, which produce a new cationic zirconium hydride or alkyl species that can reinitiate and continue the polymerization, however, the termination of the original chain serves to create a broader distribution of molecular weights in the product polymer.⁶⁰ Therefore these are non-living polymerization systems with product polymer polydispersities ($PDI = M_n/M_w$, where M_n is the number average and M_w is the weight average molecular weights for the polymer) significantly greater than the 1.10 required for a living system.¹⁶ This is not the case with the Cp*ZA catalyst system, which is living, as shown by the narrow PDI values, the absence of olefinic end groups in their ¹H-NMR spectra of its product polymers, and linear rate of monomer consumption directly related to the concentration of cationic Cp*ZA initiator in solution. This has been shown for monomers ranging from propene to higher olefins, making the Cp*ZA catalyst one of the most, if not the most, versatile stereospecific living Ziegler-Natta systems.

Evidence in support of the special β -H stability of the Cp*ZA alkyl complexes is not limited to the livingness of Cp*ZA Ziegler-Natta polymerization system. A solid state structure of the Cp*ZA isobutyl cation was solved via single crystal X-ray diffraction that showed a β -H agostic interaction with the cationic Zr center.¹¹ To confirm the presence of

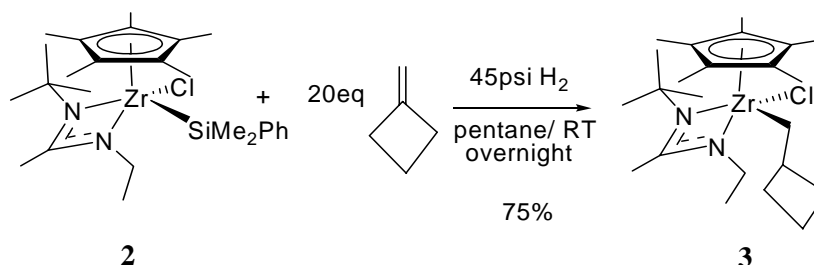
the agostic interaction, the $^1\text{H-NMR}$ spectrum of the Cp^*ZA isobutyl cation shows the $\beta\text{-H}$ upfield at a chemical shift of -0.27 ppm, and a 2D J-resolved HSQC spectrum of the Cp^*ZA isobutyl cation revealed the 96 Hz coupling constant (as opposed to the normal 125 Hz C-H coupling) between the $\beta\text{-H}$ and the $\beta\text{-C}$ confirming the presence of this secondary interaction.¹¹ The idea that agostic interactions may improve early TM-alkyl complexes' resistance to $\beta\text{-H}$ elimination by stabilizing the ground state energy can be traced back to the study of model Group 3 alkyl metallocenes by Bercaw and coworkers,⁶¹ which suggests that, in part, due to their observation of the greater reluctance of an ethyl group to $\beta\text{-H}$ eliminate from a Cp^*_2Y complex as compared to propyl and butyl groups due to the availability of 3 $\beta\text{-Hs}$ on the ethyl complex versus just 2 for in the case of propyl and butyl.

The actual causes of the remarkable stability of both the neutral and cationic Cp^*ZA complexes were not yet investigated, whether it be within or outside the context of the living Ziegler-Natta process. For example, it is known that upon insertion of an internal olefin into Schartz' reagent (Cp_2ZrHCl) the isolated products are those of the rearranged chain-walking product with the Zr finding the least substituted carbon. This is not the case for Cp^*ZAs , which in the neutral form are known to have stable Zr bonds to secondary and tertiary carbons.^{11,40} In order to further probe the ability of Cp^*ZAs to stabilize sensitive alkyl groups, the relatively exotic cyclobutylmethyl and cyclopropylmethyl complexes of Cp^*ZA were identified as synthetic targets, in order to study their relative stability to other known early TM cyclobutylmethyl complexes.^{62,63}

2.2 Hydrozirconation of Methylene cyclobutane and Related Transformations

2.2.1 Hydrozirconation of Methylene cyclobutane

Although Cp_2ZrHCl is known to be highly stable, its Cp^*ZA analog ($\text{Cp}^*\text{ZrHCl}[\text{EtNC}(\text{Me})\text{N}^t\text{Bu}]$) is highly elusive and decomposes in solution via disproportionation.¹⁰ To combat this problem a procedure was devised in our group to generate Cp^*ZA hydrochloride *in situ* via hydrogenolysis of a weak Zr-Si bond of $\text{Cp}^*\text{ZrCl}(\text{SiMe}_2\text{Ph})([\text{EtNC}(\text{Me})\text{N}^t\text{Bu}]$ (**2**).⁴⁴ The insertion chemistry of methylenecyclobutane into early TM-hydride bonds had already been reported, however, these species had never before been isolated or characterized via X-ray crystallography due to decomposition such as ring opening to form a pendant olefin.^{62,63} Using the recently developed protocol for hydrozirconation by generating a Cp^*ZA hydrochloride *in situ* from **2** and reacting it with methylenecyclobutane, Cp^*ZA cyclobutylmethylchloro complex **3** was isolated in 75% yield (Scheme 8). **3** was characterized by ^1H - and ^{13}C -NMR, and ^1H assignments for the cyclobutylmethyl group were verified by COSY (Figure 1).



Scheme 8 Hydrozirconation of methylenecyclobutane

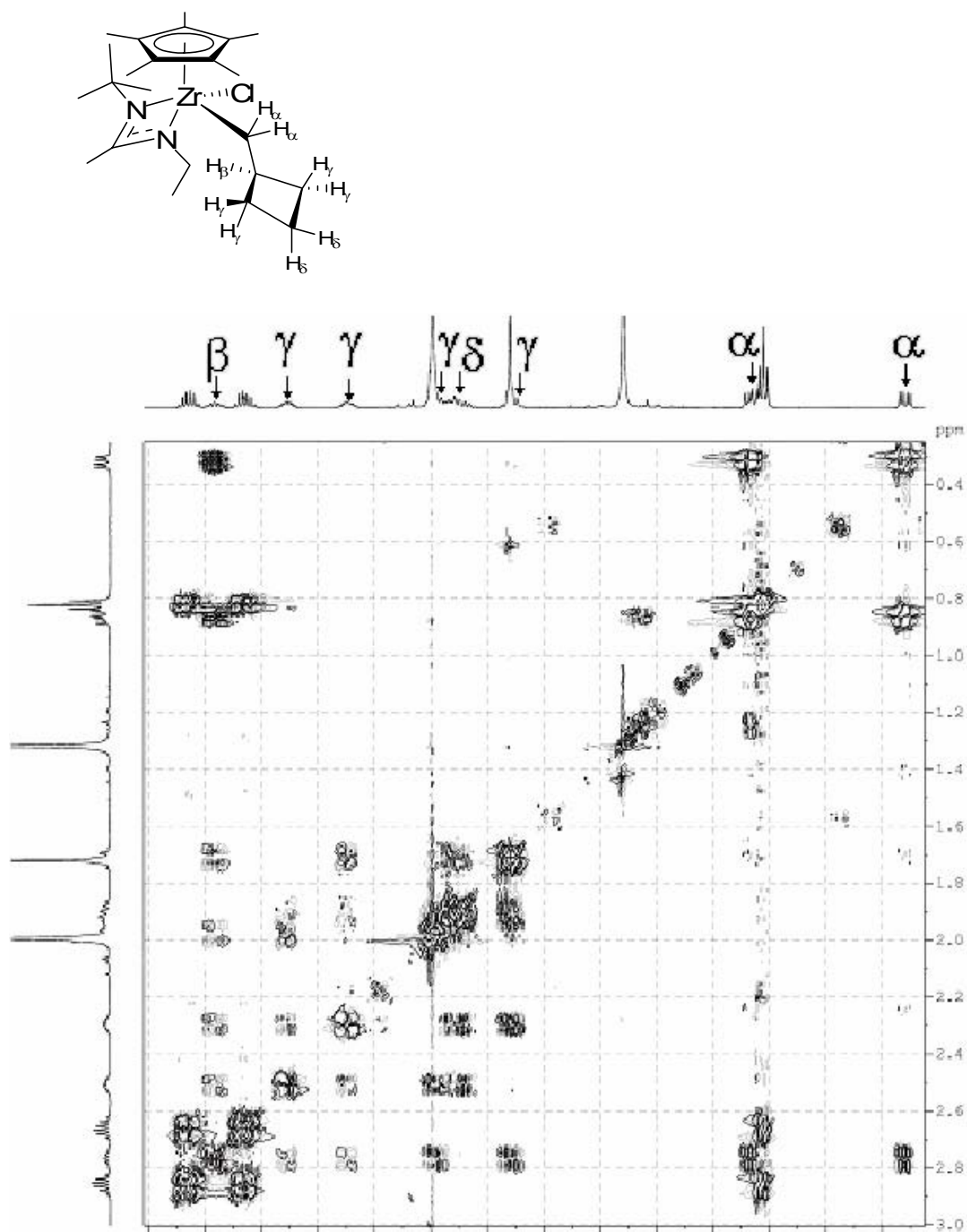


Figure 1 COSY spectrum of **3**

Single crystal X-ray diffraction confirmed the structure of the neutral alkyl chloro complex **3** (Figure 2), as similarly to all other known neutral chloro alkyl Cp*ZAs no β -agostic interaction was found in the solid state structure.

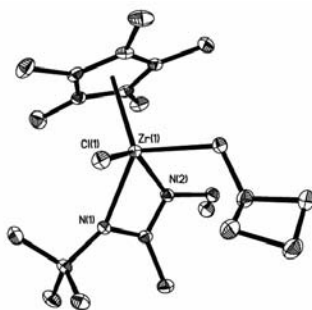
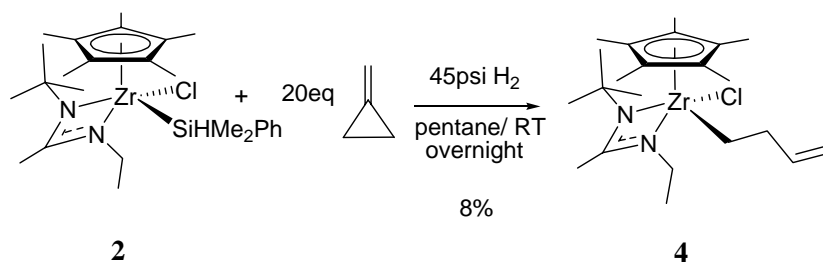


Figure 2 Solid state structure of **3** with 30% probability ellipsoids; hydrogens omitted for clarity

The crystal structure of **3** is by all parameters unremarkable, displaying the alkyl group positioned at the ethyl side of the amidinate, which has directly replaced the silyl group after hydrozirconation. It is known that in chloro Cp*ZAs the amidinate does not undergo ring flip epimerization the same way as in neutral dialkyl Cp*ZAs, and therefore it is logical that **3** would be configurationally stable at the Zr.^{64,65} At the same time, it was apparent from the structure that the bulky *tert*-butyl group on the opposite side of the amidinate is in steric conflict with the chloride, which forces the amidinate nitrogens to coordinate unsymmetrically. The crystal structure of **3** is the first example of a stable cyclobutylmethyl metal complex solid state structure, attesting to the special ability of Cp*ZAs to stabilize alkyl ligands likely stemming from a close steric ligand environment preventing secondary interactions with the metal center.

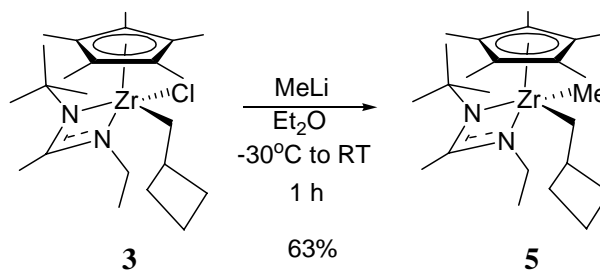
2.2.2 Hydrozirconation of Methylene cyclopropane



Scheme 9 Hydrozirconation of methylenecyclopropane

The hydrozirconation of methylenecyclopropane was also attempted, similarly to the synthesis of **3** via hydrozirconation of methylenecyclobutane. This reaction generated compound **4** in 8% crystalline yield (Scheme 9), which was the chloro butenyl Cp*ZA instead of the expected chloro cyclopropylmethyl Cp*ZA complex. The structure of **4** was confirmed by a $^1\text{H-NMR}$ comparison to an authentic sample synthesized via alkylation of Cp*ZA dichloride using butenylmagnesium chloride, the structure of which had already been confirmed by single crystal X-ray diffractometry.⁶⁶ This unexpected product could only be explained by a thermal ring opening rearrangement, such as the one observed in the literature for cyclobutylmethyl complexes.⁶³

2.2.3 Methylation of Cyclobutylmethyl Chloro Cp*ZA



Scheme 10 Methylation of **3** to generate **5**

Compound **3** was methylated with MeLi to generate **5**, which was characterized by $^1\text{H-NMR}$ showing the new methyl singlet at 0.13 ppm (Scheme 10). Single crystal X-ray analysis confirmed the structure of **5**, and as expected, in this neutral chloro alkyl Cp*ZA's structure there was no evidence of a $\beta\text{-H}$ agostic interaction (Figure 3).

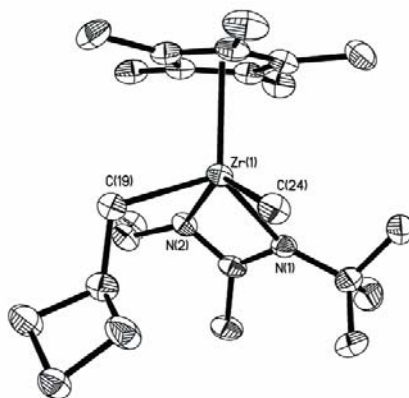


Figure 3 Solid state structure of **5** with 30% probability ellipsoids; hydrogens omitted for clarity

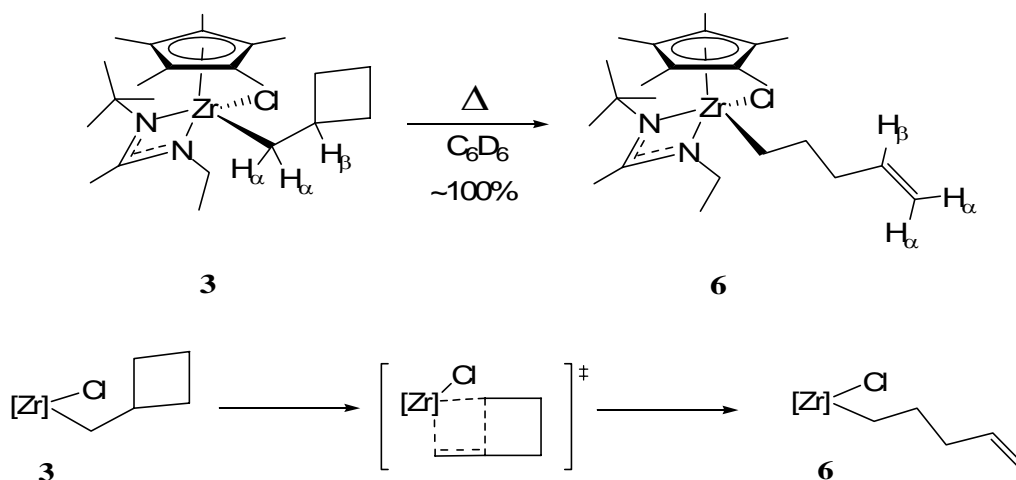
Consequently, the structural differences between **3** and **5** possess all the expected characteristics of a methyl group substitution for a chloride that have been observed for other alkyl methyl Cp*ZA complexes, such as the differences between the chloro isobutyl Cp*ZA and the methyl isobutyl Cp*ZA, which are the precursors to the isobutyl Cp*ZA cation which displays the $\beta\text{-H}$ agostic. Namely, The Zr-N distances for N1 increased from 2.2374(17) Å to 2.266(2) Å and for N2 increased from 2.2279(17) Å to 2.255(2) Å, which is consistent with going from a more electron poor chloro complex and electron withdrawing *trans*-influence to an electron rich methyl complex with an electron donating *trans*-influence. Also, there seems to be only a small amount of *cis*-influence on the cyclobutylmethyl substituent with the Zr-C distance slightly decreasing from 2.273(2) Å in **3** to 2.265(3) Å in **5**, which suggests that there is more of a steric factor with the

methyl group in **5** allowing the cyclobutylmethyl ligand to reside closer to the metal than the chloride in **3**. The Zr-C distance for the new methyl group is 2.292(3) Å, which is well within the normal range of known bond lengths for Zr-Me bonds in neutral Cp*ZA complexes.

Though **5** was stable enough to isolate and characterize in the solid state, however, it began to decompose if left for even a short period of time in solution. If the decomposition of **5** is allowed to proceed to completion it is possible to observe new signals growing in the ¹H-NMR spectrum. Upon completion the decomposition yields a mixture of several products not separable by crystallization, nor characterizable using standard NMR techniques.

2.3 Ring Opening of Neutral Chloro Cyclobutylmethyl Cp*ZA

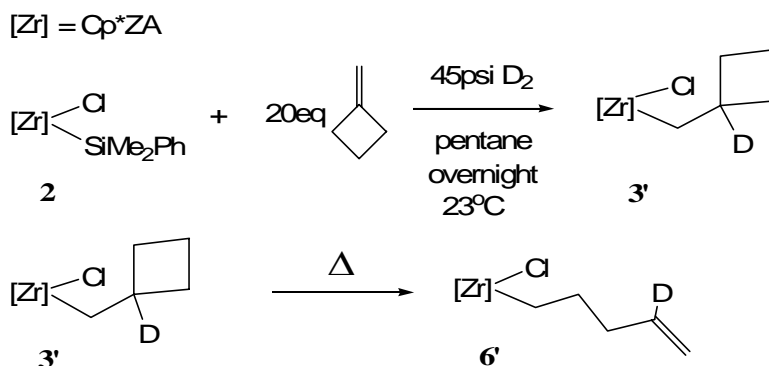
2.3.1 NMR Confirmation of Transformation



Scheme 11 Ring opening rearrangement of **3** to pendant olefin complex **6** with mechanism

The same thermal ring opening rearrangement as for hydrozirconation of methylenecyclopropane product **4** was also observed in compound **3**. When left in solution at RT overnight, **3** was observed to rearrange to a new species with resonance peaks appearing in the olefinic region of the 1H -NMR spectrum at chemical shifts of 6.00 ppm (1H), 5.15 ppm (1H), and 5.03 ppm (1H), which are characteristic of a pendant olefin on the metal complex.⁶³ Further investigations into this rearrangement showed that **3** cleanly ring-opens to **6** at temperatures ranging from RT to as high as 90°C (Scheme 11).

2.2.4 Deuterium Labeling Experiment



Scheme 12 Synthesis of **3'** and its ring opening rearrangement to **6'**

In order to probe the mechanism of this rearrangement, a deuterium analog of **3** was synthesized by substituting H₂ with D₂ gas for the deuteriozirconation of **1**. This cleanly yielded the deuterium labeled **3'** with the D substituent only present in the β position as seen in Scheme 12. As detected by ¹H-NMR, there is no observed D/H scrambling. The thermal rearrangement of the ring to the terminal olefin was also carried out for **3'** to yield **6'** with the D label exclusively occupying the δ (secondary vinyl) position (Scheme 12), which was confirmed by the complete absence (up to the NMR detection limit) of the respective multiplet resonance at 6.00 ppm in the ¹H-NMR spectrum of the decomposition product. The kinetic data showed that the rate of the ring opening for the deuterium-labeled **3'** at 60°C was exactly the same as that of **3**, exhibiting no kinetic isotope effect.

2.3.3 Kinetic Study of the Ring Opening

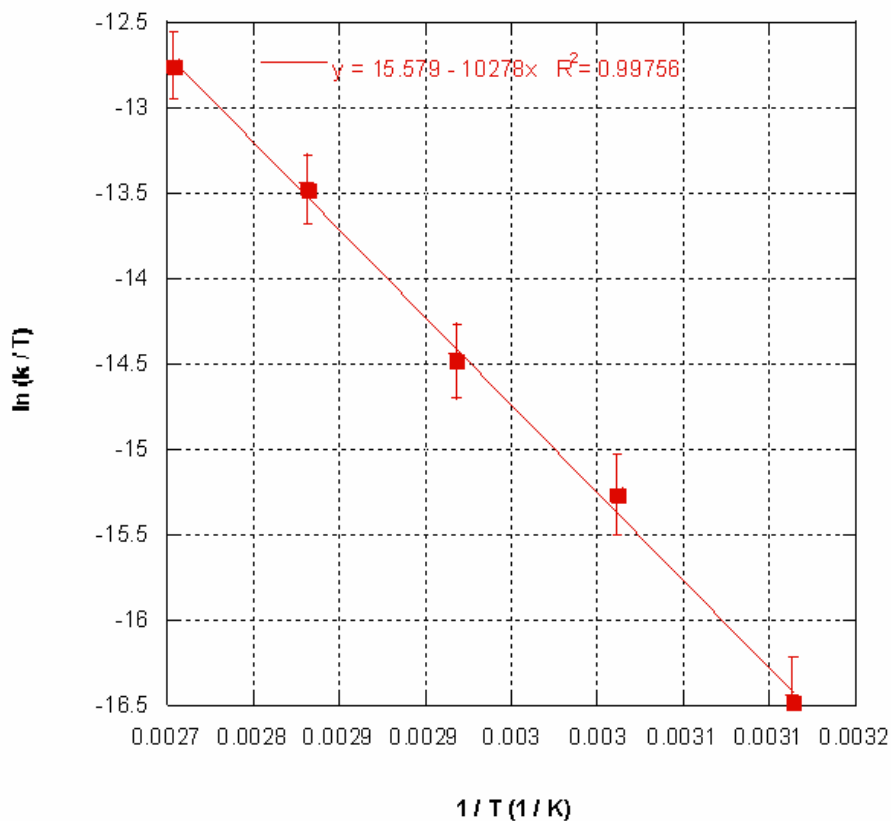


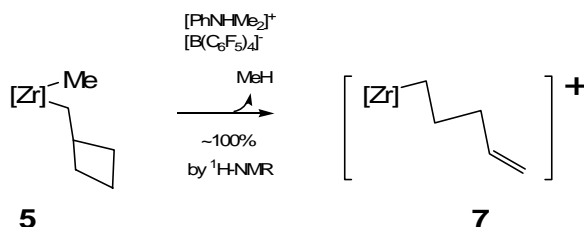
Figure 4 Eyring plot for 321 K to 363 K temperature range for the ring opening of neutral cyclobutylmethyl chloro Cp*ZA **3**

To further characterize this ring opening rearrangement, the decomposition of the chloro cyclobutylmethyl Cp*ZA **3** to make chloro pentenyl Cp*ZA **6** was followed by $^1\text{H-NMR}$ at a range of temperatures from 48°C, to 90°C. From these kinetic data the $\Delta H^\ddagger = 20.4 \pm 0.6$ kcal/mol and $\Delta S^\ddagger = -16.3 \pm 0.9$ cal/mol·K were extrapolated for the transition state (TS ‡) of the ring-opening process using the Eyring equation (Figure 4). These values of ΔH^\ddagger and ΔS^\ddagger are consistent with a β -alkyl elimination mechanism found in other similar systems, however, the barrier for this process in the Cp*ZA complex is greater than any other known cyclobutylmethyl metal complex, such as the

cyclobutylmethylmagnesium chloride, cyclobutylmethyl lithium and cyclobutylmethyl decamethyltitanocene (Cp_2Sc) reported in the literature. It was confirmed that a similar rearrangement does not occur when the methyl cyclobutylmethyl Cp^*ZA **5** is allowed to stand in solution at RT, since no identifiable product was isolated from that reaction. This made it impossible to propose a mechanism for its decomposition, however, the fact that the $^1\text{H-NMR}$ of the reaction mixture showed no olefin resonances is strong evidence supporting that the thermal decomposition process occurring in the case of **5** is different from the ring opening of **3**. All the kinetic and NMR data point to the ring opening being a deinsertion with a four-centered TS^\ddagger , confirming the proposed mechanism in Scheme 11.

2.4 Cation Studies

2.4.1 Generation of Cation from Cyclobutylmethyl Methyl Cp*ZA



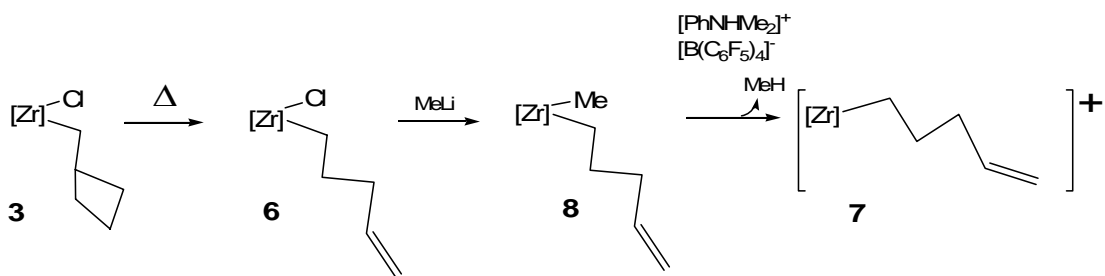
Scheme 13 Protonation of **5** generates pentenyl cation **7**

One of the goals of this project was to test the stability and general behavior of the cyclobutylmethyl Cp*ZA cation. Using the same methodology as with the Cp*ZA Ziegler-Natta polymerization system, the methyl Cp*ZA alkyl **5** is protonated using dimethylanilinium perfluorotetraphenylborate, $([\text{PhN}(\text{H})\text{Me}_2][\text{B}(\text{C}_6\text{F}_5)_4])$, which produces CH_4 from the protonated methyl group and a Cp*ZA cationic species **7** (Scheme 13).

Upon examination of the $^1\text{H-NMR}$ of **7** it became evident that the cyclobutyl ring opens transforming the cyclobutylmethyl group into a pentenyl group, which likely occurs in the same fashion as the ring opening process observed for the neutral **3** transforming into **6**. A 2D-COSY spectrum of the cation allowed for a positive identification of the resonance of protons on the pentenyl moiety. A phase sensitive HSQC of **7** allowed for an assignment of the carbon resonance in the $^{13}\text{C-NMR}$, and showed no evidence of an agostic interaction with all $J_{\text{C-H}}$ values in the normal range between 125 and 132 Hz. Considering that for **3** the ring-opening only occurs at temperatures above RT, the cation **7** is generated at -30°C , and even at this temperature the ring opening still cannot be prevented and occurs immediately. This suggests that the

barrier to the ring opening process is significantly reduced for the cationic species **7** as compared to the neutral **3**, which probably has something to do with the now available neighboring open coordination site, as well as the positive charge on Zr. This follows the general reactivity trend of known cyclobutylmethyl complexes of early transition metals, as was shown by Casey and coworkers,⁶³ the decamethylyittrcene cyclobutylmethyl complex ring opens at -78°C . Yet another testament to the stability of Cp*ZA alkyl species is the instability of the decamethylyittrcene pentenyl product, which at -78°C is only stable for a couple of weeks and once allowed to warm up to -50°C it decomposes with a half-life of 30 min., whereas the Cp*ZA pentenyl cation is stable in PhCl up to -10°C indefinitely, in the same manner as other known Cp*ZA alkyl cations, and possibly even higher temperatures in non-chlorinated solvents.

2.4.2 Generation of Cation from Pentenyl Methyl Cp*ZA



Scheme 14 Another route to generate cation **7**

To conclusively show that **7** was indeed the ring opened product cation, a straightforward synthetic pathway was chosen to initially generate a pentenyl methyl Cp*ZA cation precursor that could be directly protonated to generate a pentenyl cation

and show that it is the same species as **7**. This was achieved by allowing **3** to cleanly rearrange to **6** isolated as a pure oil, with its purity confirmed by $^1\text{H-NMR}$. The product **6** was then methylated to produce **8** in quantitative yield also as a pure oil, which was confirmed by $^1\text{H-NMR}$. Finally, **8** was protonated using $[\text{PhN}(\text{H})\text{Me}_2][\text{B}(\text{C}_6\text{F}_5)_4]$ to make a cation, which by $^1\text{H-NMR}$ appears to be identical to **7**. This independent synthetic route confirmed that **7** can be generated through either pathway, and supporting that **7** is in fact the pentenyl Cp^*ZA cation.

2.4.3 Conformational Analysis of Pentenyl Cp^*ZA Cation by Selective $n\text{Oe}$

Upon examination of its $^1\text{H-NMR}$, it is evident that the olefinic resonances of cationic complex **7** have a different chemical shift pattern than a pendant olefin such as **6**. Although **6** is a neutral complex and **7** is cationic, nevertheless, the terminal double bond of the pentenyl moiety is located four carbons away from the cationic metal center, which should make it too far removed to feel its effect, and yet the resonance of the secondary olefinic proton was shifted from a chemical shift of 6.0 ppm, as it appears in the spectrum of **6**, to 7.4 ppm in the cationic species **7**. This type of deshielding is characteristic of the olefin binding the cationic metal center, and has been observed in other similar systems.^{62,63,67,68}

The significance of the conformation of **7** is its resemblance of the polymeryl olefin Ziegler-Natta polymerization intermediate immediately before the insertion of monomer occurs. Though it has been claimed in other reports of pendant olefin coordination to Ziegler-Natta active complexes that this type of coordination is a model

for olefin coordination to the propagating center, it is far from being ideal, considering that in the case of this pentenyl Cp*Zr cation the olefin is physically tethered to the Zr. Its conformation is directly dependant on the ring strain of the coordinated system, as well as the ring's steric interactions with the complex's ligand sphere. This is particularly well illustrated by the previously unreported observation that the hexenyl Cp*Zr cation, which is analogous to **7** except for having an extra carbon on the pendant olefin chain, undergoes an insertion to give a cyclopentylmethyl Cp*Zr product.⁶⁶ This is the product of the ring-opening/closing equilibrium lying in the opposite direction from the pentenyl **7**, and these observations can be explained by Baldwin's rules.⁶⁹

Therefore it would be difficult to make the argument for the inherent value of this system as a model for the polymeryl olefin intermediate, because the conformation of the olefin in **7** is influenced by the sterics of the system. Based on the structure of **7** it would be impossible to show the conformation of free monomer upon coordination to the cation, however, this coordination of the pendant olefin does confirm the existence of the coordinated olefin intermediate.

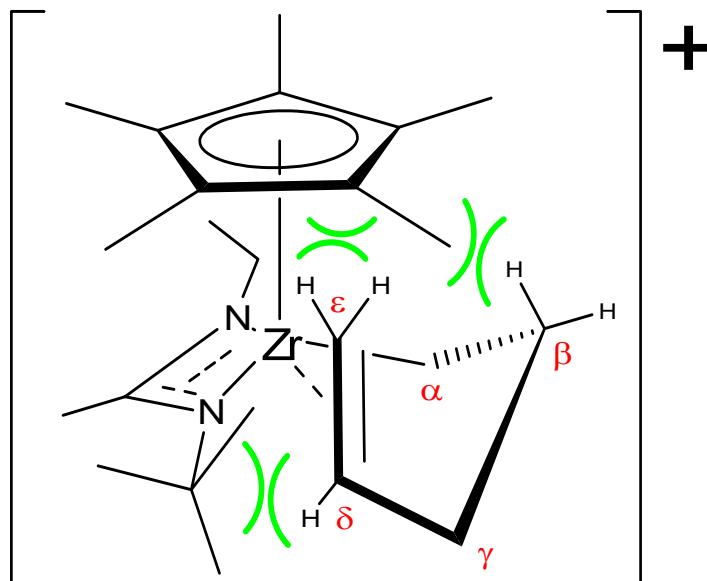
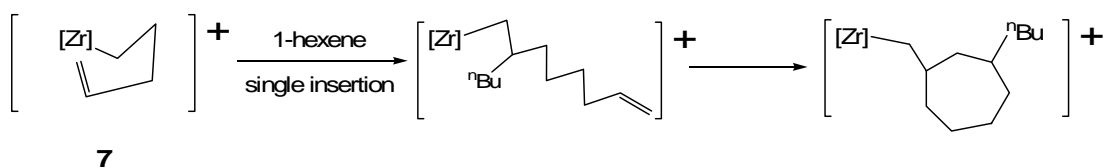


Figure 5 Diagram depicting the solution structure of **7** and also showing the nOe interactions found in **7**

Figure 5 shows the proposed conformation for cationic **7** based on a series of selective (1D) nuclear Overhauser effect (nOe) experiments that confirmed that the olefin is in close proximity to the zirconium center on the NMR timescale, yielding high nOe correlations between the ¹Bu group of the amidinate and the δ (secondary vinyl) hydrogen. Also, strong nOe communication was found between the Cp* and the two terminal olefin protons. Notably, the converse was not found: the secondary olefinic hydrogen (δ) does not display proximity to the Cp* hydrogens, nor does the ¹Bu group of the amidinate have nOe interaction with the terminal olefin protons (ϵ) of the pentenyl. Another important result was significant nOe spin transfer from the ethyl group on the amidinate to the α -Hs of the pentenyl, but not to any other signal. Also, there was a strong nOe found between the Cp* signal and the β -Hs of the pentenyl. The γ -Hs experienced an nOe transfer from the δ -H and a weak nOe from the ¹Bu group of the amidinate. All these results support a

folded envelope conformation with the olefin coordinated to the zirconium cation such that the terminus of the pentenyl double bond is pointing toward the Cp* ligand, as proposed in Figure 5. This folded envelope conformation is in agreement with one of the conformations proposed for the neutral decamethyltitricene pentenyl complex studied by Casey.^{62,63}

2.4.4 1-Hexene Polymerization Studies With Pentenyl Cp*ZA Cation

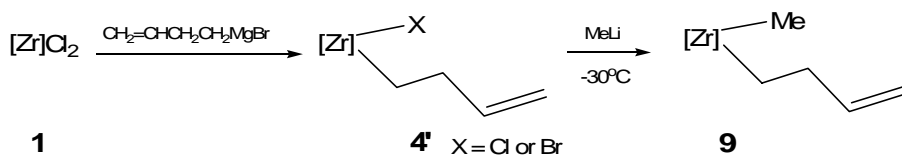


Scheme 15 Proposed mechanism of disappearance of end-group olefinic groups during polymerization of 1-hexene by cation **7**.

To further characterize **7**, it was tested for polymerization of 1-hexene, yielding isotactic PH with PDI < 1.05 in the same manner that a methyl Cp*ZA cation catalyst does. However, end group analysis performed on a sample with 50 equivalents of monomer added ($M_n \leq 4100$) of the product polymer showed no olefinic resonances. This suggests not only that incoming 1-hexene monomer can successfully compete with the pendant olefin, but also that after at least one monomer insertion occurs, the olefin end-group must somehow be consumed. This is likely accomplished via its insertion into the polymer thereby effecting the cyclization of the polymer end to make a seven-membered ring, which according to Baldwin's rules is a favorable process.⁶⁹

2.5 Study of the Methyl Butenyl Cp*ZA

2.5.1 Synthesis of Methyl Butenyl Cp*ZA



Scheme 16 Synthesis of methyl butenyl Cp*ZA **9**

To further study the properties of pendant olefin Cp*ZAs, a precursor butenyl complex **4** was synthesized via alkylation of Cp*ZA dichloride **1** using butenylmagnesium bromide. By ¹H-NMR it became evident that the product of the Grignard alkylation was a 1:2 mixture, respectively, of the chloro:bromo butenyl Cp*ZA (ratio established via integration of ¹H-NMR peak intensities), and since it's chemically different from the purely chloro-substituted **4**, this product is designated **4'**. The mixture of different halide substituents on the product was likely due to halide exchange of the zirconium chlorides with the Grignard reagent bromides. The compound **4'** was subsequently treated with a stoichiometric equivalent of MeLi in an attempt to produce the methyl butenyl Cp*ZA complex **9** (Scheme 16), however, when the reaction was allowed to warm to RT from its initial -30°C, **9** was not the isolated product. Rather, a red product was isolated and later determined to be butadiene complex **10a** (vide infra). The methylation of **4'** was then carried out successfully when the reaction was carried out at -30°C for the 18h duration of the reaction and under dilute conditions (11.0 mM). The white crystalline product **9** was characterized by ¹H-NMR as well as single crystal X-ray diffraction (Figure 6 and Table 1).

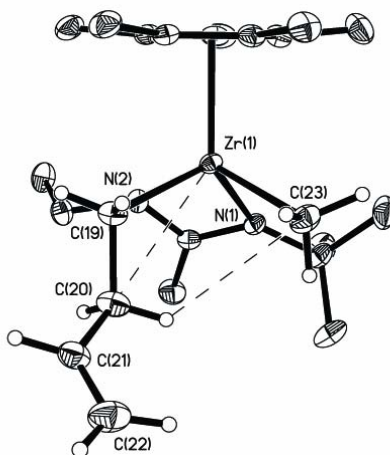


Figure 6 Solid state structure of **9** depicting possible secondary interactions drawn with 30% probability ellipsoids; some hydrogens have been omitted for clarity

Zr(1) – C(19)	2.2583(18)	C(19) – C(20)	1.539(3)
Zr(1) – C(23)	2.285(2)	C(20) – C(21)	1.487(3)
		C(21) – C(22)	1.302(3)

Table 1 Selected bond distances for **9** in angstroms (Å)

The $^1\text{H-NMR}$ of **9** exhibits three olefinic signals at chemical shifts of 6.12 ppm, 5.17 ppm, and 4.99 ppm, which are consistent with the pattern seen for the pendant olefin pentenyl complex **6**. The solid state structure of **9** is interesting and is worth examining closer. The most obvious feature of the solid state structure of **9** is the disparity in bond lengths of C(20) (β carbon of the butenyl ligand) to its neighboring carbons. It has two single bonds – one to C(19) and the other to the sp^2 hybridized C(21) (Figure 6). Interestingly, the C(20)-C(21) bond length is 1.487(3) Å, versus the normal single bond length for the C(20)-C(19) of 1.539(3) Å. This differential is significant enough at 0.05 Å to be well outside the range of error for these bond lengths, but this single aspect of the structure is only one piece of the story, and there are two other important features of the solid state structure of **9** that embody important contributing factors to complete the

picture. A second interesting observation about the crystal structure of **9** is that the distance between the Zr and C(20) is about 3.09 Å, which is too long to deem as conclusive evidence of an agostic interaction, however, it is close enough that the shortening of the C(20)-C(21) bond can be viewed as relevant to the possible Zr-C(20) secondary interaction. The third important feature of this structure is the short distance of about 2.91 Å between the Zr methyl group carbon C(23) and the butenyl group β-H H20B, which is the β-H closest to the methyl group side. This close proximity of the methyl group to the β-H suggests that there may also be a secondary interaction between them, which due to the polarity of the interaction can be likened to a reverse hydrogen bond. The shortening of the C(20)-C(21) bond, the apparent short distance between Zr and C(20), as well as the short distance between the Me group on the metal and the β-H on the butenyl group closest to it, all suggest the the structure of **9** is one of a conformation that is close to the Me group hydride abstraction TS[‡], and can be viewed as a stunted TS[‡] kinetically trapped by the very secondary interactions that are involved in its pathway toward hydride abstraction. This not only foreshadows the mechanism of the decomposition of **9**, which will later be discussed in more detail (*vide infra*), but is also relevant to the general discussion of stability of Cp*ZA alkyl species against common decomposition pathways, showing that various secondary interactions can at lower temperatures provide kinetic stability for these generally unstable types of compounds.

2.5.2 Decomposition of Methyl Butenyl Cp*ZA

As reported earlier, the synthesis of **9** was initially unsuccessful when the reaction was allowed to warm to RT and yielded a red crystalline material **10a**, which when characterized by $^1\text{H-NMR}$ was recognized immediately to be a Cp*ZA butadiene complex, which can also be viewed as a zirconacyclopentene. This was determined from the characteristic signals at chemical shifts of 6.17 ppm and 6.09 ppm corresponding to the two β -Hs on **10a**, which appear at different chemical shifts due to the asymmetry of this C_1 symmetric molecule. Characteristic of such a Cp*ZA butadiene complex, these β -H proton signals are shifted downfield due to diamagnetic anisotropy from the homoaromatic “ring current” of the butadiene fragment and the metal center.⁷⁰

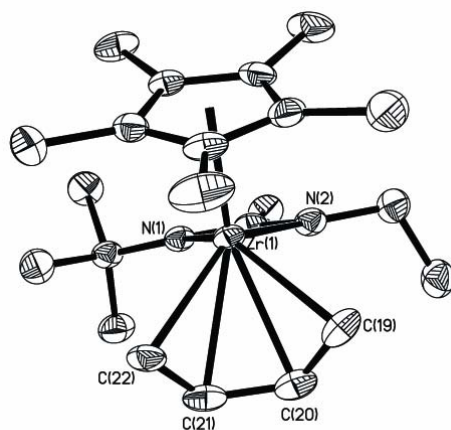
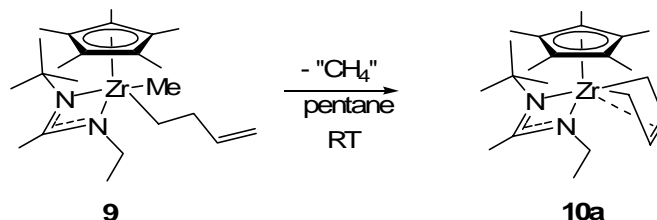


Figure 7 Solid state structure of **10a** with 30% ellipsoids; hydrogens omitted for clarity

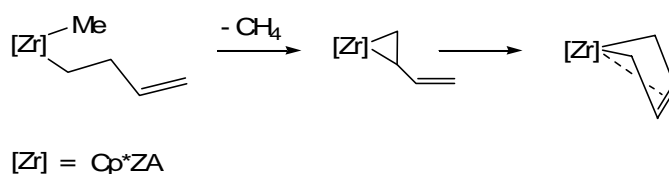
Zr(1) – C(19)	2.336(6)	C(19) – C(20)	1.461(10)
Zr(1) – C(20)	2.485(6)	C(20) – C(21)	1.414(10)
Zr(1) – C(21)	2.494(6)	C(21) – C(22)	1.427(9)
Zr(1) – C(22)	2.358(6)		

Table 2 Selected bond distances for **10a** in angstroms (Å)

The solid state structure of **10a** was obtained from single crystal X-ray diffraction (Figure 7 and Table 2), confirming that indeed **10a** is analogous to a previously reported zirconacyclopentane (Cp*ZA butadiene) **10b**. Once **9** was successfully isolated and allowed to stand in pentane solution at RT overnight, **10a** was produced quantitatively with loss of CH₄ (Scheme 17).



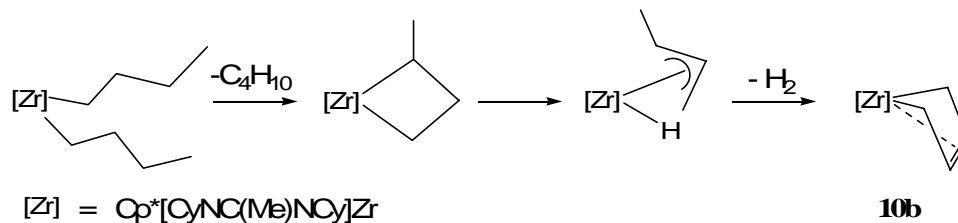
Scheme 17 Decomposition of **9** to **10a**



Scheme 18 Proposed stepwise mechanism for the decomposition of **9** to **10a**

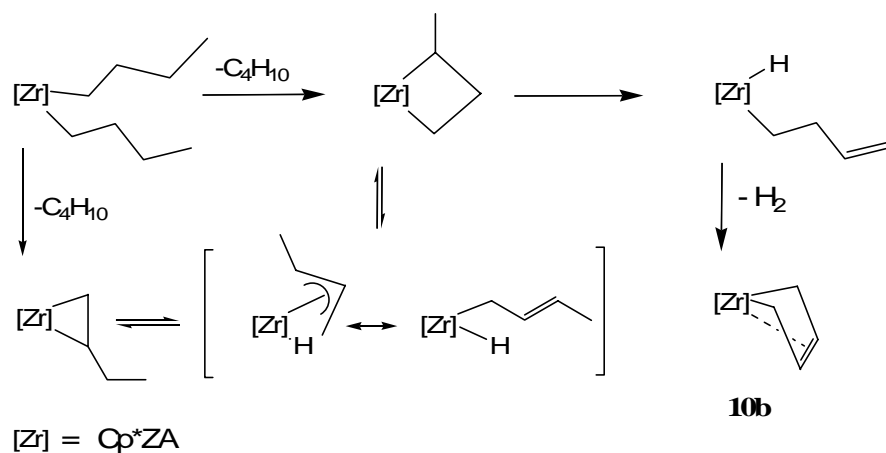
Based on the analysis of possible secondary interactions in the solid state structure of **9** and the observation of the facile formation of **10a** from **9** with loss of CH₄, it is possible to envision the mechanism of the formation of **10a** to proceed via immediate abstraction of a β -H from the butenyl ligand by the Me group producing an η^2 -butadiene Cp*ZA, which subsequently rearranges to the η^4 -butadiene Cp*ZA **10a** (Scheme 18). This new evidence somewhat clarifies the route through which **10b** is obtained from the thermolysis of dibutyl Cp*ZA.⁴³ The mechanism proposed for that transformation as published involved an initial γ -H abstraction with loss of butane and formation of a

transient zirconacyclobutane intermediate (Scheme 19), which was based on work conducted by Dioumaev and Harrod.⁷¹



Scheme 19 Pathway originally proposed for thermolysis of $[Zr]nBu_2$ to make **10b**

Originally it was suggested that the strained 4-membered ring of the aforementioned zirconacyclobutane presumably undergoes a facile β -hydride elimination to alleviate the ring strain. As seen in Scheme 19, the mechanism originally proposed for this transformation proceeded through the lowest energy hydrido η^3 -allyl intermediate, which would be the product of β -H elimination of one of the zirconacyclobutane ring β -Hs. It has been observed by Whitesides and coworkers, that the decomposition of robust bis-Cp titanocyclopentanes does not normally go via β -H elimination due to steric strain, however, upon the synthesis of an analogous titanocyclopentane bearing an α -methyl substituent, facile β -H elimination is observed.⁷² If γ -H abstraction is in fact the first step of the decomposition process of dibutyl Cp^*ZA , then the α -methyl substituent in the zirconacyclobutane intermediate may be the key to the next step in the process. In light of the evidence from the titanocyclopentane work by Whitesides and coworkers,⁷² and the facile decomposition of **9** to make **10a**, the actual mechanism of the decomposition of dibutyl Cp^*Za is probably more like the one shown in Scheme 20.



Scheme 20 New proposed mechanism for decomposition of $[\text{Zr}]^n\text{Bu}_2$ to **10b** based on decomposition of **9** to **10a**

The original mechanism was proposed based on work conducted by Dioumaev and Harrod,⁷¹ which dealt with zirconocene based alkyl complexes. It is apparent that the Cp*ZA ligand scaffold has a different reactivity profile than analogous zirconocene compounds. Dioumaev and Harrod state that they observe both a zirconacyclobutane and a zirconacyclopentadiene in solution upon addition of 2 equivalents of $^n\text{BuLi}$ to zirconocene dichloride.⁷¹ Based on kinetic analysis they suggested that the initial decomposition based on their evidence probably occurs via a γ -H abstraction to make a zirconacyclobutane intermediate, while the zirconacyclopentadienes observed in the NMR experiments appear to be the products of a zirconacyclobutane rearrangement that amounts to a formal hydride shift achieved via a series of elimination/insertion steps, and not from direct β -H abstraction (Scheme 20).

Since no evidence exists against direct β -H abstraction in Cp*ZAs, it is impossible to definitively assert via which pathway the decomposition proceeds with the Cp*ZA ligand manifold. It is possible that in the case of Cp*ZAs both β -H and the γ -H

abstraction processes occur, but it is not known whether only β -H abstraction occurs, or only γ -H abstraction occurs, or both occur, in any case it is still possible to envisage a plausible mechanistic pathway proceeding through a zirconacyclobutyl intermediate, as originally suggested (Scheme 20).

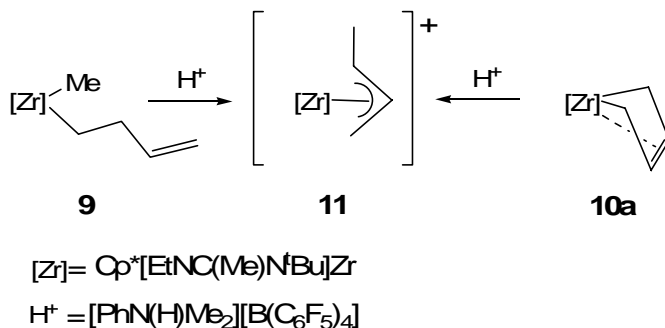
More importantly, the new evidence that has come to light as a result of the conversion of **9** to **10a** and the analysis of the solid state structure of **9**, which shows the proximity of the metal-based Me group to the β -H on the butenyl group and of the Zr to the β -carbon, all seemingly poised to undergo the β -H abstraction. This suggests that the most likely intermediate directly preceding the formation of **10a** is a hydrido butenyl Zr species (Scheme 20), which would be analogous to the methyl butenyl Cp*ZA **9**. This means that though it is theoretically possible that the transannular β -hydride elimination/deinsertion occurs to form a hydrido allyl Cp*ZA, it likely does not affect the formation of **10b**, and is only a spectator equilibrium.

2.5.3 Study Of Butenyl Cp*ZA Cation

The cation **11** produced by protonating **9** with [PhN(H)Me₂][B(C₆F₅)₄] is deep red in color, as opposed to other known alkyl or alkenyl Cp*ZA cations, which are yellow. Its ¹H-NMR spectrum showed a set of two resonances in the olefin region at 6.2 ppm and 6.0 ppm, integrating for 1 H each, and a new set of resonance in the allyl region at 4.2 ppm, which appears to be two asymmetric superimposed multiplets integrating for 2 Hs. In an attempt to characterize this cation, a polymerization of 1-hexene was carried out and yielded 2.8% by mass of purely isotactic (as determined by ¹³C-NMR) poly-1-hexene

(PH) with M_n nearly 3 times greater than expected and a PDI value of 1.08 after a 2 h polymerization attempt. These numbers are characteristic of the Cp*ZA Ziegler-Natta catalyst originally produced by Sita and coworkers,¹ and they suggest that during the activation of **9** with [PhN(H)Me₂][B(C₆F₅)₄] some portion of the precatalyst was protonated not at the metal-based methyl group, but instead at the butenyl group, producing an active methyl Cp*ZA cation, with the majority of the cation (~99% from polymer yield and M_n) was inactive toward 1-hexene polymerization.

Based on the ¹H-NMR spectrum, which showed signals in the allyl region, and the lack of polymerization activity, it was supposed that **11** could be an allyl cation. To show that this was the case, and having little success crystallizing **11** by diffusion of pentane into chlorobenzene, it became necessary to find an alternative route to prove the structure of **11**. It was recognized that if it were possible to generate the same allyl cation via another route and show that it is the same as the one being generated by protonation of **9**, then that would be good evidence that **11** is indeed the allyl cation. Drawing on past experience with allyl Cp*ZA cations generated by protonation of a Zp*ZA(TMM) complex, **10a** was protonated using [PhN(H)Me₂][B(C₆F₅)₄]. The product cation appeared to be nearly identical by ¹H-NMR to the spectrum of **11** (Scheme 21).⁷³



Scheme 21 Protonation of **9** or **10a** gives the same allyl cation **11**

Chapter 3: Reactivity of a Non-Base Stabilized Styrene Complex of Zirconium

3.1 Oxidative Coupling of Alkenes and Alkynes With The Styrene Cp*Zr

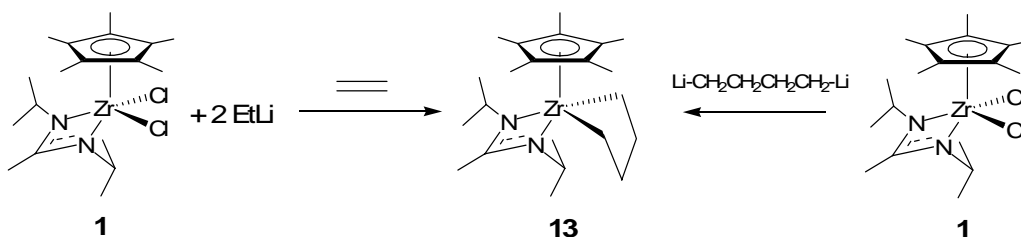
3.1.1 Background

Investigations into the chemistry of zirconacyclopentanes initially emerged after the synthesis and isolation of the first known base-free zirconacyclopropane complex Cp*Zr[(Me)₂CHNC(Me)NCH(Me)₂](CH₂CHPh) (**12**), which has been previously reported.¹⁹ The alkene and alkyne insertion chemistry exhibited by **12** is related to the chemistry pioneered by Negishi, Erker, and Buchwald, among others.^{19-21,25,74,75} The major difference is that the non-zirconacene Cp*Zr species is a 14e⁻ zirconium complex, which is formally more electron deficient than the 16e⁻ zirconacene-based species used in studies carried out by those who pioneered this chemistry. Though at first glance it may seem that the 14e⁻ species would be less stable, our zirconacyclopentane products are stable enough to isolate and characterize by X-ray crystallography, which previously has not been successfully accomplished with such a variety of substituted zirconacyclopentanes. Gratifyingly this chemistry has yielded a rich variety of products using a single ligand system, which has enabled us to study the stability of zirconacyclopentanes due to effects from various substituents.

Upon isolation of **12**, the initial investigations of its reactivity with C-C unsaturations were carried out with a variety of substrates. Due to the relative stability and isolability of our zirconacyclopentanes, we can study the effects of various substituents on the stability and reactivity of Cp*Zr zirconacyclopentanes.

3.1.2 Synthesis of an Unsubstituted Zirconacyclopentane

Synthesis of **13** was accomplished via two different methods. One method involved reacting Cp*ZA dichloride **1** with two equivalents of EtLi under an atmosphere of ethene, yielding **13** in excellent yield (by NMR). An alternative synthetic method was used to confirm the identity of **13** where 1,4-dilithiobutane was generated *in situ* from 1,4-dibromobutane with two equivalents of ^tBuLi per bromide, and then reacted with the Cp*ZA dichloride **1**. Both methods produced the same compound as confirmed by ¹H-NMR (Scheme 22).⁷⁶



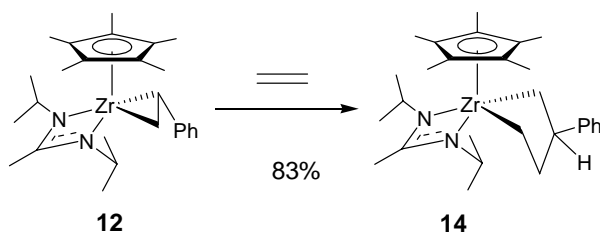
Scheme 22 Two different syntheses of **13**

It is presumed that the first method, borrowed from Negishi,¹⁹ which has been extensively studied,^{46,77-79} most likely produces an olefin complex of zirconium via β -H abstraction, which then undergoes an insertion with ethene. The novelty of this compound is in its thermal stability relative to known zirconocene-based zirconacyclopentanes.⁷⁹⁻⁸⁴

Zirconocene-based zirconacyclopentanes are species that are difficult to isolate or characterize due to their instability. This makes them relatively exotic and crystal structures that have been published in the literature are either limited as to the type of substituents that can be present on the metallocycle, or as in the case of Sun, and coworkers, there is some question as to the validity of the published crystal structures due

to a severe contraction in the $C_{\beta}-C'_{\beta}$ single bond, which is reported to be 1.33 Å. As a rule either the zirconacycle or the Cp ligands on the metal must have enough steric bulk to block any interaction between the metal center and the β -Cs or β -Hs of the ring, otherwise the zirconocene-based zirconacyclopentane species are unstable, and cannot be isolated. In comparison, the Cp*ZA zirconacyclopentane **13** is stable for days at 100°C in toluene.

3.1.3 Ethene Insertion



Scheme 23 Reaction of **12** with ethene to form **14**

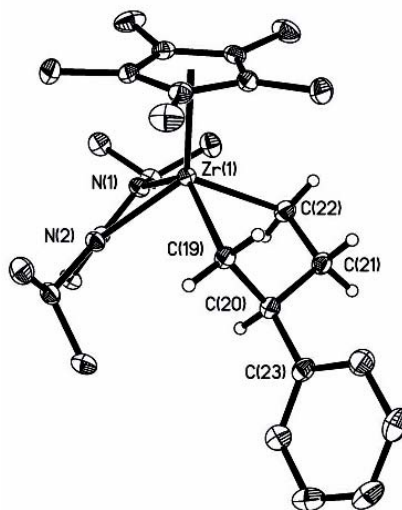


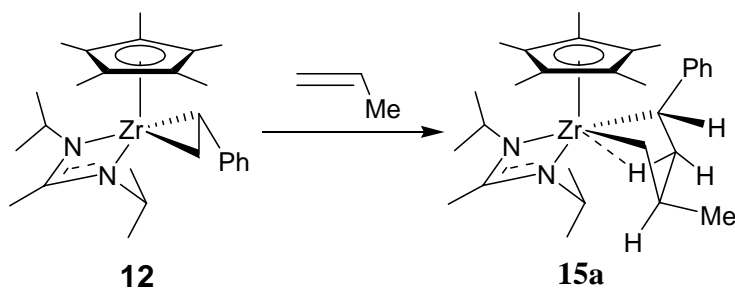
Figure 8 Solid state structure of **14** with 30% probability ellipsoids; Cp* and amidinate hydrogens have been omitted for clarity

Zr(1) – C(19)	2.3073(14)	Zr(1) – C(22)	2.2839(15)
C(19) – C(20)	1.548(2)	C(20) – C(21)	1.529(2)
C(21) – C(22)	1.527(2)	C(20) – C(23)	1.521(2)

Table 3 Selected bond distances for **14** in angstroms (Å)

When **12** was exposed to an atmosphere of ethene, the β -Ph substituted Cp*ZA zirconacyclopentane **14** was produced in high yield (Scheme 23). The $^1\text{H-NMR}$ of **14** shows two isomers which at RT always appear in the same ratio with respect to one another. The solid state structure of **14** was unremarkable, however, it revealed that ethene inserted on the more hindered side of zirconacyclopentane **12** and that all the C-C bond distances are of normal single bond length, which is in contrast to a contraction of $\text{C}_\beta\text{-C}'_\beta$ bond in other known zirconacyclopentanes (Figure 8 and Table 3).⁸⁴ **14** was not found to be as thermally stable as **13**, and even though it was indefinitely stable in solution at RT, the solution turned brown and its $^1\text{H-NMR}$ spectrum exhibited new resonances due to decomposition following incubation of the sample at 50°C for 30 min.

3.1.4 Propene Insertion



Scheme 24 The isolated product of propene reaction with **12** is **15a**

Allowing **1** to be under 45psi of propene overnight turned the solution from a deep green to a dark brown color. After volatiles were removed *in vacuo* the remaining

solids were redissolved in a minimum amount of pentane, and recrystallized at -30°C to provide a 58% yield of **15a**, a yellow crystalline material (Scheme 24). The solid state structure of **15a** revealed an agostic interaction between the Zr center and the lower β -H on the unsubstituted β -carbon [Zr(1)-H(21B) 2.38(2) Å, Figure 9]. When a single crystal of **15a** was dissolved in C_6D_6 , it immediately appeared as two interconverting species by NMR (Figure 10), in the same manner as a single crystal of **14** appeared as two species. After standing at RT for 15 min, the solution began to turn from a light yellow to dark brown and by ^1H -NMR the appearance of two new species was observed (Figure 11).

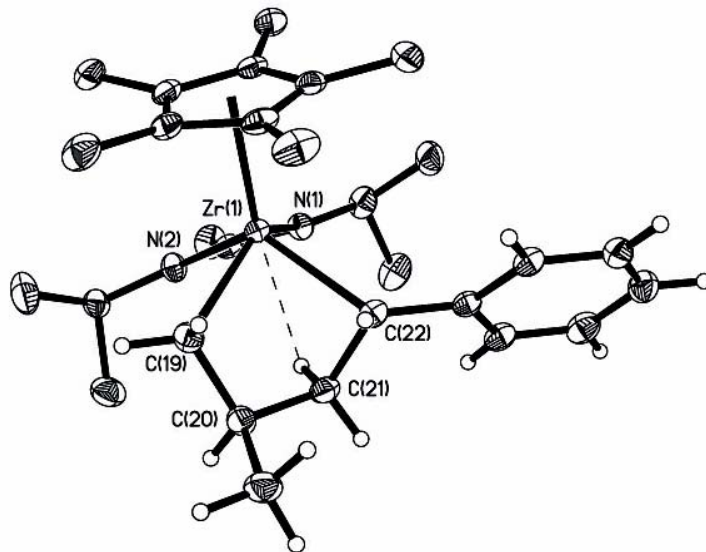


Figure 9 Solid state structure of **15a** with 30% probability ellipsoids; all but the metallocycle hydrogens have been omitted for clarity.

Zr(1) – C(19)	2.296(2)	C(19) – C(20)	1.511(3)
Zr(1) – C(22)	2.326(2)	C(20) – C(21)	1.545(3)
Zr(1) – H(21)B	2.38(2)	C(21) – C(22)	1.529(3)

Table 4 Selected bond distances for **15a** in angstroms (Å)

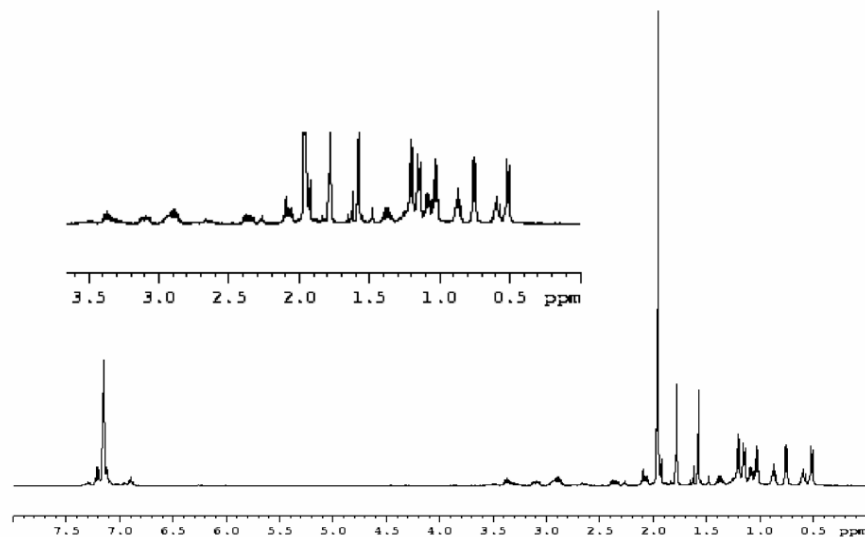


Figure 10 $^1\text{H-NMR}$ spectrum of crystals of **15a** at RT in C_6D_6

As can be seen in Figure 11, one of these was identified as the corresponding $\text{C}_\beta\text{-C}_\beta'$ unsaturated butadiene (zirconacyclopent-3-ene) complex **16a**, and the other can be identified by its characteristic resonance at (3.8 ppm) as being a zirconanorbornadiene product **17**, the initial synthesis of which from the reaction of **12** with H_2 has been reported and its reaction with H_2 is shown in Scheme 23 (vide infra).⁷⁷

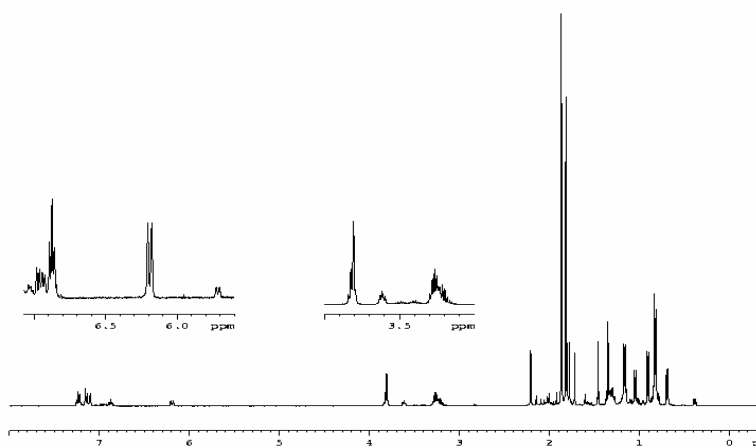
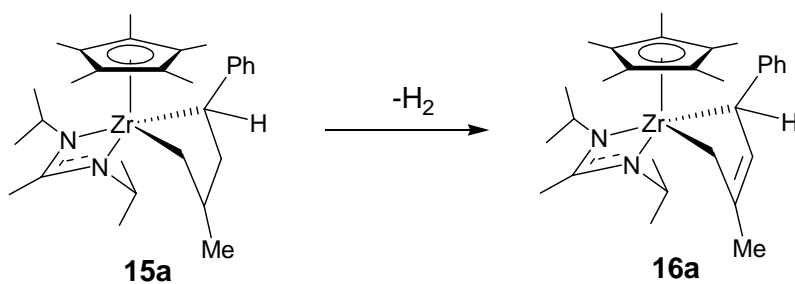


Figure 11 $^1\text{H-NMR}$ in C_6D_6 of the product of decomposition of **15a** after overnight at RT to produce **16a** and **17**

The production of **17** likely occurred due to H₂ that was present in solution after it formed as a byproduct of **15a** converting to **16a** (Scheme 25). **16a** was isolated in a 28% yield and its solid state structure was determined by X-ray crystallography, confirming that it has lost an equivalent of H₂ and has become a Cp*Zr butadiene complex, with the plane of the butadiene at a 98° angle with the plane of the Zr-C_α bonds, yet it appears from its solid state structure that **16a** still retains some metallocyclopentene character, with the C_β-C_{β'} bond being shorter than the other C-C bonds in the metallocycle (Figure 12 and Table 5).



Scheme 25 Decomposition of **15a** yields **16a**

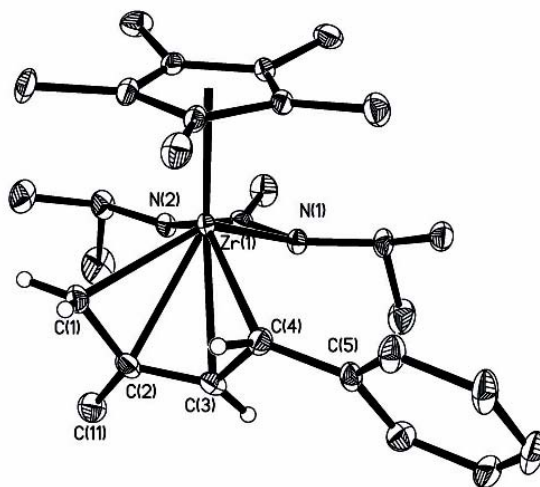


Figure 12 Solid state structure of **16a** with 30% probability ellipsoids; all but the metallocycle hydrogens have been omitted for clarity

Zr(1) – C(1)	2.347(5)	Zr(1) – C(2)	2.497(5)
Zr(1) – C(3)	2.497(5)	Zr(1) – C(3)	2.377(5)
C(1) – C(2)	1.454(8)	C(2) – C(3)	1.376(7)
C(3) – C(4)	1.463(7)	C(4) – C(5)	1.471(7)

Table 5 Selected bond distances for **16a** in angstroms (Å)

3.1.5 Styrene Insertion

Compound **12** was dissolved in neat styrene at RT, and the solution color changed from dark green to a light brown. The solution was then placed under high vacuum for 5h at RT to remove the residual styrene. During the procedure yellow crystalline material formed from the crude oil. The crude material was dissolved in Et₂O and recrystallized at –30°C providing **15'b** as a dark yellow-orange crystalline product in an 82% yield (Figure 13).

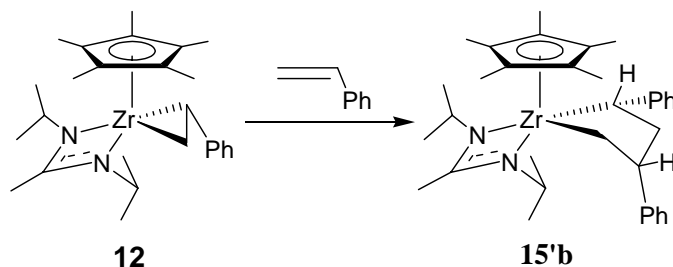


Figure 13 Styrene insertion into **12** yields **15'b**

The crystalline material was characterized by X-ray crystallography and **15'b** was shown to have an unremarkable solid state structure with all normal single bond distances around the zirconacyclopentane ring (Figure 14 and Table 6). This is the very thing that is notable about **15'b**, this its crystal structure unequivocally showing that all of the zirconacycle C-C bonds are about 1.52 Å in length, whereas the only other known structure of a diphenyl substituted zirconacyclopentane published by Rosenthal has a C_β-C'_β length of 1.34 Å, with the authors asserting that it is saturated ring.⁸⁴

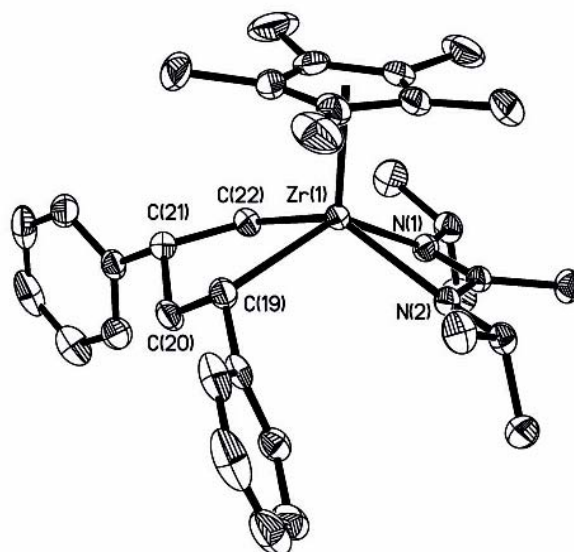


Figure 14 Solid state structure of **15'b** with 30% probability ellipsoids; hydrogens omitted for clarity

Zr(1) – C(19)	2.375(2)	C(19) – C(20)	1.540(3)
Zr(1) – C(22)	2.292(2)	C(20) – C(21)	1.516(3)
		C(21) – C(22)	1.538(3)

Table 6 Selected bond distances for **16a** in angstroms (Å)

The notation for the styrene product **15'b** is changed from the propene insertion product **15a** because the stereochemistry of **15'b** is the opposite of **15a**. The Ph group in the β -position in **15'b** that resulted from the insertion of styrene is *cis* to the α -Ph substituent, whereas the Me group that was the result of propene insertion in **15a** is *trans* to the Ph substituent. Hence, the “prime” notation will connote a *syn* stereochemistry, as **15'b** will be designated as *syn* as related to the Ph group, and **15a** will be designated as *anti*.

The $^1\text{H-NMR}$ of a single crystal of **15'b** shows a second isomer similar to the behavior observed for **15a** (Figure 15). Based on investigations by Negishi and by Takahashi into the organic chemistry of zirconacyclopentane rearrangements from the

cleavage of the $C_{\beta}-C'_{\beta}$ zirconacyclopentane bond and more recently by Rosenthal into the organometallic chemistry of substituted zirconacyclopentanes, it can be inferred that zirconacyclopentanes are fluxional species that are in equilibrium undergoing C-C bond cleavage to reform a bis-olefin complex.^{79,82,84-86} In the case of the bis-olefin complex, a different molecule of olefin or alkyne may displace one of the olefins forming a different zirconacycle, or the olefin may rotate to a lower energy conformer thereby isomerizing the ring.^{79,85-87}

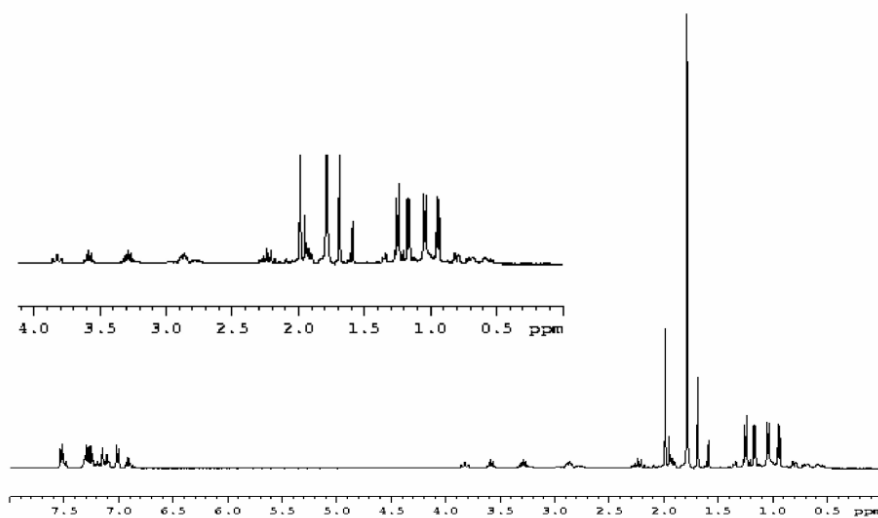


Figure 15 ¹H-NMR of **15'b** at RT in C₆D₆

Upon remaining in solution at RT for 15-20 minutes, a sample of **15'b** visibly changes to a darker color. This continues until the solution turns dark green. By ¹H-NMR it is evident that all three species: **12**, **15'b**, and styrene are present in the sample after 1h at RT confirming that the compound undergoes a deinsertion of styrene to produce **12** (Figure 16).

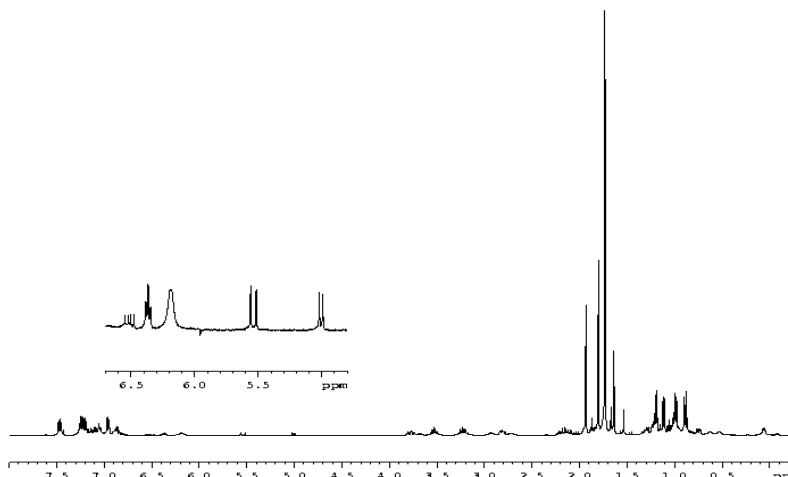
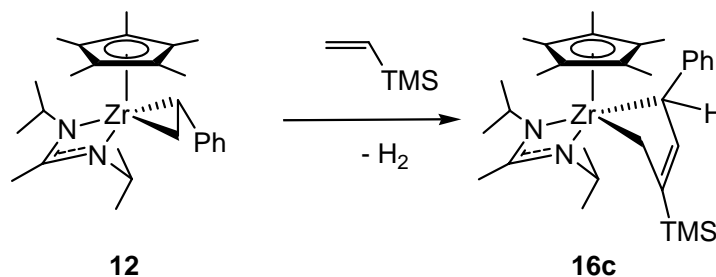


Figure 16 $^1\text{H-NMR}$ of **15'b** after 1 h at RT in C_6D_6

3.1.6 Vinyl-TMS Insertion

The addition of vinyl-TMS to **12** in pentane yields a violet compound **16c** (Scheme 26).



Scheme 26 The only pure product isolated from reaction of **12** with vinyl-TMS is **16c**

The crystalline yield of **16c** from this reaction after several harvests by concentrating the successive mother liquors is 31% with respect to zirconium. The product is a violet-purple compound and appears as a single isomer by $^1\text{H-NMR}$ (Figure 17).

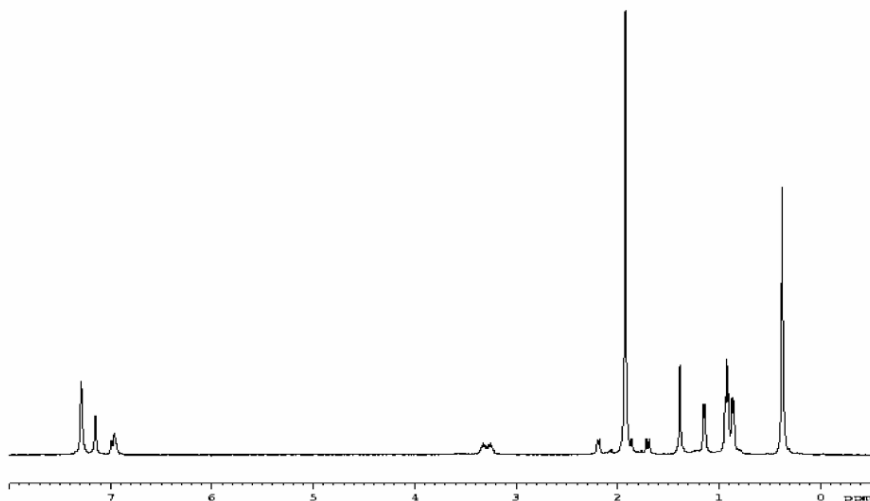


Figure 17 $^1\text{H-NMR}$ spectrum of **16c** in C_6D_6

An interesting aspect of this $^1\text{H-NMR}$ spectrum of **16c** is in the resonance frequencies of the unsaturated zirconacycle protons, which lie upfield of even the allyl region rather than the expected higher chemical shift. This is particularly noteworthy when compared to the methyl analog **16a**, which shows the deshielded vinyl resonance at 6.2 ppm. Without structural information, one would predict this to be a saturated compound, but just as for **16a**, the bond lengths and locations of hydrogens in the crystal structure of **16c** prove that this ring is, in fact, unsaturated (Figure 18 and Table 7).

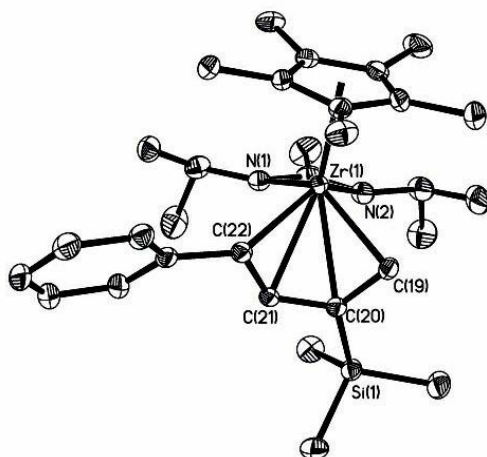


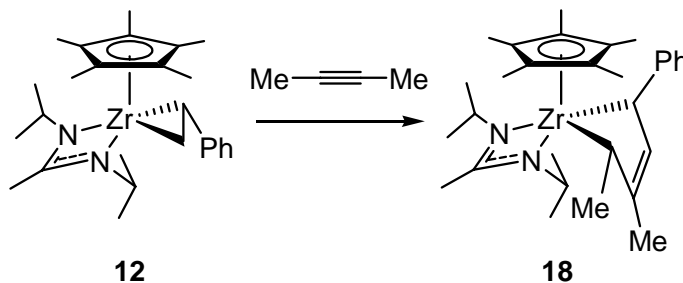
Figure 18 Solid state structure of **16c** with 30% probability ellipsoids; hydrogens omitted for clarity

Zr(1) – C(19)	2.295(2)	C(19) – C(20)	1.464(3)
Zr(1) – C(20)	2.485(2)	C(20) – C(21)	1.378(3)
Zr(1) – C(21)	2.486(2)	C(21) – C(22)	1.432(3)
Zr(1) – C(22)	2.422(2)	C(21) – C(22)	1.477(3)

Table 7 Selected bond distances for **16c** in angstroms (Å)

Any attempts to isolate the saturated zirconacyclopentane **15c**, which is the logical intermediate precursor to **16c**, were fruitless, presumably due to its instability.

3.1.7 2-Butyne Insertion



Scheme 27 The product of reaction of **12** with 2-butyne is Cp*ZA butadiene complex **18**

When 2-butene is mixed with **12**, stoichiometrically, or in excess, the reaction proceeds to change color from dark green to purple-violet overnight. This reaction proceeds nearly quantitatively in the presence of only one equivalent of 2-butyne in 18h (Scheme 27). It is significantly faster in the presence of excess 2-butyne. Upon removal of volatiles **18** is isolated as a violet crystalline solid by recrystallizing the solid residues from Et₂O at -30°C. The solid state structure of **18** reveals that it is not the direct product of 2-butyne insertion into **12**, but it is rather the isomer of a formal 1,3 hydride shift on the zirconacyclopent-3-ene ring (Figure 19 and Table 8).

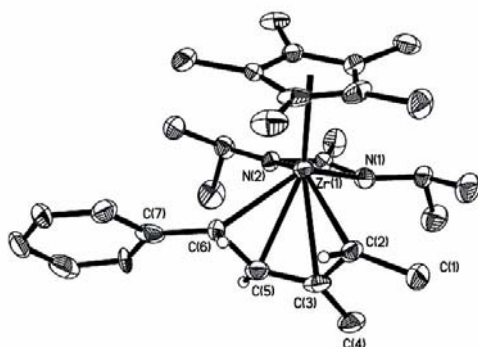


Figure 19 Solid state structure of **18** with 30% probability ellipsoids; hydrogens omitted for clarity

Zr(1) – C(2)	2.388(4)	C(2) – C(3)	1.453(5)
Zr(1) – C(3)	2.507(4)	C(3) – C(5)	1.381(5)
Zr(1) – C(5)	2.442(4)	C(5) – C(6)	1.449(5)
Zr(1) – C(6)	2.376(4)	C(6) – C(7)	1.472(5)

Table 8 Selected bond distances for **18** in angstroms (Å)

By ¹H-NMR it is apparent that the resultant product is a mixture of two isomers (Figure 20), similar to that of **16a**. A 2D-EXSY spectrum showed clear exchange peaks between the two isomers (Figure 21).

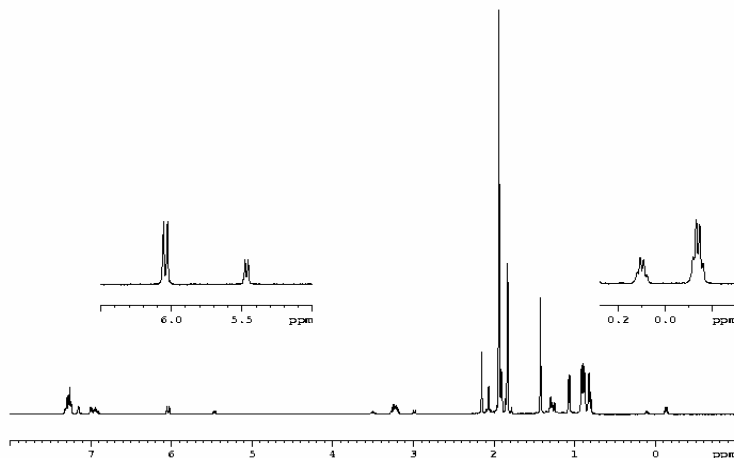


Figure 20 $^1\text{H-NMR}$ of **18** at RT in C_6D_6

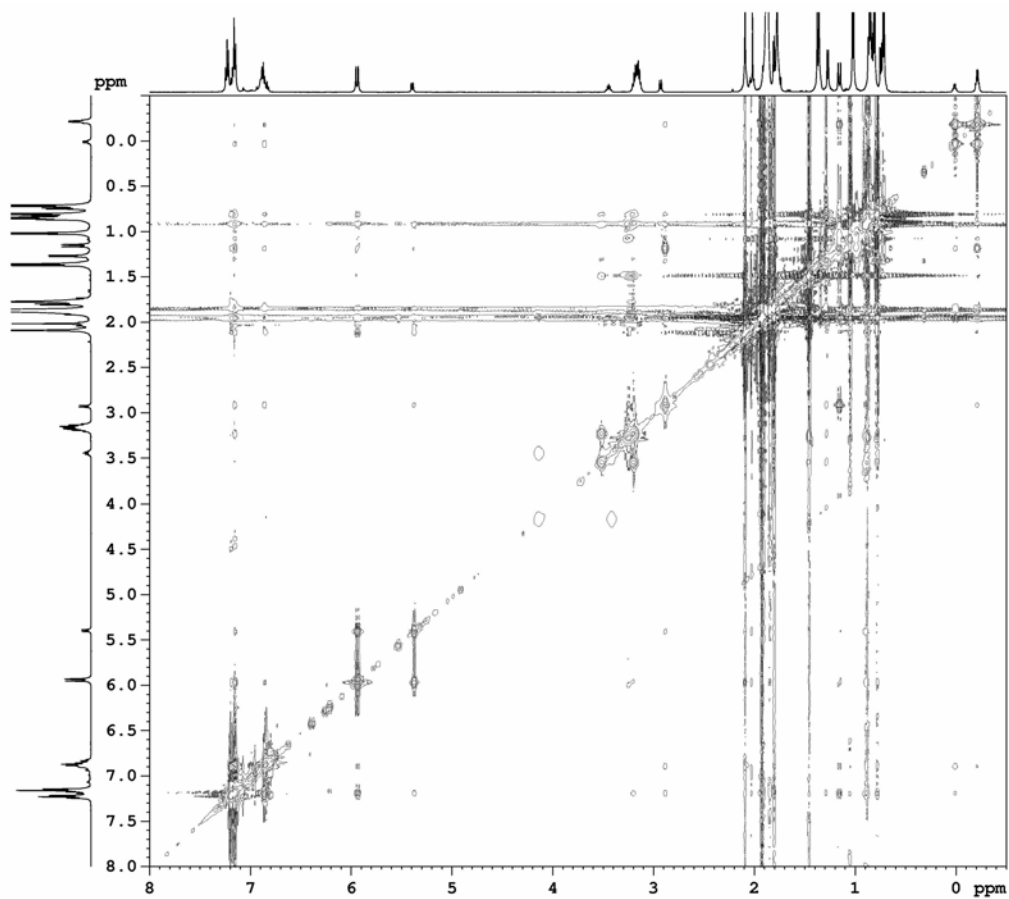
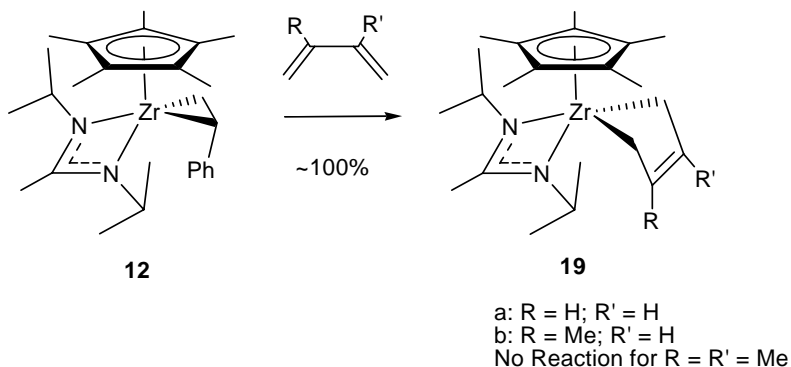


Figure 21 EXSY (800ms mixing time) of **18**; Bruker 500MHz spectrometer at RT in C_6D_6

3.2 Oxidative Addition To The η^2 -Styrene Cp*ZA

3.4.1 Oxidative Addition of 1,3-Butadienes

Unlike the alkene and alkyne chemistry described above, 1,3-butadienes do not undergo cycloinsertions with **12**; instead a displacement of the styrene by the 1,3-butadiene occurs to form a zirconacyclopent-3-ene (**18b,c**, Scheme 28).



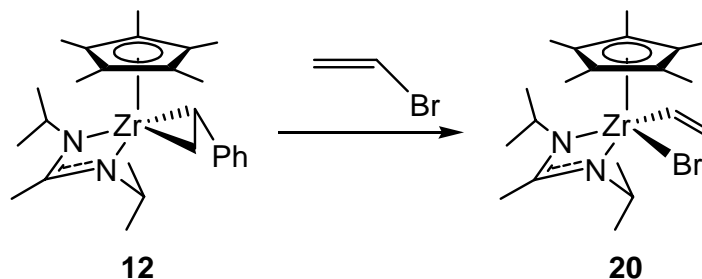
Scheme 28 Oxidative addition of butadienes to a formal Zr(II) to form **19b,c**

An important result of reactions of various 1,3-butadienes with **12** was that unsubstituted 1,3-butadiene, and 2-methyl-1,3-butadiene both react readily to form **19a** and **19b**, while 2,3-dimethyl-1,3-butadiene is unreactive toward **12** even at 60°C. This result, when viewed together with the unsuccessful attempts of reacting *cis*- and *trans*-2-butene with **12**, which were inert up to 60°C, shows that the steric environment of **12** is constrained, and can only accommodate α -olefin substrates.

3.4.2 Vinyl Bromide Oxidative Addition

The attempted insertion of vinyl bromide into **12** yielded a surprising result and produced yet another example of **12** behaving like an η^2 -olefin Zr(II) complex, which

preferentially undergoes oxidative addition, versus the insertion chemistry or the earlier reported σ -bond metathesis processes,⁷⁷ where it behaves more like a zirconacyclopropane (Scheme 29).



Scheme 29 Vinyl bromide reaction with **12** to produce **20**

The solid state structure of compound **20** was ascertained by single crystal diffractometry (see Figure 22).

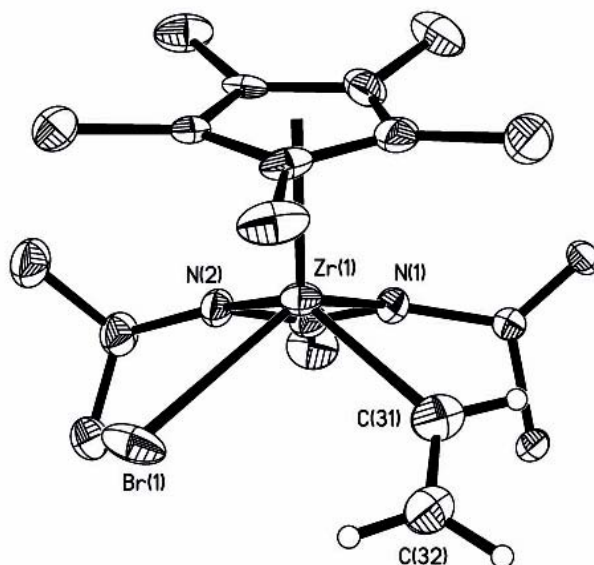


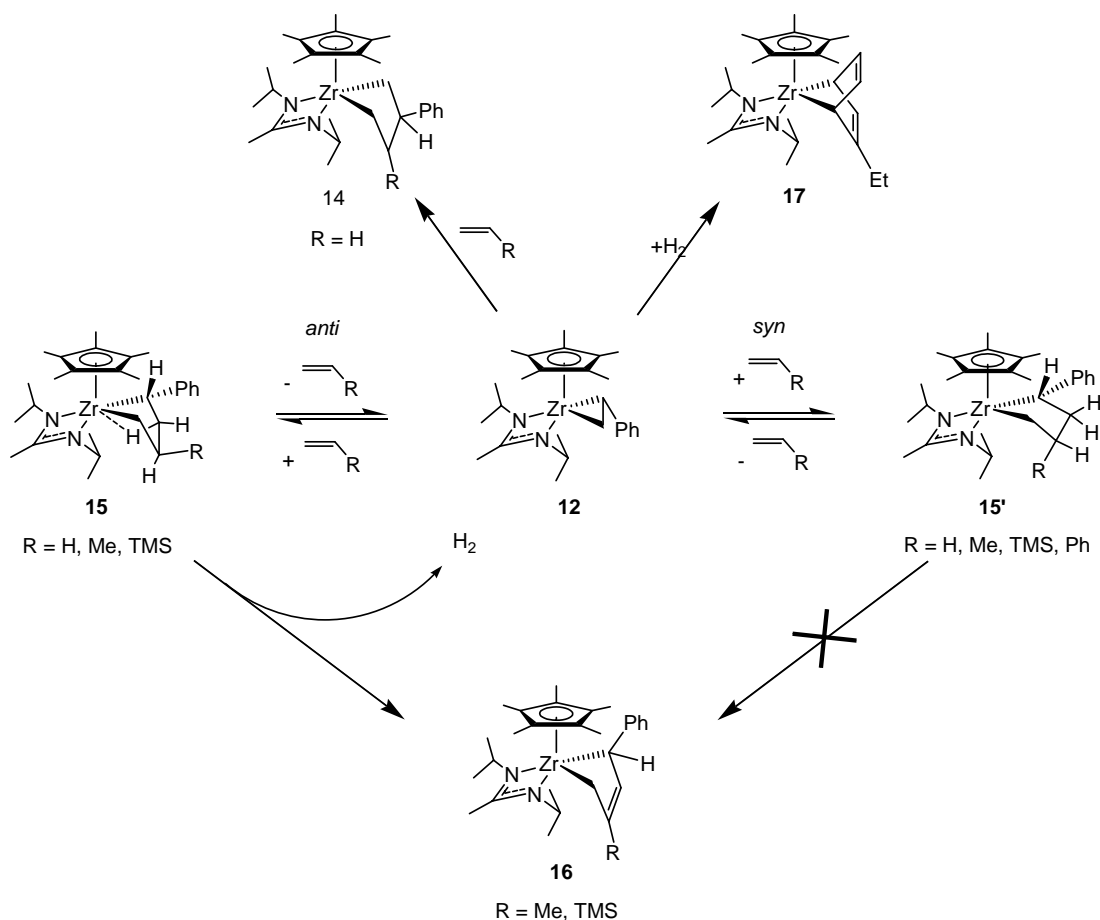
Figure 22 Solid state structure of **20**

It is noteworthy, that **20** is a rare example of a vinyl zirconium species, and to the best of our knowledge, it is only the second example of a solid state structure of such a species,

after the structure of the chloro 1-methylvinyl bis-tertbutylzirconocene reported by Takahashi and coworkers in 1995.⁸⁸ One major difference observed between the two structures is the C=C bond shortening to 1.250(5) Å in **20**, versus the 1.342(6) Å in the Takahashi structure. The only precedent from literature for a vinyl complex C=C bond shortening was reported by Gambrotta and coworkers, where an deficient calyx-pyrrole Sm-vinyl complex exhibited a C=C bond distance of 1.209(16), which is significantly shorter than the C=C bond length in **20**. What the samarium complex and **20** have in common is probably electron deficiency. Therefore the C=C bond shortening is probably attributable to a σ electron withdrawing effect. This evidence shows the relative electron deficiency of the Cp*ZAs relative to zirconocenes, for example , as compared to Takahashi's zirconocene, which yet again highlights the paradox of Cp*ZA alkyl complexes having greater β -H stability than zirconocene alkyl complexes.⁸⁸

3.5 Mechanistic Discussion of Alkene and Alkyne Coupling with the η^2 -Styrene Cp*ZA

3.5.1 Unified Explanation For The Styrene Cp*ZA Complex Reactivity With Alkenes



Scheme 30 Proposed reaction scheme for observed reactivity of **12** with α -olefins

When all the gathered data are carefully reviewed, it is possible to begin to see patterns in the reactivity of **12**, which are not readily apparent from any single reaction, but each reaction fits into Scheme 30 as though pieces of a puzzle. However, based on all the pieces of the puzzle it is possible to reconstruct the mechanisms of the reaction pathways to explain the variety of products observed using the various substrates to react

with **12**. Scheme 30 outlines the patterns of reactivity for **12** with ethene, propene, styrene and vinyl-TMS. The following discussion will attempt to explain how each piece of the puzzle fits into the grand scheme of this reactivity, and the general logic of how Scheme 30 was constructed.

3.5.2 Mechanistic Discussion of Insertion of Ethene

From the zirconacyclopentane products **14**, **15a**, and **15'b** of insertion of olefins into zirconacyclopropane **12** (Figure 23), which show different regio- and stereo-selectivities for the insertion, it is evident that both steric and electronic aspects are at play in deciding the regio- and stereo-selectivity of the final ring product.

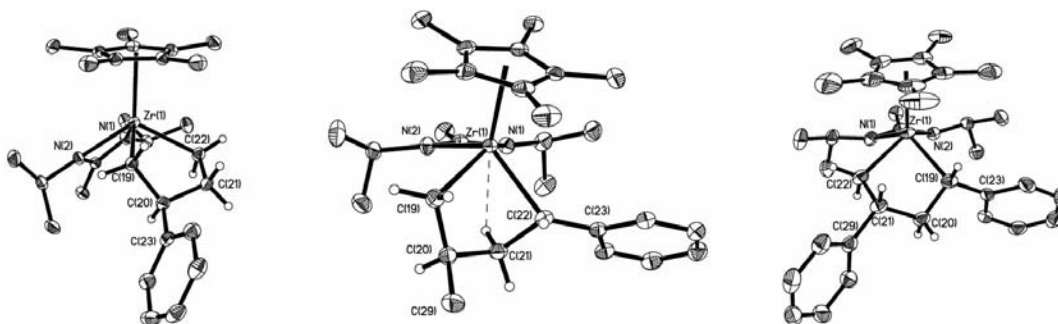


Figure 23 Solid state structures of **13**, **15a**, **15'b**

Of note is the regioselectivity of the ethene insertion, which produces **14** by inserting on the substituted, and therefore more sterically hindered, side of zirconacyclopropane **12**. This is most likely governed by the ability of the unsubstituted, and therefore smaller, ethene to coordinate on that side of the zirconacyclopropane **12**. In this case the formation of product **14** is probably controlled by the alleviation of steric strain with the phenyl substituent appearing in the β position in the product.

This process, however, is not as simple as just a matter of immediate steric control forcing the phenyl group into the β position. It is a more likely scenario that the insertion can take place on both faces of the zirconacyclopropane. It is also likely that the reaction on the less hindered side does occur at an even faster rate than the insertion on the more hindered side. However, the phenyl group placed in the α -position seems to have a destabilizing effect on zirconacyclopentanes, as observed with the instability of **15a**, **15'b**, and the never isolated, but likely, intermediate **15c**. By $^1\text{H-NMR}$ we observed a fluxional quality to the molecule. This fluxionality is also exhibited by the presence of two species in the $^1\text{H-NMR}$ of compounds **14**, **15a** and **15'b**; presumably, one is the zirconacyclopentane observed in the solid state, and the other is likely the deinserted *bis*-olefin complex intermediate. Once a deinsertion takes place and the *bis*-olefin complex intermediate is in solution with a large amount of ethene, which can eventually coordinate on the other side of the styrene and produce the more stable product. If this is true, then the reaction of **12** with ethene is under thermodynamic control, with **14** being the energy-well toward which eventually all products are shunted, accounting for why **14** was the only isolated product.

Another interesting observation worth considering is that there is the absence of a Ph group in the α position for **13** and **14**, which may account for the increased thermal stability of these compounds as compared to **15a**, **15'b**, and **15c**. This could be attributed to both steric and electronic effects of the large and electron rich Ph being close to the metal center.

3.5.3 Mechanistic Discussion of Insertion of Propene

By looking at **15a**, **15'b**, and **16c** the products of propene, styrene, and vinyl-TMS insertion into zirconacyclopropane **12**, and by taking into account the results of ethene insertion, it is possible to conclude that the added steric bulk of any substituent on the olefin, other than a hydrogen, disallows the insertion to occur on the more substituted side of **12**. Another interesting aspect of this chemistry is the preference of the methyl group in the propene insertion product **15a** to be pointing up, as seen in its solid state structure.

The reason for isolation of only the *syn*-insertion product **15'b** is probably that the phenyl group in the β position would simply be too large to coordinate in an *anti* fashion to **12** due to significant interference with Cp*, however, the Me group of the propene is just small enough that its steric interactions with the Cp* ligand are cancelled out by the stabilization energy of the transannular agostic interaction with a β -H, as seen in the solid state structure of **15a** (Figure 9), which makes the *trans*-inserted propene product just stable enough to isolate at lower temperatures. This is also supported by the instability of the intermediate **15c**, which was never isolated, presumably due to the large steric bulk of the TMS substituent producing significantly larger steric strain, and therefore a β -H agostic interaction, such as the one seen for **15a** would not be enough to compensate for that steric stress increasing the energy of the zirconacyclopentane intermediate **15c**.

The mechanism of the decomposition of **15a** to **16a** will be discussed in section 3.5.6.

3.5.4 Mechanistic Discussion of Insertion of Styrene

A reasonable explanation for the isolation of styrene *syn*-insertion product **15'b** as opposed to the *anti* isomer, lies in that the Ph group on the styrene is sterically large and due to its π -conjugation with the olefin the barrier of rotation about the Ph group bond to the olefin is high. This makes styrene a relatively rigid monomer and its insertion into **12** can only be accommodated in the *syn* conformation with the styrene Ph group “tucked” underneath the metal center. Both this steric bulk, as well as the π -conjugation probably account for a high barrier to insertion, and can explain why **15'b** had to be prepared in neat styrene utilizing L'Chatelier's principle to push the reaction toward formation of **15'b**. By the principle of microscopic reversibility, the styrene deinsertion must go through the same high energy TS[‡], which is why it was kinetically trapped and stable enough to have been isolated.

The deinsertion of styrene from **15'b** gives an important clue as to the possible existence of *syn* insertion products of propene and vinyl-TMS insertion, **15'a** and **15'c**, respectively, which presumably have not only lower barriers to deinsertion, but also have more stable isomers in **15a** and **16c** shunting the various reaction equilibria.

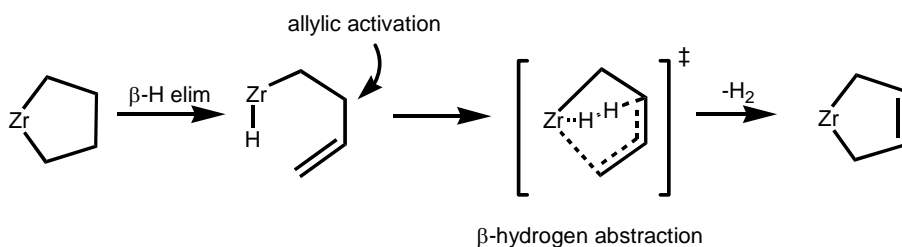
3.5.5 Mechanistic Discussion of Insertion of Vinyl-TMS

For the cycloinsertion of vinyl-TMS, the zirconacyclopentane **15c** was never isolated, and its instability likely stems from the steric interactions between the large TMS group and the Cp* ligand on zirconium, which cancel out any stabilization that could have been gained via a transannular β -H agostic, as was the case with **15a**.

3.5.6 Mechanistic Discussion of Decomposition of 15 to 16

An important aspect to examine for the explanation of the derivation of Scheme 30 is the unprecedented conversion of compounds **15a** and **15c** to **16a** and **16c**, respectively, with loss of H₂. Notably, an analogous transformation did not occur in the case of **15'b**, which is likely due to the steric bulk of the β-Ph substituent preventing any interaction with the β-H on the neighboring carbon.

There are two key observations that can shed light on the possible pathway for the transformation of **15** to **16**. The first is the transannular β-H agostic found in the solid state structure of **15a**. According to the traditional view of agostic interactions, **15a** is a stunted TS[‡] for the transannular β-H elimination. The second important piece of evidence supporting the β-H elimination mechanism is that the direct product of such a process would be a Cp*ZA hydrido butenyl intermediate (Scheme 31), and would be analogous to the methyl butenyl Cp*ZA **9**, which was shown to produce the Cp*ZA butadiene **10a**. These observations are highly suggestive that the transformation from **9** to **10a** shares similar mechanistic aspects with the transformation of **15a,c** to **16a,c**.



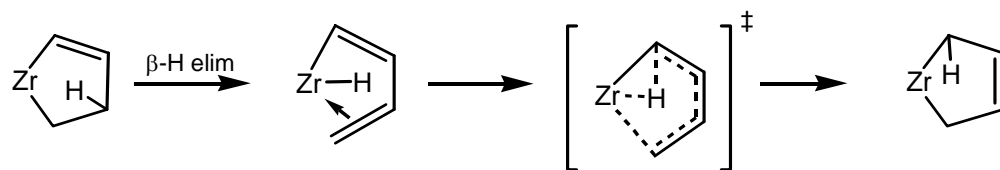
Scheme 31 Proposed mechanism of decomposition of **15** to **16**

3.5.7 2-Butyne Insertion and Rearrangement

The reaction of 2-butyne with **12** produces **18** in a nearly quantitative yield with just one equivalent of 2-butyne. These results are in sharp contrast with the attempted insertion of *cis*- and *trans*-2-butene into **12**, which did not yield insertion products even at 45psi of butane and elevated temperatures. These observations suggest that it may not be the steric hindrance of but rather the fast deinsertion of 2-butenes that are to blame. As was suggested for the insertion of ethene, it is possible that the insertion occurs with 2-butene, however, the equilibrium lies heavily to the side of starting materials, and the product is never isolated. With ethene it was another story, since **14**, the product of the insertion of ethene into **12** on the more substituted side is very stable. 2-Butene is significantly larger than ethene, and cannot insert on the more hindered side of the zirconacyclopentane **12**, hence there were no isolable insertion products.

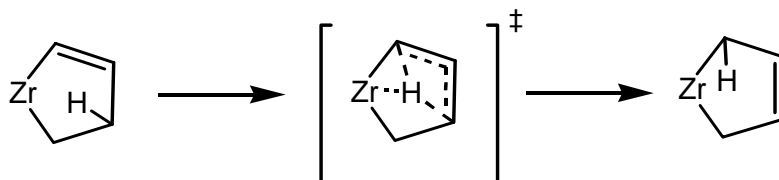
Though the reactions of **12** with 2-butene did not yield isolable products, the reaction of **12** with 2-butyne yielded **18**. As already mentioned, **18** is not the direct product of the insertion of 2-butyne into **12**, but is rather the product of a secondary rearrangement via a formal migration of a hydride. The rearrangement from the initial insertion product to make the butadiene Cp*ZA **18** served to trap the butadiene disallowing its deinsertion and shedding light on the dynamic processes underlying these transformations. This H-shift is a novel transformation, and to the best of our knowledge has never before been reported in literature, since the general reactivity of olefin complexes of zirconocene and its derivatives yields the direct insertion product zirconacyclopent-2-enes.⁴⁵

The driving force for this process is yet again the thermodynamic stabilization of the neutral homoaromaticity of the product. The question stands as to what type of mechanism leads to the observed product. Unlike the transformation of **15** to **16** with elimination of H₂, involving 2 Hs, the rearrangement to produce **18** involves the movement of a single H atom from a β position to an α position on the zirconacycle, in turn changing the position of the double bond from 2 to 3, and producing the Cp*ZA butadiene **18**. This process can potentially happen via 2 possible pathways, in a similar fashion to the transformation of **15** to **16**. The first is a stepwise process of an initial β-H elimination, followed by a cyclic 6-membered TS[‡] leading to the final product, which is depicted in Scheme 32.



Scheme 32 Stepwise mechanism for formation of **18**

The second possible mechanism for this transformation is a concerted process, which is best depicted as a zirconium-mediated transannular hydride shift, as shown in Scheme 33.

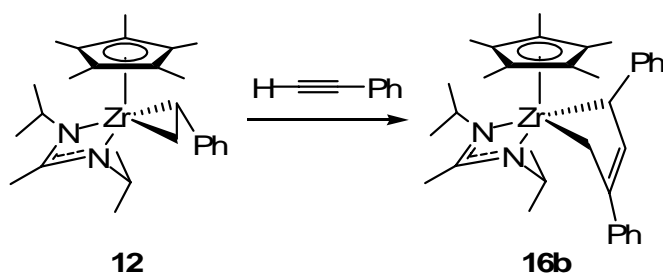


Scheme 33 Proposed concerted mechanism for formation of **18**

This type of TS[‡] state is not unprecedented, and similar TS[‡]s have been considered for butene elimination from metallocyclopentanes in olefin oligomerization processes.^{89,90}

There is no evidence in support of one process over the other, and possibly the only good way to get an idea on whether the step-wise or the concerted process is the true reaction pathway is via DFT calculations to map out the relative energies of all the TS[‡]s and intermediates.

This rearrangement also sheds light on another interesting transformation published recently. As reported, it is the formation of **16b**, but from the formal insertion of phenylacetylene into **12**, probably followed by the same H-shift rearrangement observed in formation of **18** (Scheme 34, Appendix).⁷⁷



Scheme 34 Synthesis of **16b** from insertion of PhCCH into **12**

3.6 Conclusions About The Chemistry Of The Styrene Cp*ZA

In the course of this study the mechanistic details the reactivity of zirconacyclopropane **12** with α -olefin substrates bearing various substituents have been elucidated (Scheme 30). It was found that depending on the mode of insertion, the resultant products have varying degrees of stability. Some of these are stable zirconacyclopentanes, as in the case of unsubstituted **13**. In another instance the product zirconacyclopentane reverts back to zirconacyclopropane **12**, such as the case of **15'b**, and presumably it's so with all olefin insertions which bind **12** via the *syn* binding mode. In yet another decomposition mode, some of the zirconacyclopentanes actually eliminate H₂ to form a Cp*ZA butadiene, as in the case of conversion of **15a,c** to **16a,c**, respectively.

It was shown that all these products were the result of differentiation in the initial insertion step. The ethene insertion product **14** is more stable than **15a,b,c** due to the lack of a phenyl group in the α -position on the zirconacycle, which is the product of ethene insertion on the more substituted side of the zirconacyclopropane **12**. Insertion on that side of the ring only occurs in the case of ethene, presumably due to greater steric demands of any substituted olefin.

Compound **15a** was the only *trans* insertion product characterized by X-ray crystallography, which is probably due to the stabilizing effect of the β -H agostic interaction found in its solid state structure.

An 2D-EXSY experiment shows ¹H-NMR exchange peaks between the two species that are present in the spectrum of **15'b**. It is likely that the second species is the

bis-olefin deinsertion intermediate, which has been shown to exist in the work of Takahashi and Rosenthal.

Not only was the origin of the varying regio- and stereoselectivities of the insertion explained, but also the mechanistic aspects of the decomposition pathways were studied via synthesis of compound **9** as a model for the intermediate of the decomposition of **15a,c** to **16a,c**. It was shown that compound **9** cleanly decomposes to Cp*ZA butadiene complex **10a** and in the process liberates CH₄. These observations coupled with the β-H agostic found in the solid state structure of **15a** further support the assertion that substituted Cp*ZA zirconacyclopentanes undergo β-H elimination to form a hydrido butenyl intermediate, which then eliminates H₂ and produces the isolated Cp*ZA butadiene complexes **16a,c**. The presence of byproduct H₂ was supported by the production of the zirconanorbornadiene **17**, as shown by the decomposition of **15a** when followed by ¹H-NMR.

Furthermore, the insertion of 2-butyne into **12** and then its subsequent rearrangement to **18** was a novel transformation, which reinforced the notion that the homoaromaticity of products as a strong thermodynamic driving force for the decomposition and rearrangement of zirconacyclopentanes and zirconacyclopent-2-enes to zirconacyclopent-3-enes.^{70,91}

All the observations and analyses paint the Cp*ZA scaffold as a novel system producing zirconacyclopentanes with a significant gain in stability over zirconocene based systems. The zirconacyclopentanes that were isolated and studied shed new light on various decomposition pathways available to metallocyclopentanes, and potentially have given us a new model system to study the decomposition of metallocyclopentanes in

the context of olefin oligomerization. It is now clear that the steric environment of the inner sphere, the relative electron deficiency of the complex, and the various substituents on the metallocyclopentane ring affect the stability of the metallocycle significantly, and as in the case of the Cp* acetamidinate system, can produce a large variety of novel chemistry.

Though there is no realistic potential for a Cp*ZA-based catalytic olefin oligomerization, this study has given us a significant amount of information elucidating the factors involved in decomposition of metallocyclopentane rings. This can potentially be used in designing a finely tuned olefin oligomerization catalyst with not only regio- and stereo-control, but also of a set number of monomer units. As already mentioned in the introduction to this chapter, several systems are known to dimerize and trimerize ethene, as well as other α -olefins. The object of this study was to shed light on the possible factors involved in the mechanism of control over these processes, and that goal has been achieved.

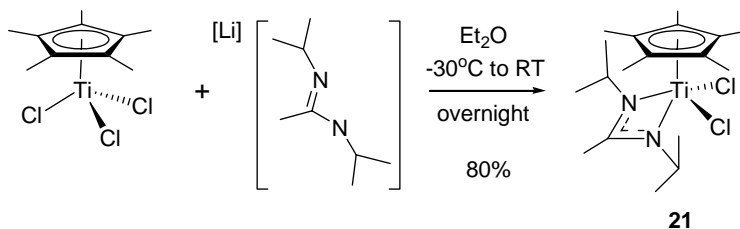
Chapter 4: Pentamethylcyclopentadienyl Acetamidinate Titanium Chemistry

4.1 Titanium In Ziegler-Natta Polymerization and Olefin Oligomerization

Recently there have been other exciting discoveries in the field of Ti organometallic chemistry outside the Ziegler-Natta catalysis realm, such as the recently reported Ti-based ethylene trimerization catalyst by the Teuben group.^{53,55} The pursuit of Ti-based Cp* acetamidinate chemistry was undertaken considering the known higher stability of metallocene titanocyclopentanes, as compared to zirconacyclopentanes, combined with the recent successes with isolation of a stable Cp*ZA η^2 -styrene complex **12** and the studies of its olefin insertion product zirconacyclopentanes (Chapter 3).⁷² It has been found by Whitesides and coworkers that α -alkyl substitutions bearing β -Hs of bis-Cp titanocyclopentanes allows for new β -H eliminations pathways.⁷² Isolation and studies of substituted titanocyclopentanes as well as a comparison of Cp*ZA versus the Ti analog chemistry were the original intentions of pursuing Cp* acetamidinate titanium chemistry, which could potentially have given a better understanding of the nature of reactivity of these generally unstable species, in the same manner that was found for the series of zirconacyclopentanes **13**, **14**, **15a**, and **15'b**.

4.2 Exploration of Titanium Synthesis and Reactivity

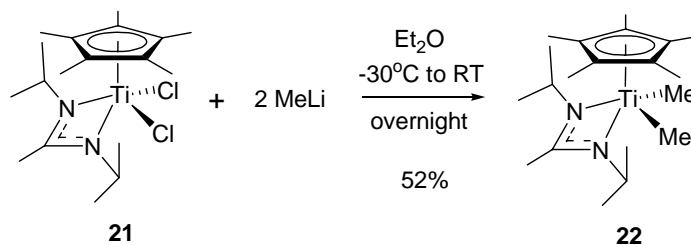
4.2.1 Synthesis of $\text{Cp}^*\text{TiCl}_2[\text{iPrNC}(\text{Me})\text{N}^{\text{iPr}}]$



Scheme 35 The synthesis of **21**

The synthesis of $\text{Cp}^*\text{TiCl}_2[\text{iPrNC}(\text{Me})\text{N}^{\text{iPr}}]$ (**21**) is carried out under the same conditions as the synthesis of its zirconium analog Cp^*ZA dichloride **1**, by starting with Cp^*TiCl_3 and reacting it with $[\text{Li}][\text{iPrNC}(\text{Me})\text{N}^{\text{iPr}}]$ that is generated *in situ* from 1,3-diisopropylcarbodiimide and MeLi (Scheme 35). Compound **21** was isolated as dark crystals with a green hue in 80% yield. The ^1H -NMR spectrum of **21** is similar to that of the previously obtained Cp^*ZA dichloride **1** and is otherwise unremarkable.

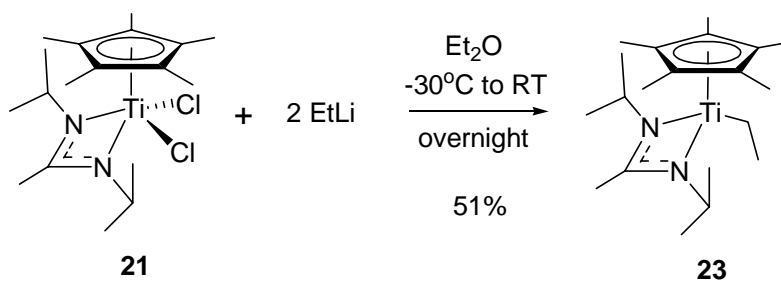
4.2.2 Alkylation of $\text{Cp}^*[\text{iPrN}(\text{Me})\text{N}^{\text{iPr}}]\text{TiCl}_2$ With MeLi



Scheme 36 Synthesis of **22** via methylation of **21**

The alkylation of **1** with two equivalents of MeLi was carried out in Et_2O and yielded 52% of red crystalline product **2** (Scheme 36). The identity and purity of **22** were confirmed by ^1H - and ^{13}C -NMR spectroscopy.

4.2.3 Alkylation of Cp*^[iPrN(Me)N^{iPr}]TiCl₂ With EtLi



Scheme 37 Synthesis of **23** from **21**

In contrast to methylation of **21** with MeLi, the alkylation of **21** with two equivalents of EtLi yielded a considerable surprise (Scheme 37). More specifically, the initial intent of the reaction was to produce a diethyl complex of Ti, which would undergo a β -H abstraction to form a titanocyclopropane complex, then forming a titanocyclopentane under ethene, which would be similar to the formation of the unsubstituted zirconacyclopentane **13** (vide supra).

The ¹H-NMR spectrum of the product **23** was obtained showing two very broad signals with one having a peak width spanning roughly 600 Hz centered at a chemical shift of 3.26 ppm, and the other spanning roughly 1400 Hz centered at 6.45 ppm. This suggested the presence of a paramagnetic species, presumably a Ti(III) complex. The structure of **23** was solved via single crystal X-ray diffraction, and it was confirmed to be the Cp*^[iPrN(Me)N^{iPr}]TiEt complex (Figure 24).

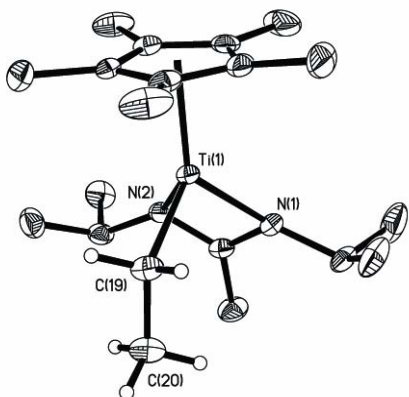
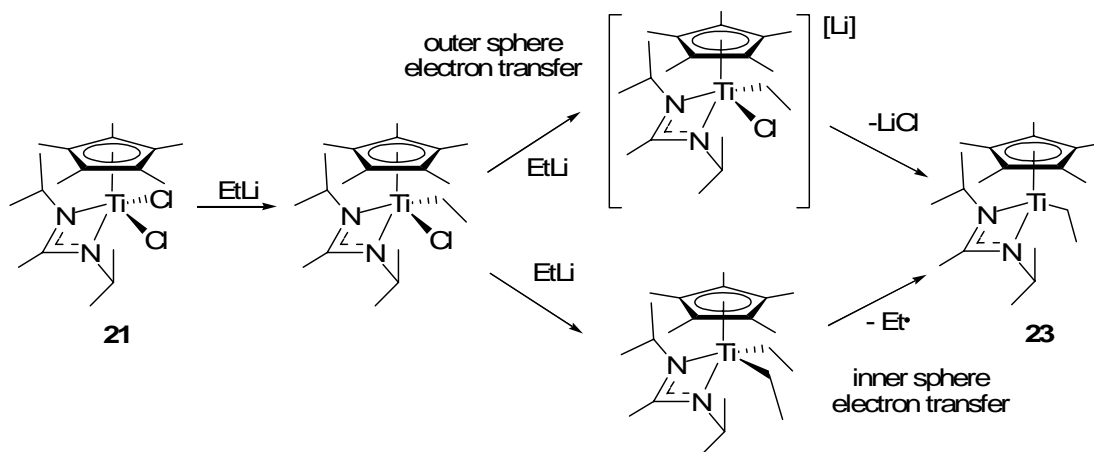


Figure 24 Solid state structure of **23** with 30% ellipsoids; all but ethyl hydrogens have been omitted for clarity

It follows that Scheme 37 accurately portrays the net result for the synthesis of **23**, with one of the ethyl lithium equivalents substituting a chloride and the other equivalent of ethyl lithium reducing the metal. The true nature of this reaction has not been investigated further, and it is difficult to say whether this is an example of an inner sphere or an outer sphere electron transfer, although based on the encumbered sterics one would in theory favor the latter.

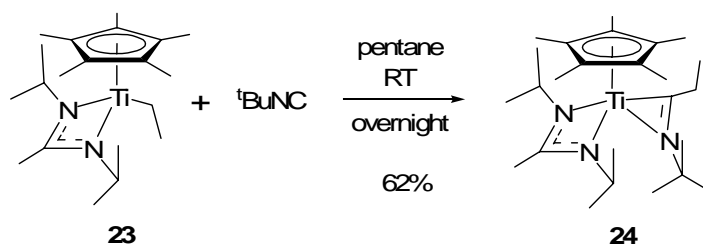
The first question that comes to mind from the above observation is what is the reason for the electron transfer reactivity? The same reaction using the Cp*ZA dichloride **1** (as discussed in chapter 2) yielded a zirconacyclopropane that was trapped with ethene to give the unsubstituted zirconacyclopentane **13**. In the case of Ti, it seems it is more favorable for one of the EtLi equivalents to effect an outer sphere electron transfer reaction to the metal than to substitute a Cl (Scheme 38). One possibility is that an outer sphere electron transfer would be a kinetically controlled process resulting from the greater steric demands for the titanium complex, as compared to the zirconium, disallowing the alkylide anion from approaching the metal. However, since there is no

evidence regarding the electron transfer pathway, there is another way to look at this result from the point of view that **23** is a thermodynamic product, with the electron transfer being the result of alleviation of steric strain on the Ti by decreasing the coordinative saturation of the complex with an inner sphere electron transfer process (Scheme 38).



Scheme 38 The possible e^- transfer pathways for the formation of **23**

4.2.4 Insertion Of ${}^t\text{BuNC}$ Into $\text{Cp}^*[\text{iPrNC}(\text{Me})\text{N}^i\text{Pr}]\text{Ti}(\text{III})\text{Et}$



Scheme 39 Synthesis of **24** via insertion of ${}^t\text{BuNC}$ into T-C bond of **23**

In order to explore the synthetic utility of **23**, its reactivity with ${}^t\text{BuNC}$ was examined. ${}^t\text{BuNC}$ is known to readily insert into early TM-alkyl bonds, and upon reacting with **3** gives the η^2 -iminoacyl insertion product **24** in a 62% crystalline yield (Scheme 39). Initially the ${}^1\text{H-NMR}$ of **24** was used to show that it is indeed different from the starting

material **3**. The structure of **24** was then verified by single crystal X-ray diffraction (Figure 25).

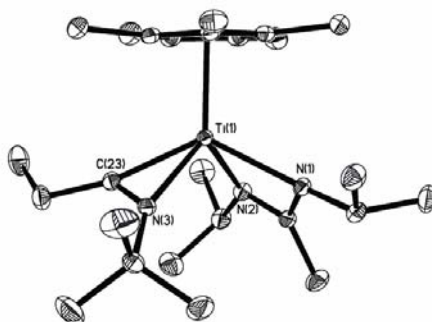


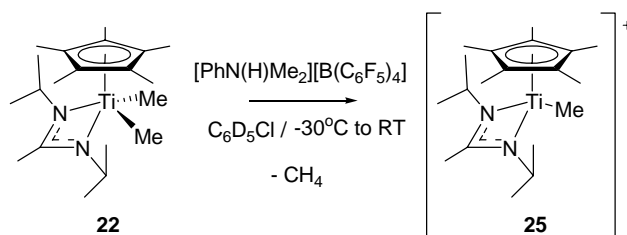
Figure 25 Solid state structure of **4** with 30% ellipsoids; hydrogens omitted for clarity

The solid state structure of **24** is remarkable in the unsymmetrical binding of the η^2 -iminoacyl ligand to the metal. Presumably due to steric interactions the *tert*-butyl group on the iminoacyl nitrogen is forced downwards, which in turn forces the iminoacyl carbon and its ethyl substituent upward. This demonstrates the tight coordination sphere around the metal center, and assuming that the initial step of the ^tBuNC insertion process is its coordination to **23**, this reactivity shows that the titanium ligand sphere can at least accommodate the coordination of a σ -donor ligand with a small cone angle such as ^tBuNC.

4.2.5 Generation Of Cp*[iPrNC(Me)NiPr]Ti(IV)Me Cation

The living stereospecific Ziegler-Natta polymerization of α -olefins by [Cp*[EtNC(Me)N^tBu]ZrMe][B(C₆F₅)₄] was reported in 2000, and currently this system remains the benchmark for stereospecificity and livingness for Ziegler-Natta polymerization of propene as well as higher α -olefins.¹ It is known that titanium based

Ziegler-Natta initiators possess higher activity than zirconium systems, hence **22** was used as precatalyst to test for polymerization activity of the titanium(IV) methyl cation **25**, to compare its activity to the original Cp*ZA cationic Ziegler-Natta system.



Scheme 40 Protonation of **22** to make cationic **25**

Before testing its polymerization activity **25** was generated in situ on NMR scale in order to directly observe the cation. The standard method of protonation of a methyl group on the precatalyst with $[\text{PhN}(\text{H})\text{Me}_2][\text{B}(\text{C}_6\text{F}_5)_4]$ was used to generate **25** with methane leaving (Scheme 40). Although the integration of the ^1H -NMR spectrum at RT was in agreement with the predicted structure of **25**, it revealed a significant broadening of all the signals on the cation, with the remaining aniline signal exhibiting a normal line-width. This suggests that the normal dynamic processes of Cp* and alkyl group rotation **25** undergoes at RT may have been slowed by steric congestion near the metal, but eliminated the possibility of the formation of the dimethyl bridging dication, which is known to occur in the analogous Cp*ZA Ziegler-Natta system,⁴ since the methyl resonance for **25** was also significantly broadened. Another logical explanation is a collapse of the cation ligand sphere so close to the metal center that all dynamic processes have been slowed on an NMR timescale even at RT. The severe shortening of the Ti-ligand bonds would also explain the lack of reactivity of **25** with ethene at 60 psi ethene pressure.

4.3 Conclusions About Cp* Acetamidinate Titanium Chemistry

Although the alkylation of **21** with EtLi did not yield the intended Negishi-like chemistry, it has instead yielded Ti(III) ethyl complex **23**, giving the first known crystal structure of a Ti(III) alkyl species bearing β -Hs. The Teuben group⁹² has extensively explored bis-Cp Ti(III) chemistry, and has reported decamethyltitanocene(III) alkyls, which were shown to undergo various modes of decomposition even at low temperatures. Other known compounds of Ti(III) that have been reported include phosphoylide, μ -oxo dimer, hydride and tetrahydroborate, as well as allyl complexes, just to name a few.⁹³⁻¹⁰³ The amount of Ti(III) chemistry that has been carried makes it all the more interesting that stable Ti(III) alkyl compounds with β -Hs have never before been isolated, and underscore the unique nature of **23**.

The question as to why this type of electron transfer reactivity is observed is difficult to approach using the evidence that has been collected so far. One may be tempted to speculate as to the steric environment around the metal center being crowded, and the reduction of the metal relieving the steric strain. It is certainly reasonable, considering the relative strength of Ti-Cl bonds in **21**, versus the much weaker Ti-C bond strength. However, to conclusively find what driving forces govern the reduction more investigations must be carried out into mechanism of the electron transfer.

Chapter 5: Exploration of Cp*TaXn[iPrNC(Me)N*i*Pr] Chemistry (X= Cl, H, Alkyl, Alkylidene)

5.1 Brief Overview of Pertinent Tantalum Chemistry

Schrock's earlier studies that were fundamental in developing olefin metathesis, included the discovery of the first known olefin oligomerization (dimerization) catalyst based on tantalum.^{13,14,47} As mentioned in Chapter 3, since then other Ta, Cr and Ti selective olefin trimerization systems have been reported, and these are thought to proceed via successive olefin insertions/ring expansions of metallocycles, with the final products formed from β -H eliminations as permitted by metallocyclopentane or metallocycloheptane ring sterics for dimerization or trimerization, respectively, then followed by reductive elimination to form the product olefin and regenerate the active metal catalyst to which another equivalent of olefin can coordinate to reinitiate the oligomerization process.^{49,51-54,56-59} Since evidence exists for the β -H agostic interaction from the investigations of Cp* acetamidinate Zr metallocyclopentane chemistry in support of theoretical calculations,^{89,90} investigations into Cp* acetamidinate tantalum chemistry were undertaken to ascertain the ability of the Cp* acetamidinate ligand set to stabilize tantalocycles.

Over the years several sporadic reports of Ta-based MAO-activated Ziegler-Natta polymerization systems also have surfaced, but no follow-up work with well defined initiators and fully characterized mechanistic investigations has been published for any of these systems, suggesting a certain difficulty in finding the actual active species responsible for the Ziegler-Natta catalysis in Ta systems.¹⁰⁴⁻¹⁰⁹ In 1997 Antonelli and

coworkers¹¹⁰ reported the polymerization of ethylene with a Ta allyl catalyst which upon activation with trityl tetrakis(perfluorophenyl)borate or with tris(perfluorophenyl)borane produced polyethylene, but once again, there have been no follow-up studies published on this system since. One report regarding the chemistry of Cp* acetamidinate tantalum complexes was published by the Meyer group in 1999.¹⁰⁴ The polymerization of ethene was found to occur when the Cp* acetamidinate tantalum trichloride (**26**) was activated by MAO. Though MAO-activated polymerization of ethene with **26** was successful, attempts to generate a well defined and fully characterized cationic initiator using this ligand system with Ta failed, as it was reported by the Meyer group¹⁰⁴ that **26** could be alkylated via reaction with an excess of MeMgCl, which yielded the trimethyl complex **27**, however, both B(C₆F₅)₃ and [H(OEt₂)₂][B(3,5-(CF₃)₂C₆H₃)₄] were used to activate **27** *in situ* and no polymer activity was observed from this type of activation, suggesting that the active species is not a Ta(V) dialkyl cation, but rather another species which is the product of the reaction of **27** with MAO.

The report by Meyer and co-workers¹⁰⁴ was intriguing for several reasons, including that the traditional research efforts in Cp* acetamidinate Zr chemistry have concentrated in the past on the development of living stereospecific polymerization of α -olefins in the Sita group.^{1,3-9,11,12,40,41,43,111-116} Considering the unprecedented β -H stability of the Cp* amidinate group 4 alkyl complexes of Zr and Ti, and the fruitful investigations into the synthesis and stability of Cp* amidinate zirconacyclopentanes, studies into the synthesis of Cp* amidinate tantalocycles were initiated and immediately yielded unprecedented results producing a great variety of species (*vide infra*) prompting further

investigations into the fundamental chemistry of Ta-alkyl species where Ta is present in the Ta(III), Ta(IV), and Ta(V) formal oxidation states.

5.2 Reactions of Cp*TaCl₃[ⁱPrNC(Me)NⁱPr] with Alkyl Lithiums

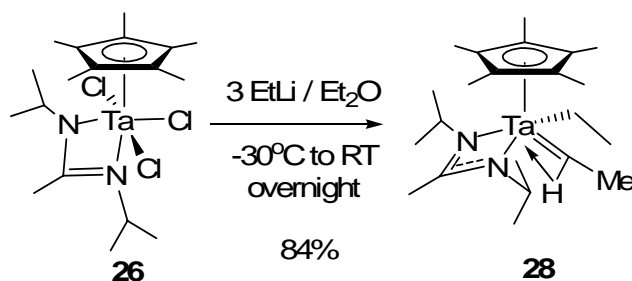
5.2.1 Reaction with 3 Equivalents of MeLi

The synthesis of Cp*TaMe₃[ⁱPrNC(Me)NⁱPr] (**27**) was originally reported along with the synthesis of **26**, however, in order to ascertain the reactivity of **26** with MeLi, the reaction was carried out in Et₂O starting at -30°C and allowed to warm to RT overnight, and **27** was isolated in low (22%) yield.¹⁰⁴ The identity of **27** was verified by comparison of its ¹H-NMR spectrum with the one reported in the literature.¹⁰⁴ For comparison, the original synthesis of **27** was carried out using 4 equivalents of MeMgCl and yielded the product **27** in a 60% yield. Our own efforts yielded **27** in a 96% yield from the reaction of **26** with 3 equivalents of MeMgI. The low yield of **27** from the reaction of **26** with MeLi suggests that there are possibly parasitic processes taking place other than the expected salt metathesis, producing a mixture of products.

5.2.2 Reaction with 3 Equivalents of EtLi

The salt metathesis reactivity of **26** with EtLi was the next logical step in the series of alkyl lithium reagents to examine. The major product of this reaction was the Ta(V) ethyl, ethylidene complex **28**, which was isolated in 84% crystalline yield (Scheme 41). The ¹H-NMR of **28** revealed that the compound possessed no plane of symmetry, and apart from the resonances corresponding to the Cp* and the amidinate ligands there were four other signals that were indicative of an ethyl and an ethylidene groups on the metal. It is reasonable to conclude that this compound formed via the well-accepted

mechanism for formation of early TM-alkylidene complexes that proceeds through α -H abstraction and the formation of alkane.¹¹⁷



Scheme 41 Synthesis of **28**

The unambiguous ¹H-NMR assignments for **28** were resolved via ¹H, ¹³C – HSQC, with the ethylidene α -H signal appearing at a chemical shift of 4.16 ppm in the ¹H-NMR spectrum and the α carbon resonance of the ethylidene appearing at 236.9 ppm in the ¹³C-NMR spectrum. The J-resolved-HSQC spectrum of **28** showed that the C _{α} -H coupling constant is 89 Hz, which is significantly smaller than the normal C-H coupling frequencies, which tend to lie in the 130-140 Hz range.¹¹⁷ This evidence shows the existence of a strong α -agostic interaction between the metal center and the α -H, and according to earlier published work conducted with tantalum alkylidenes, these chemical shifts and the very low C _{α} -H _{α} coupling constant are characteristic of a very strong α -agostic interaction and a highly electron deficient metal center.¹¹⁷

The solid state structure of **28** was obtained by single crystal X-ray diffraction confirming the NMR analysis and revealing more interesting structural features (Figure 1). Notably, **28** is the first isolated example of a Ta alkylidene species bearing β -Hs.

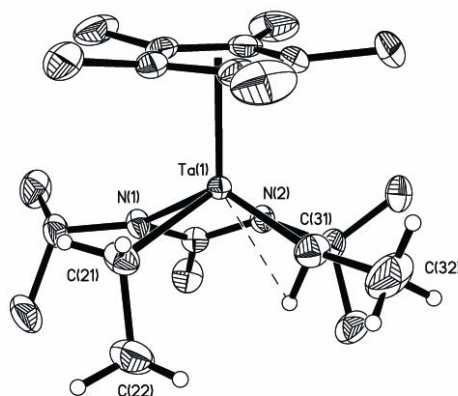


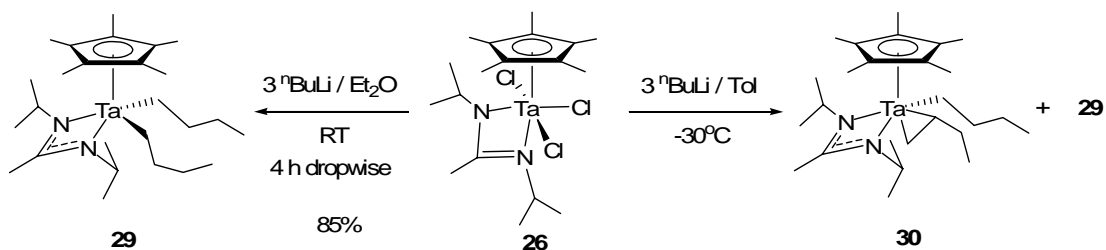
Figure 26 Solid state structure of **28** with 30% ellipsoids; Cp* and amidinate hydrogens have been omitted for clarity

Ta1 - C31	1.965(3) Å	Ta1 - C21	2.236(3) Å
Ta1 - N1	2.235(2) Å	Ta1 - N2	2.2044(19) Å
C32-C31-Ta1	161.5(3)°	C22-C21-Ta1	112.6(2)°

Table 9 Selected bond distances and bond angles for solid state structure of **28**

The important bond lengths and bond angles are listed in Table 9, however, a key structural aspect that was revealed and cannot be overlooked in a detailed structural analysis was the Ta-C_α-C_β bond angle for the ethylidene ligand, which was found to be 161.5°, hence emphasizing that the extent of the α-agostic interaction is significant enough to cause the C_α to be nearly *sp* hybridized. The electron deficiency of the metal was further revealed by the shortness of the Ta-C_α and the Ta1-H_α distances of 1.965(3) Å and 2.236(3) Å, respectively, which is within the normal range of other known tantalum alkylidene complexes.

5.2.2 Reaction with 3 Equivalents of ⁿBuLi



Scheme 42 Reaction of **26** with ⁿBuLi under varying conditions producing **29** and **30**

The reaction of **26** with ⁿBuLi is interesting because it reveals something germane about the potential wealth of results inherent for the chemistry of **26** and its derivatives. When the reaction of **26** with ⁿBuLi was carried out at -30°C in toluene there were two resultant products that were present in a 1:1 mixture (Scheme 42). The identity of the products was revealed only after the solid state structure was solved by single crystal X-ray diffractometry and the two compounds were found to co-crystallize in a 1:1 ratio with one another. One of these products was found to be the a(IV) dibutyl product **29**, which presumably forms when one the third equivalents of ⁿBuLi engages in an electron transfer reaction rather than substituting a chloride in a metathesis process. The other product of this reaction was found to be the Ta(III) butyl, η^2 -1-butene complex **30**, which most likely formed via a β -H abstraction process.¹⁹ However, when the same reaction was carried out at RT in Et₂O, and the ⁿBuLi solution was added drop-wise to the slurry of **26**, the reduction product **29** was formed exclusively in an 85% yield (Scheme 42). This suggests that the reduction product is kinetically favored, and it may be possible to synthesize the Ta(III) η^2 -1-butene complex **30** in pure by carrying out its synthesis at even lower temperatures.

5.2.3a Cp*Ta^{IV}Bu₂[ⁱPrNC(Me)NⁱPr]

The Ta(IV) dibutyl complex **29** is paramagnetic and there is no valuable structural information to discern from its ¹H-NMR spectrum, which manifests as two very broad peaks. The solid state structure of **29**, however, is interesting in that it is a Ta(IV) compound that is nearly isostructural with the previously published Cp*Zr^{IV}Bu₂[CyNC(Me)NCy] (Figure 27).¹¹⁸

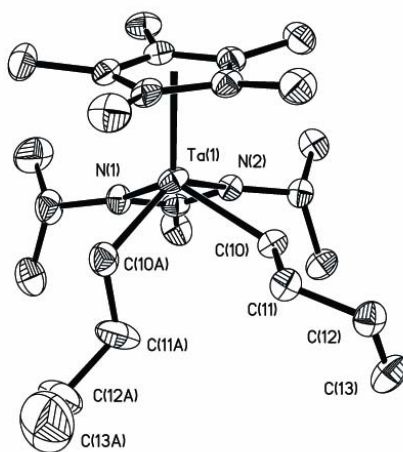


Figure 27 Solid state structure of **29** with 30% probability ellipsoids; hydrogens omitted from clarity

One of the results of isolating the variety of Cp* tantalum amidinate (Cp*TaA) complexes is the new ability to conduct a structural comparison of Ta(IV) *d*¹ complexes to the known isostructural *d*⁰ complexes of Zr(IV) and Hf(IV). Unfortunately there is a difference between the N-alkyl substituents on the amidinate between **29** and the published Zr(IV) dibutyl complex, and so it is important to try to discern the steric effects of the larger Cy groups from the electronic effects of the differing metals.

	Ta(IV) ⁿBu₂ (29)	Zr(IV) ⁿBu₂
M - N_a	2.1791(19) Å	2.262(3) Å
M - N_b	2.184(2) Å	2.305(3) Å
M - C_a	2.210(2) Å	2.288(4) Å
M - C_b	2.233(3) Å	2.269(3) Å
M - CENT	2.0895(9) Å	2.2519(19) Å

Table 10 Selected bond distances for **29** and its isostructural Zr(IV) analog

In Table 10 are listed the Ta-N and Ta-C bond lengths for both complex **29** and its Zr(IV) analog. The fact that the M-ligand bond distances for the Ta complex are significantly shorter than for the Zr complex is immediately apparent. One must take into account that third row TMs have smaller radii than the second row metals of the same group due to the Lanthanide contraction.¹¹⁹ However, the Lanthanide contraction has been found to produce roughly about a 0.02 Å decrease in bond length from Zr(IV) vs. Hf(IV) Cp* acetamidinate complexes.¹¹⁶ The bond length difference for the amidinate ligand in **29** and its Zr(IV) analog is approximately 0.11 Å for each M-N bond. Furthermore, the difference in the distance from the metal center to the Cp* centroid is 0.16 Å. Even taking into account that the amidinate is bulkier on Zr due to the N-Cy substituents it is possible that some of this bond length difference is the product of the extra steric bulk from the Cy groups on the Zr compound. However, there is also approximately a 0.06 Å difference in bond length for the Ta-C bonds of the two butyl substituents. For these ligands the steric bulk of two isopropyl groups in the Ta complex is similar to that of two cyclohexyl groups in the Zr compound, and therefore this difference in bond length to the butyl group carbons between the Ta and the Zr complexes is more due to electronics stemming directly from the differences in the metal centers.

A possible explanation as to why the Ta(IV) d^1 complex is more electron deficient than the Zr(IV) d^0 species can be related to the electron affinities of the metals, however, that explanation is unsatisfactory. The two metals are in the same oxidation state, and the complexes have the same exact ligands, so the actual difference lies in a more fundamental principle altogether; it must be the well known general periodic trend that atomic radii get smaller with each increasing atomic number due to the addition of a proton to the nucleus, which exerts a greater force on the inner shells of electrons thereby collapsing them. This general trend will be observed and its ramifications further explored for all Ta(IV) complexes for which isostructural Hf(IV) species exist for comparison (vide infra).

5.2.3b $\text{Cp}^*\text{Ta}^n\text{Bu}(\eta^2\text{-CH}_2\text{=CHCH}_2\text{CH}_3)[\text{PrNC}(\text{Me})\text{N}^i\text{Pr}]$

The second product of the low temperature reaction of **26** with 3 equiv of $^n\text{BuLi}$ in toluene was found to be the Ta(III) n-butyl, η^2 -1-butene complex **30**, which perhaps can also be described as a Ta(V) metallocyclopropane complex. From the $^1\text{H-NMR}$ spectrum of **30** it is evident that the metallocyclopropane hydrogens located on C10B with a chemical shift of 2.55 ppm are quite distinct from the hydrogen located on C11B, which is at a chemical shift of 3.92 ppm. Notably, all three of the metallocyclopropane hydrogens are in the allyl region of the $^1\text{H-NMR}$ spectrum.

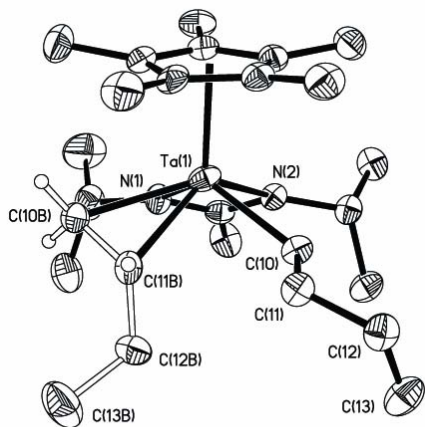
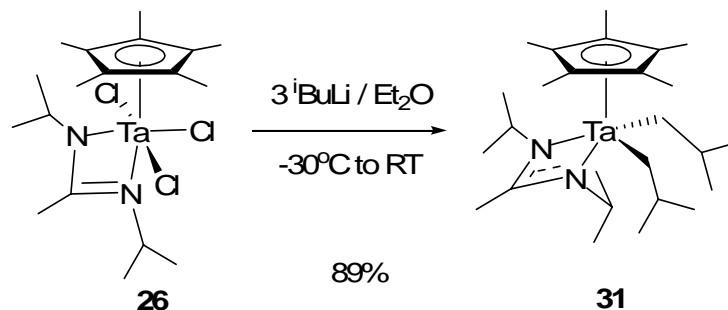


Figure 28 Solid state structure of **30** with 30% probability ellipsoids; all but the C10B and C11B hydrogens have been omitted for clarity

The solid state structure of **30** is more revealing of the nature of this compound, considering that the Ta1-C10B and Ta1-C11B bond distances are 2.404(9) Å and 2.347(15) Å, respectively (Figure 28). The length of these bonds suggests that the binding mode of the 1-butene ligand to the metal is closer to a π bonding mode.^{120,121} A relevant Cp* acetamidinate Zr(IV) η^2 -styrene complex **12** was recently reported in the literature, and in comparison the Zr-C bond distances of 2.28 Å and 2.30 Å observed for **12**, the Ta-C distances in **30** are significantly longer, especially considering that one would expect a bond distance contraction from Zr to Ta.⁷⁷ The comparison between **30** and the Zr(IV) η^2 -styrene complex **12** is imperfect for three reasons: 1) there are too many variables due to the metals being from different groups and periods, and the Ta having an odd electron count, 2) the coordination sphere around the metal is coordinatively, and therefore sterically, more congested for the Ta complex **30** due to an extra ligand, and 3) the styrene ligand is electronically different from the 1-butene ligand, and a case can be made that the Zr complex is η^3 rather than η^2 , with the phenyl ring carbon that is connected to the olefin having a distance of just 2.48 Å to the Zr.

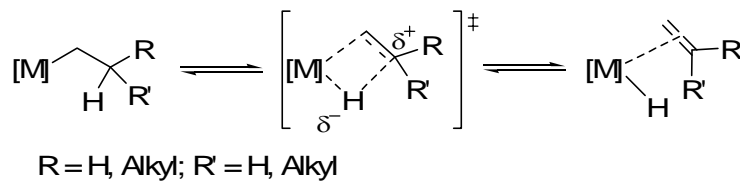
The chemistry of **30** is yet to be investigated, and here **30** is presented as only one piece of evidence to emphasize the special steric environment produced by the Cp* acetamidinate ligand set that alters the reactivity of the alkyl lithium reagents toward metal chlorides based on the size of the alkyl group (steric bulk) on the lithium reagent. This is due to the changes in the steric environment around the metal with each successive Cl→Alkyl exchange. So far this reactivity has been shown to produce a Ta(V) trimethyl with MeLi, a Ta(V) ethyl, ethylidene with EtLi, a Ta(V) butyl, η^2 -1-butene and a Ta(IV) bis-*n*-butyl with ⁿBuLi. Such an unprecedented variety of reactivity suggests that with more tuning by varying the amidinate substituents the affect the steric environment around the metal it may be possible to produce a great variety of Ta alkyl complexes for further study of Ta(III) olefin complex chemistry with ramifications for olefin oligomerization and maybe even C-H activation chemistry.

5.2.3 Reaction with 3 Equivalents of ⁱBuLi



Scheme 43 Reaction of **26** with ⁱBuLi to produce **31**

The reaction of **26** with 3 equivalents of ⁱBuLi was carried out in Et₂O by rapidly mixing the reactants at -25°C and allowing the reaction to stir at RT overnight. The Ta(IV) diisobutyl complex **31** was subsequently isolated in an 89% yield (Scheme 43). The relative stability of **31** alone is remarkable, since the isobutyl group β-H is on a tertiary carbon. During the a β-H elimination in early TMs, the TS[‡] polarization causes the C_β to bear much of the positive charge (Scheme 44). One would predict that the barrier for the β-H elimination process should be lowest for the isobutyl group as compared to other alkyls.



Scheme 44 Polarization of the TS[‡] during a β-H elimination

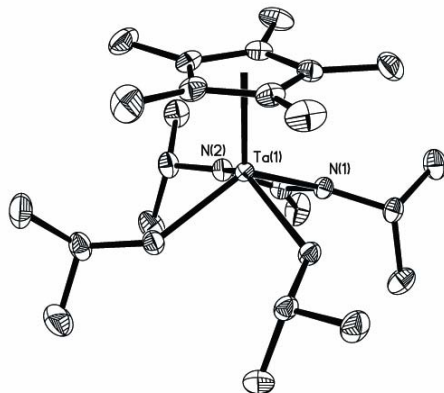


Figure 29 Solid state structure of **31** with 30% ellipsoids; hydrogens omitted for clarity.

The solid state structure of **31** was determined via single crystal X-ray diffraction (Figure 2). Similarly to the availability of a Zr(IV) analog of **29** for a structural comparison, there are also a Zr(IV) and a Hf(IV) analogs for **31** that have been reported.^{116,118} This allows a better comparison, since when comparing **29** to its Zr(IV) analog we could not eliminate the variable associated with the Lanthanide contraction, which slightly decreases the atomic radius of the third row TM, as compared to the second row TM of the same group.¹¹⁹ In this case, however, we can compare three species. The differences between the Zr and the Hf species show the Lanthanide contraction effect, and therefore, the differences between the Ta and the Hf species should only be due to the differences in electron deficiency between the Hf(IV) d^0 and the Ta(IV) d^1 metal centers.

	Ta(IV) ⁱBu₂	Hf(IV) ⁱBu₂	Zr(IV) ⁱBu₂
M-N_a	2.1807(14) Å	2.3248(12) Å	2.3113(15) Å
M-N_b	2.2028(14) Å	2.2003(12) Å	2.2471(16) Å
M-C_a	2.2538(17) Å	2.2801(14) Å	2.2702(19) Å
M-C_b	2.2025(18) Å	2.2733(15) Å	2.301(2) Å
M-CENT	2.0881(8) Å	2.2301(7) Å	2.2508(7) Å

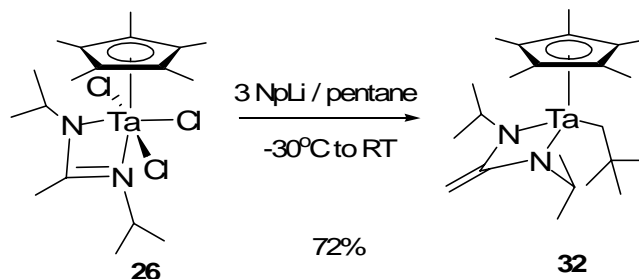
Table 11 Selected bond distances for **31** and its Zr(IV) and Hf(IV) isostructural analogs

Table 11 shows the list of pertinent bond distances for the Ta(IV), Zr(IV) and Hf(IV) diisobutyl complexes. The major difference between the Ta versus the two group 4 complexes is the difference in the M-N distances for the amidinate and the M-centroid distance for the Cp* ligand. The Ta was synthesized using N-isopropyl substituents, while the Zr and the Hf complexes have an ethyl and *tert*-butyl substituent, making them asymmetric. The difference between the two N-substituents on the amidinate causes the M-N bond lengths to be significantly different, while for the Ta complex they are more symmetric. However, the average distance of the two nitrogens to the metal is about 0.05 Å closer in the Ta complex than the Hf, even with the asymmetry of the amidinate ligands in mind. This is also true for the M-C bonds, where the Ta-C bonds are about 0.05 Å shorter than in both the Zr and the Hf complex. Furthermore, the difference in the distance of the centroid of the Cp* ligand to the metal is about 0.14 Å between the Ta and the Hf and even greater at about 0.16 Å between the Ta and Zr.

5.2.4 Reaction with 3 Equivalents of NpLi

With every iteration of reacting **26** with successively larger alkyl lithiums, as the steric bulk of the alkyl lithium reagents has increased the observed reactivity with **26** has changed and has given new products through yet another new process. This is true in case of NpLi as well, when it is reacted with **26**. So far the observed modes of reactivity have been 1) substitution of the Cl ligand with an alkyl group and 2) α hydride abstraction to form an alkylidene, 3) β -H abstraction to form a Ta(III) olefin complex, and 4) reductive electron transfer to the metal have been discussed. In case of NpLi there is yet another new mode of reactivity for **26** that has been revealed. Upon the reaction of 3 equiv. of

NpLi with **26**, the Ta(IV) bright green complex **32** was isolated in a 72% crystalline yield (Scheme 6).



Scheme 45 Synthesis of **32** via reaction of NpLi with **26**

7 is a paramagnetic compound and no useful structural information could be obtained from its NMR spectra. Its solid state structure was determined via single crystal X-ray diffraction verifying its identity as a Cp* amidinate Ta(IV) Np complex (Figure 30).

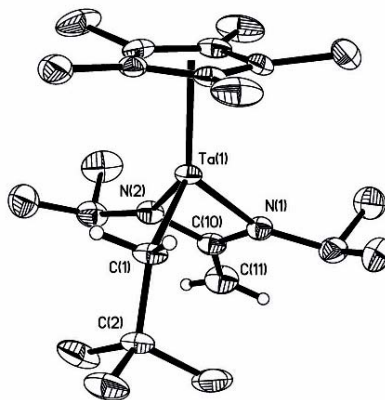


Figure 30 Solid state structure of **32** with 30% probability ellipsoids; all but the C(1) and C(11) hydrogens have been omitted for clarity

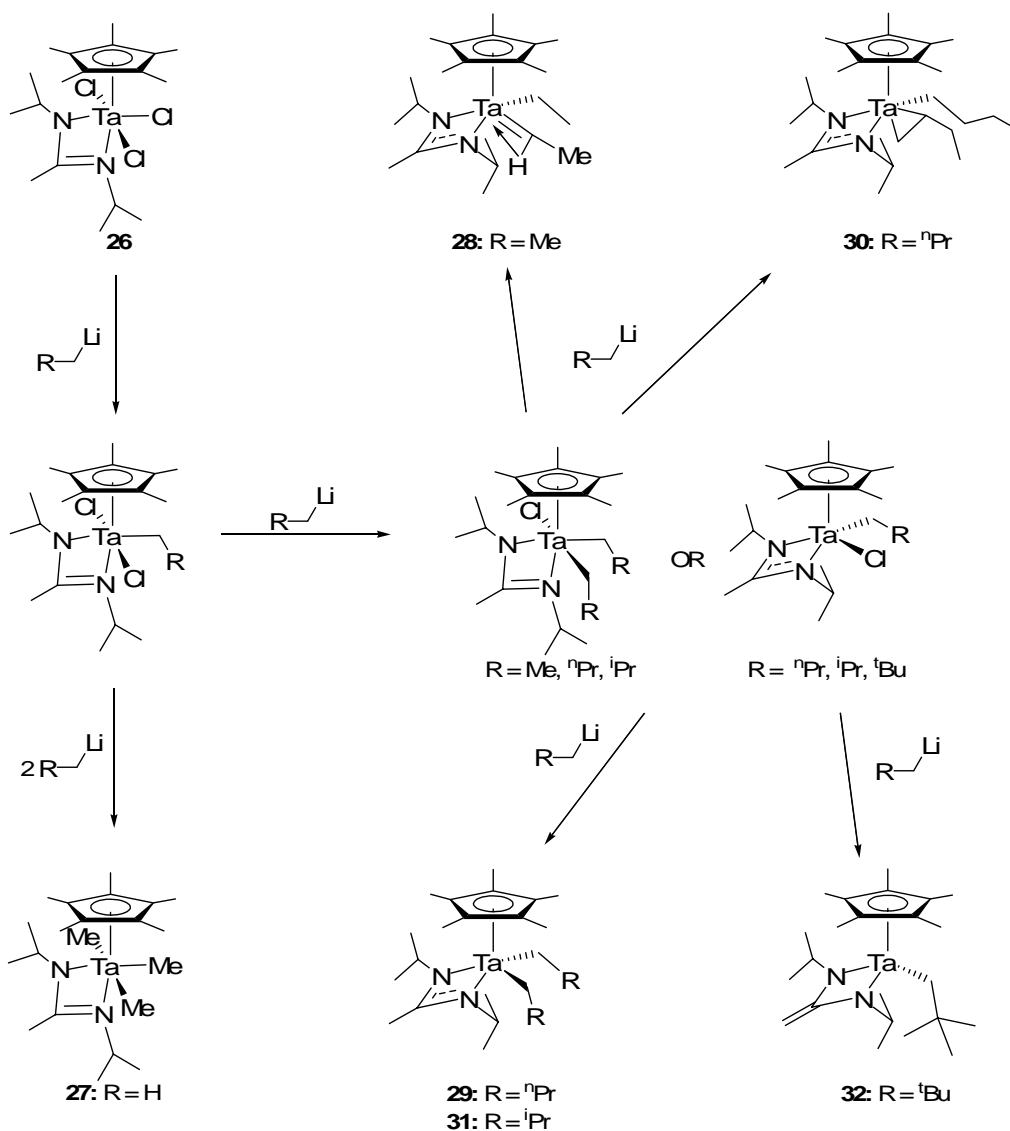
This revealed the reason for the uncharacteristically bright green color of this compound, as compared to the range of orange to brown colors for all other alkyl Cp* acetamidinate Ta complexes that had been isolated prior to the synthesis of **32**. Compound **32** was no

longer an acetamidinate complex, but in the process of reacting with NpLi the methyl group in the distal position on the amidinate was deprotonated producing this amidenamidate. This is also evident from the shortened M-N bond distances of 2.021(3) Å and 2.027(3) Å observed for **32**, which are in the range of a single covalent M-N bond, confirming that the amidenamidate is a -2 ligand.

The deprotonation of the distal position on the acetamidinate ligand has been previously observed with Cp* acetamidinate Zr compounds effected by a silyl lithium base.^{7,115} The mechanistic explanation for this reactivity, though not yet studied in detail, is similar to those proposed for the other two modes of reactivity with alkyl lithium salts, in that the steric characteristics of the base play a key role in directing via which pathway the reaction will proceed. In the case of NpLi following the initial substitution of a Np for a Cl ligand the complex is so sterically encumbered that the direct approach of the second NpLi is precluded, and an electron transfer to the metal occurs with elimination of LiCl, which is a process observed for the addition of the third equivalent of alkyl lithium reagent as earlier described for smaller alkyl lithium reagents (*vide supra*). At this point there is still a Ta(IV) alkyl chloride intermediate and another equivalent of NpLi in the reaction mixture, and due to the steric environment around the complex in combination with the bulky nature of the Np group, it acts as a base in this process, and deprotonates the distal methyl group and transforming the amidinate, which is a -1, 4e⁻ ligand, into a -2, 4e⁻ amidenamidate ligand.

5.2.5 Conclusions Regarding Reactivity of Cp*TaA Trichloride with Alkyl Lithiums

In regard to the reaction of **26** with various alkyl lithium species, it has been shown that due to the restricted steric environment around the Ta metal center in **26**, the size of the alkyl group in the alkyl lithium reagent plays a crucial role in controlling the mode of reactivity for each iterative equivalent of the alkyl lithium reagent and therefore controls the identity of the major product that is observed for each process (Scheme 7). Assuming that the initial reaction is always a substitution of one alkyl ligand for a Cl, then it must be the steric environment in that first alkyl dichloro intermediate that is the branch-point responsible for sterically controlling which reaction will take place with the next equivalent of alkyl lithium. The available modes of reactivity observed include: 1) direct alkyl substitution of a Cl ligand via a salt metathesis reaction; 2) α -H abstraction to produce a Ta(V) alkylidene; 3) β -H abstraction to produce a Ta(V) metallocyclopropane (can also be viewed as a Ta(III) olefin complex) 4) electron transfer to the metal; and 5) deprotonation of the amidinate to produce an amideenamidate complex.



Scheme 46 Possible intermediates for the reactivity pathways in the reactions of **26** with three equivalents of various alkyl lithium reagents.

The rich variety of reactivity and products observed from the reactions of **26** with a gamut of alkyl lithium reagents ranging in steric bulk testifies not only to the sensitivity of the steric environment around the metal produced by the Cp* acetamidinate ligand set, but also to its ability to stabilize a variety of high oxidation state early TM alkyl complexes. Further investigations into the stability and reactivity of the compounds **27-32** will be discussed in the subsequent sections of this chapter.

5.3 Reduction Chemistry of Cp*TaCl₃[ⁱPrNC(Me)NⁱPr]

5.3.1 Synthesis of Cp*TaCl₂[ⁱPrNC(Me)NⁱPr]

The discovery of Cp*TaCl₂[ⁱPrNC(Me)NⁱPr] (**33**) was serendipitous, and originally the result of an exploratory reaction between Ta(V) ethyl, ethylidene complex **27** and a three-fold excess of Me₃SnCl. Upon workup and recrystallization the bright red-orange crystals were of a paramagnetic compound, as shown by ¹H-NMR. The crystal structure of **33** was solved confirming its identity (Figure 31).

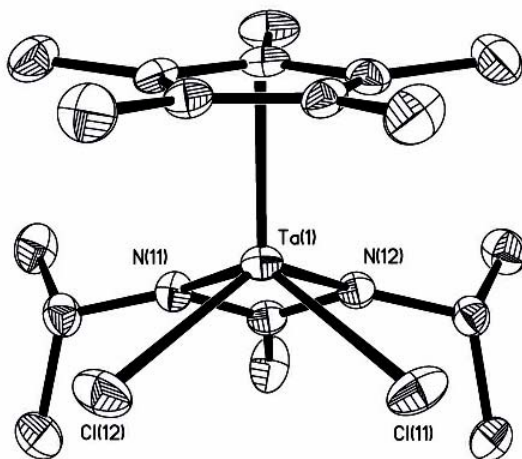


Figure 31 Solid state structure of **33** with 30% probability ellipsoids; hydrogens omitted for clarity

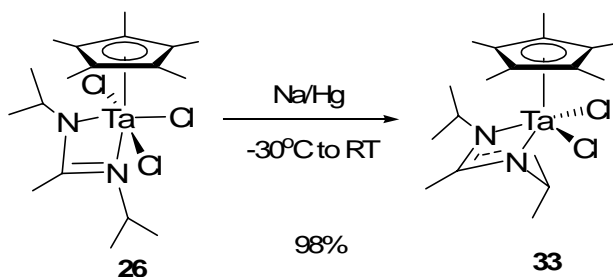
A direct comparison with the Hf(IV) analog Cp*HfCl₂[EtNC(CH₂CH₂TMS)N^tBu] of **33** was now possible, and even though the Hf(IV) compound contains an amidinate differing in the identity of the distal substituent, it has been shown that the distal substituent on the amidinate sterically or electronically affects the metal complex in the same way as a methyl group as long as it is also an alkyl group and is not bulky in nature.¹²² Once again, as seen with the previous comparisons of

isostructural Ta(IV) and Hf(IV) complexes, all the Ta-ligand bonds are significantly shorter as compared to the H(IV) analog (Table 4).

	Ta(IV)	Hf(IV)
M - N _a	2.123(3) Å	2.162(2) Å
M - N _b	2.129(3) Å	2.237(2) Å
M - Cl _a	2.4046(11) Å	2.4160(9) Å
M - Cl _b	2.4140(11) Å	2.4225(9) Å
M - CENT	2.0711(17) Å	2.1877(15) Å

Table 12 Selected bond distances for **33** and the isostructural Hf(IV) analog

Although the mechanism of the transmetallation reaction of **27** with tin was never studied, it was recognized that **33** is isostructural with the Cp*ZrCl₂[ⁱPrNC(Me)NⁱPr] complex **1**, which is commonly used for the synthesis of homoleptic, as well as asymmetric zirconium alkyl species for the purposes of evaluating their reactivity and polymerization competence upon activation to a cationic state.^{1,3-9,11,12,43,77,111,113,115,116,123,124} Therefore, an opportunity was recognized to directly access a variety of Ta(IV) alkyl species via alkylation of **33** using Grignard and alkyl lithium reagents. This recognition of the potential synthetic utility of **33** prompted investigations into the synthesis of **33** from **26** via sodium amalgam reduction.



Scheme 47 Synthesis of **33** via N/Hg reduction of **26**

Sodium amalgam (Na/Hg) reduction of TM halide complexes is a common method of accessing lower oxidation state species. In the case of the Cp* amidinate tantalum species the 1 equivalent Na/Hg reduction of **26** yielded **33** in an almost quantitative (98%) yield (Scheme 47). This facile synthesis of **33** provided a route to access a variety of homoleptic and mixed dialkyl Cp* acetamidinate Ta(IV) complexes.

5.3.2 Synthesis of $\{\text{Cp}^*\text{TaCl}[\text{iPrNC}(\text{Me})\text{N}^i\text{Pr}]\}_2(\mu\text{-}\eta^1, \eta^1\text{-N}_2)$

In the process of investigating Na/Hg reduction chemistry of **26** several different procedures were attempted. The initial reaction was carried out in Et₂O under the atmosphere of N₂, with 4 equivalents of Na sand. 10 mol % of Hg were added after cooling the reaction to -25°C, and after stirring overnight at RT the reaction was worked up by evacuating all volatiles followed by a pentane extraction, which yielded two species as determined by ¹H-NMR. Through successive recrystallization purification it was finally possible to obtain **34**, which was one of those two species, in a pure crystalline form, and its solid state structure was solved via single crystal X-ray diffraction. The other product of the reaction has been isolated, and though a single crystal was produced, single crystal diffractometry has not yet produced a plausible structure, though it is thought to be the dinuclear Ta(III) complex $\{\text{Cp}^*\text{Ta}[\text{iPrNC}(\text{Me})\text{N}^i\text{Pr}]\mu\text{-Cl}\}_2$.

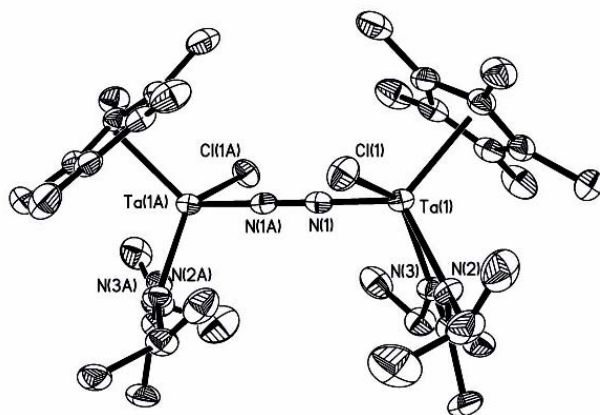


Figure 32 Solid state structure of **34** with 30% probability ellipsoids; hydrogens omitted for clarity

Figure 32 shows the structure of **34** to be a molecule of N_2 trapped between two equivalent Ta centers. This dimer exhibits Ta-N bond distances of 1.813(5) Å, and a N-N bond length of 1.288(10) Å, and the Ta-N-N bond angle of 178.5(6)°, with all 4 Ta-N-N-Ta atoms collinear and hence formally still sp hybridized. The Ta-N distance is at the lower limit and the N-N is at the upper limit of known distance ranges for group 5 N_2 end-on complexes, with the Ta-N bond distance best described as a double bond, and the N-N bond order being reduced to less than 2.¹²⁵⁻¹²⁸

A recent report of a ditantalum dinitrogen complex reported by the Messerle group $(Cp^*TaCl_2)_2(\mu-\eta^1, \eta^1-N_2)$,¹²⁹ was found to have Ta-N bond lengths of 1.804(3) Å and the N-N distance is 1.280(6), with these bonds less than 0.01 Å shorter than in **34**. Although the difference in bond lengths between **34** and $(Cp^*TaCl_2)_2(\mu-\eta^1, \eta^1-N_2)$ is relatively small, the Ta-N-N bond angles in complex $(Cp^*TaCl_2)_2(\mu-\eta^1, \eta^1-N_2)$ have been reduced to 166.3(4)°, which shows a significant change in N hybridization closer to sp^2 . It is impossible that this significant difference in hybridization of the bridging N atoms in **34** and the Messerle structure is purely due to the slight variation in Ta-N and N-N bond

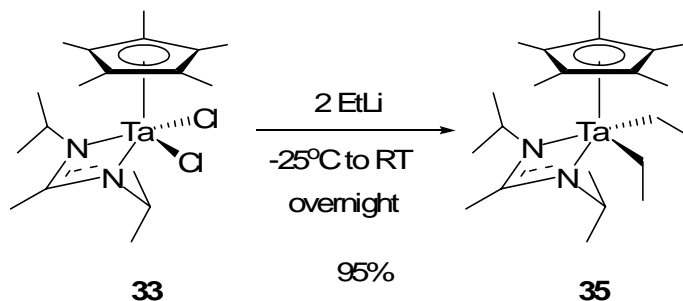
lengths. A more plausible explanation is that the difference in the coordinative saturation and the steric environment of the inner sphere of the species plays a significant role, where the more substituted Ta center in **34** is more sterically congested, which in turn likely changes the allowed electronic interactions between the N₂ ligand and the Ta atoms.

5.3.3 Alkylation Reactions of Cp*TaCl₂[ⁱPrNC(Me)NⁱPr]

The ability to access a variety of homoleptic and asymmetric Ta(IV) dialkyl complexes was the main objective in obtaining the Ta(IV) dichloride **33**. This goal was chosen since it is known that Cp* amidinate Zr(IV) dialkyl complexes are precursors for highly active living stereospecific Ziegler-Natta polymerization catalysts and a direct comparison between group 5 *d*¹ and group 4 *d*⁰ isostructural initiators would be of great value to understanding of the steric and electronic factors involved in Ziegler-Natta olefin insertion, as well as other reactions. The exploration of polymerization activity and other transformations of Ta(IV) dialkyl complexes will be described in subsequent sections of this chapter, while the synthesis and characterization of these complexes will be described here.

5.4 Alkylations of Cp*TaCl₂[ⁱPrNC(Me)NⁱPr]

5.4.1 Synthesis of Cp*TaEt₂[ⁱPrNC(Me)NⁱPr]



Scheme 48 Synthesis of **35**

Based on the reactivity of the Zr(IV) diethyl complex generated *in situ*, which decomposed via β -H abstraction and under an atmosphere of ethene produced the unsubstituted zirconacyclopentane **13**, the reaction of **33** with EtLi was carried out under 40psi of ethene.⁷⁶ Upon workup crystalline product **35** was isolated, and later the reaction was optimized in a pure argon atmosphere at low T to produce **35** in a 95% yield (Scheme 48).

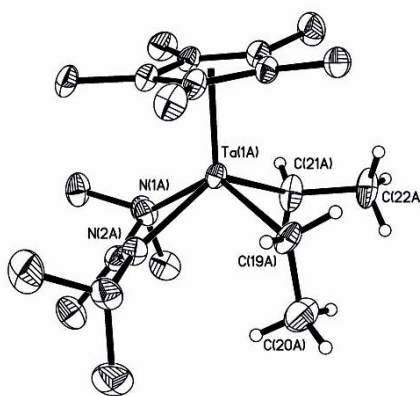


Figure 33 Solid state structure of **35** with 30% probability ellipsoids; all except ethyl group hydrogens have been omitted for clarity

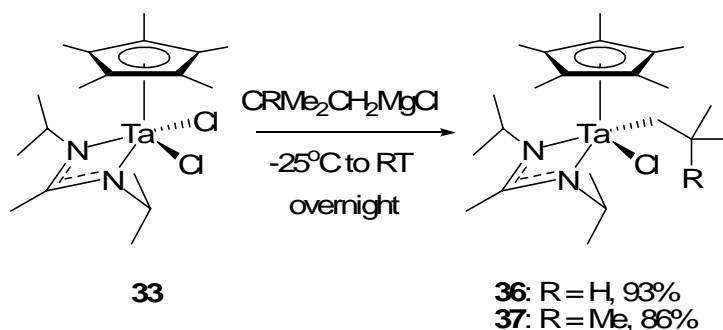
Rather than the expected tantalocyclopentane product, **35** was identified to be the Ta(IV) diethyl complex by single crystal diffractometry (Figure 33). When compared to other homoleptic Ta(IV) dialkyl species, the bonds distances in **35** of 2.171(6) Å and 2.178(6) Å for the Ta-N bonds and 2.222(8) Å and 2.239(7) for the Ta-C bonds, are very similar to bond lengths for the dibutyl **29** and diisobutyl **31**. Isolation and characterization of **35** was an important addition to the already impressive collection of stable dialkyl Ta(IV) complexes. The stability of **35** is remarkable, and may be explained by steric congestion that is observed in **35** like in the other Ta(IV) dialkyl complexes already mentioned, which prevents secondary interactions between the metal center and the alkyl substituents.

5.4.2 Synthesis of $\text{Cp}^*\text{TaCl}(\text{CH}_2\text{CRMe}_2)[\text{PrNC}(\text{Me})\text{N}^i\text{Pr}]$ for R = H or Me

A known phenomenon for early TM methyl complexes that serve as homogeneous Ziegler-Natta polymerization initiators is the formation of μ -Me dimers.⁴ It has also been recognized that an effective strategy to circumvent this problem is the use of initiators that only have larger metal-based alkyl groups, such as isobutyl or benzyl. These are sometimes difficult to initiate in a clean and well defined fashion because the Lewis acid cocatalysts such as trityl perfluorotetraphenylborate or perfluorotriphenylborane may react with higher alkyl groups by either abstracting the entire alkyl group from the metal, or by β -H or β -Me abstraction, causing the formation of a cationic olefin complex, and therefore producing a mixture of cationic species, rather than a pure single species. In order to have a well defined and controlled activation it is necessary to have a heteroleptic species with one larger alkyl group together with a

methyl group, so that activation occurs only at the methyl group, which can either be abstracted or protonated producing a well defined alkyl cation that cannot engage in bridging interactions with another cation due to prohibitive sterics.

In order to have well defined initiators for polymerization activity testing, the synthesis of a methyl neopentyl and a methyl isobutyl Ta(IV) complexes were undertaken. The synthetic methodology used employed the significantly faster reactivity of the first over the second equivalent of Grignard reagent with early TM chloro species.⁴³ Upon reaction of **33** with 1 equiv. of $\text{ClMgCH}_2\text{CRMe}_2$ ($\text{R} = \text{H}$ or Me) the corresponding chloro alkyl Ta(IV) isobutyl **36** and neopentyl **37** complexes were isolated in good to excellent yields (**36**: $\text{R} = \text{H}$, 93%; **37**: $\text{R} = \text{Me}$, 86%;) as shown in Scheme 49.



Scheme 49 Synthesis of **36** and **37**

The solid state structures of **36** and **37** were determined via single crystal diffractometry, and the structures proved to be similar, both crystallizing in the same $\text{P2}_1\text{2}_1\text{2}_1$ space group with nearly identical cell parameters. Structurally **36** and **37** were shown to be similar as can be qualitatively observed in Figure 34.

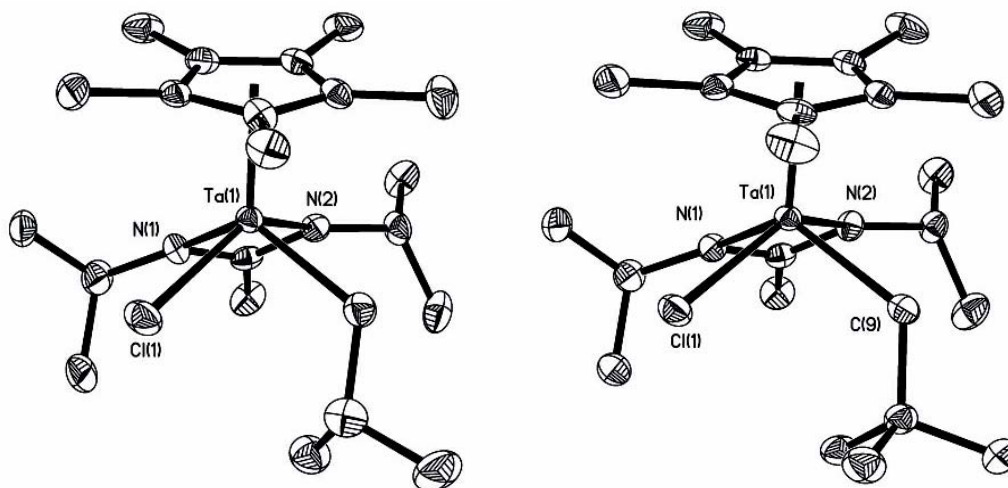


Figure 34 Solid state structures of **36** and **37**, respectively, with 30% probability ellipsoids; hydrogens have been omitted for clarity

Compounds **36** and **37** are also interesting from the point of view that they are, to the best of my knowledge, the first known examples of Ta(IV) chloro alkyl compounds. The Hf(IV) chloro isobutyl complex that is almost isostructural with compound **36**, other than the variation in the acetamidinate with Et and ^tBu substituents on the nitrogens, also crystallized in the same P₂₁2₁2₁ space group with very similar cell parameters and cell volume to those of **36** and **37**.⁴³ Although the cell parameters are similar between the group 4 and group 5 compounds, a bond distance comparison between the Ta(IV) and the Hf(IV) complexes in Table 5 shows the same pattern seen in the previous two group 4 *d*⁰ to group 5 *d*¹ comparisons earlier in this chapter (*vide supra*), that is, in the Ta(IV) compounds the metal is found to have significantly shorter bonds to the Cp* and the amidinate ligands, empirically evidenced by the 0.05 to 0.10 Å longer bond distances observed for the amidinate nitrogens and 0.10 to 0.15 Å for the centroid of the Cp*. As seen in Table 13, the differences between the chloro alkyl compound **36** and its Hf(IV)

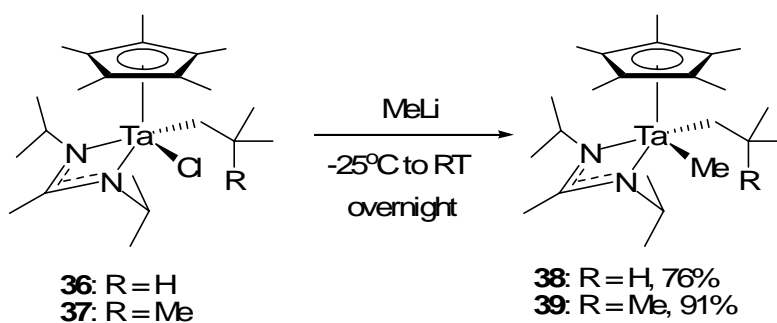
analog are well within the same range as those of the Ta(IV) vs. Hf(IV) and Zr(IV) dialkyl species already discussed.

	Ta(IV)	Hf(IV)
M - N _a	2.146(8) Å	2.199(7) Å
M - N _b	2.161(8) Å	2.238(6) Å
M - C	2.224(9) Å	2.257(6) Å
M - Cl	2.437(3) Å	2.4314(19) Å
CENT	2.098(4) Å	2.208(3) Å

Table 13 Selected bond distances for **11** and the isostructural Hf(IV) analog

5.4.3 Synthesis of Cp*TaMe(CH₂CRMe₂)[iⁱPrNC(Me)NⁱPr] for R = H or Me

After the Ta(IV) chloro alkyl species **36** and **37** were isolated in pure form, they were reacted with a single equivalent of MeLi to effect a salt metathesis and substitute the Cl with a Me ligand (Scheme 50). As a result, the corresponding Ta(IV) methyl isobutyl and methyl neopentyl complexes **38** and **39**, respectively, were isolated in good to excellent yields (**38**: R = H, 76%; **39**: R = Me, 91%).



Scheme 50 Synthesis of **38** and **39**

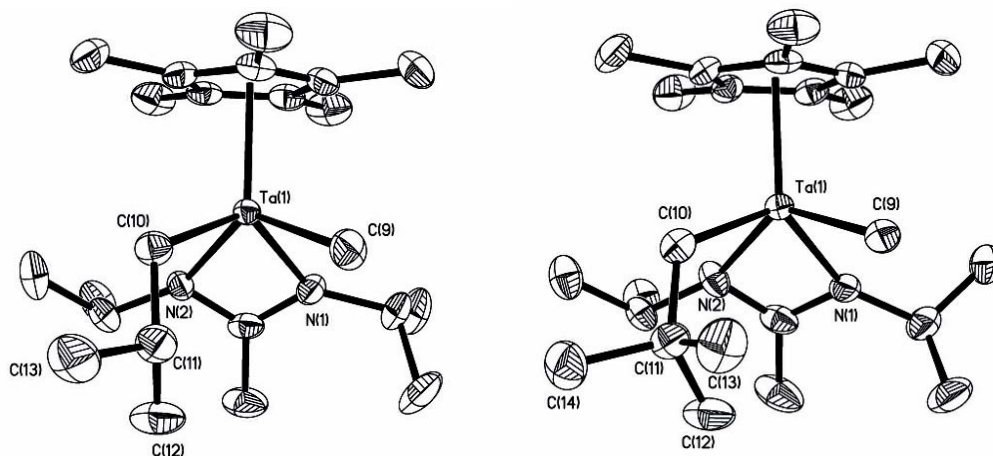


Figure 35 Solid state structures of **38** and **39**, respectively, with 30% probability ellipsoids; hydrogens have been omitted for clarity

The solid state structures of **38** and **39** were found via single crystal diffractometry, and though they appear to be similar in structure they crystallize in different space groups of $P2_1/n$ for **38** and $P2_12_12_1$ for **39**, with **39** crystallizing in the same space group as its chloro precursor **37**, while the crystal packing for **38** occurred in a different fashion (Figure 35).

5.5 Generation of Ta(IV) and Ta(V) Cations

5.5.1 Introduction to Generating Early Transition Metal Cations

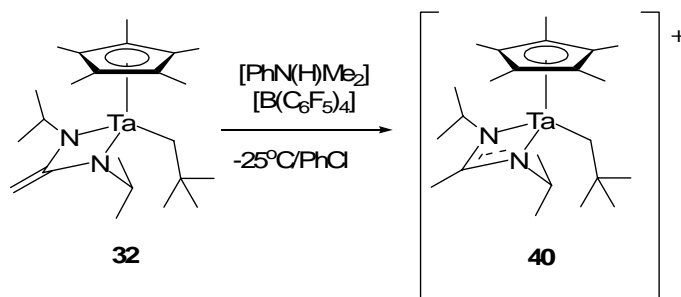
The traditional method of generating homogeneous Ziegler-Natta cationic initiators is considered to be via activation with methylaluminoxane (MAO), the first controlled synthesis of which is attributed to Kaminsky for work published in 1980.³⁶ Bintzinger is also credited with aiding the development of MAO as an initiator for Ziegler-Natta olefin polymerization utilizing ansa-metallocenes and working in conjunction with Kaminsky.³⁷ Not until 1991 was another breakthrough in Ziegler-Natta activation reported by Marks,¹³⁰ when a Lewis acid in the form of a perfluorinated triphenyl borane ($B(C_6F_5)_4$) was used with a group 4 metallocene dimethyl species to produce a high activity α -olefin polymerization system. Marks confirmed the identity of the active species by obtaining the solid state structure of the metallocene cation with the weakly coordinating methyl borate anion.¹³¹ This was the beginning of the development of well defined cocatalysts for homogeneous Ziegler-Natta polymerizations of α -olefins.

The coordinating nature of the methyl borate anion generated via an abstraction of a methide from the metal is thought to interfere with the polymerization process by competing with the incoming monomer for a coordination site, as was shown by the Me-bridged structure that Marks reported,¹³¹ as well as subsequent kinetic studies of the borane-activated metallocene systems.^{132,133} The inherent coordination behavior of the Me-borate makes studying living polymerization systems difficult, hence the development of novel cocatalysts with non-coordinating anions was necessary for the study of well defined homogenous Ziegler-Natta polymerization systems.

In conjunction with the discovery of the perfluorinated triaryl borane activation, acidic salts of perfluorinated tetraphenyl borate $[B(C_6F_5)_4]$ with either N,N-dimethylanilinium $[PhN(H)Me_2]$ or trityl $[Ph_3C]$ cations were found to be particularly effective in activating group 4 dialkyl complexes toward cationic Ziegler-Natta polymerization with the non-coordinating $B(C_6F_5)_4^-$ anion having negligible, if any discernable, effect on the rate of propagation.^{130,134} The discoveries of these better cocatalysts has been instrumental in the further development of novel homogeneous Ziegler-Natta polymerization systems, and provides the necessary tools to generate well defined early TM alkyl cations in order to study their structural properties, stability and reactivity toward relevant substrates.

5.5.2 Generation of $\{Cp^*TaNP[iPrNC(Me)NiPr]\}[B(C_6F_5)_4]$: The First Stable Ta(IV) Alkyl Cation

5.5.2a Protonation of Amidenaminate Ta(IV)



Scheme 51 Protonation of **32** to make cation **40**

The deprotonation of the acetamidinate ligand in the synthesis of Ta(IV) amidenaminate complex **32** presented an ideal opportunity to cleanly generate a Ta(IV), since it is known that the amidenaminate, similarly to an enolate, possesses nucleophilic and Lewis base character.^{7,115} With this in mind, protonation of **32** was carried out by

reaction with 1 equiv. of $[\text{PhN(H)Me}_2][\text{B(C}_6\text{F}_5)_4]$, which chemoselectively regenerated the acetamidinate from the amidenaminate to produce the Ta(IV) cationic complex **40** in a 98% crystalline yield following pentane diffusion crystallization from PhCl solution (Scheme 51).

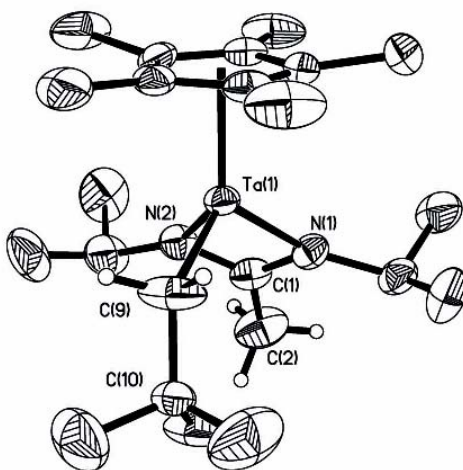


Figure 36 Solid state structure of **40** with 30% probability ellipsoids; all but C(2) and C(9) hydrogens have been omitted for clarity

The solid state structure of **40** was determined by single crystal X-ray diffraction as shown in Figure 36. This is an exciting discovery, since it has been thought for a long time that cationic Ta(IV) alkyl species are unstable. Work conducted by Chirik and Bercaw¹⁷ with decamethyl tantalocenes has shown that alkyl complexes of Ta(III) undergo β -H elimination to form a stable hydrido olefin complexes. A recently published work by Bergman and coworkers¹³⁵ report the synthesis of a non-metallocene imido Ta(V) benzyl cation. However, until now, there has not been a report of a Ta alkyl cationic species that contains a β -Me group.

	32	40
Ta - N_a	2.021(3) Å	2.085(3) Å
Ta - N_b	2.027(3) Å	2.104(3) Å
Ta - C	2.199(3) Å	2.110(4) Å
Ta-C_α-C_β	126.4(2) ^o	129.9(3) ^o

Table 14 Selected bond distances for **32** and **40**

An interesting comparison can be drawn between the structures of **32** and **40**, as shown in Table 6. The M-N bond distances are shorter for the neutral compound **32** than in the cationic **40**, however, in **32** the amidenamidate ligand is formally a -2 ligand, where each of the M-N bonds is covalent, whereas in **40** the Ns are part of the acetamidinate ligand, which carries a -1 charge and formally there is only a single covalent M-N bond with the other N datively coordinating to the metal center. The difference in the M-C bond length to the N_p ligand between **32** and **40** reveals and underscores the difference in electron deficiency of the metal, with the cationic complex **40** drawing the N_p ligand closer in than the neutral **32**. The Ta-C_α-C_β bond angle is another aspect of the structures worth considering, with the angle in the cationic **40** being slightly greater than in the neutral **32**, but the angles are close enough in value that the difference could be just the product of crystal packing.

5.5.2b Protonation of Methyl Neopentyl Ta(IV)

One of the goals for the synthesis of **38** and **39** was to attempt to generate the corresponding cations via a well defined Me group protonation or abstraction using one of the popular cocatalysts discussed in section 5.5.1. In the case of **39** the product should be the already isolated cation **40**, which would have been further proof of concept, however, the reaction of **39** with any of the cocatalyst failed to produce crystals of **40**. Upon mixing **39** with any of the cocatalysts the color of solution turned from the deep red of the Ta(IV) neutral species to a very light yellow solution; however, any attempts to crystallize it from PhCl or toluene using pentane diffusion failed. This was presumably due to the different method of cation generation, which possibly produced more impurities and therefore did not allow the proper growth of clean single crystals.

5.5.3 Generation of $\{\text{Cp}^*\text{Ta}^i\text{Bu}[\text{PrNC}(\text{Me})\text{N}^i\text{Pr}]\}\text{[B}(\text{C}_6\text{F}_5)_4\text{]}$

5.5.3a Attempts in PhCl

As already mentioned, there is only one known example of a Ta-alkyl cation reported in 2006 by Arnold and Bergman,¹³⁵ however, it is a Ta(V) benzyl cation. Our goal was to isolate and study both Ta(IV) and Ta(V) cations. Initial attempts to generate the $\{\text{Cp}^*\text{Ta}^i\text{Bu}[\text{PrNC}(\text{Me})\text{N}^i\text{Pr}]\}\text{[B}(\text{C}_6\text{F}_5)_4\text{]}$ cationic species in PhCl by the protonation of **38** at -25°C produced a diamagnetic species that was crystallized from the PhCl solution by pentane diffusion, and was shown to be the dichloro bridging dication **41** by single crystal X-ray diffractometry (Figure 37).

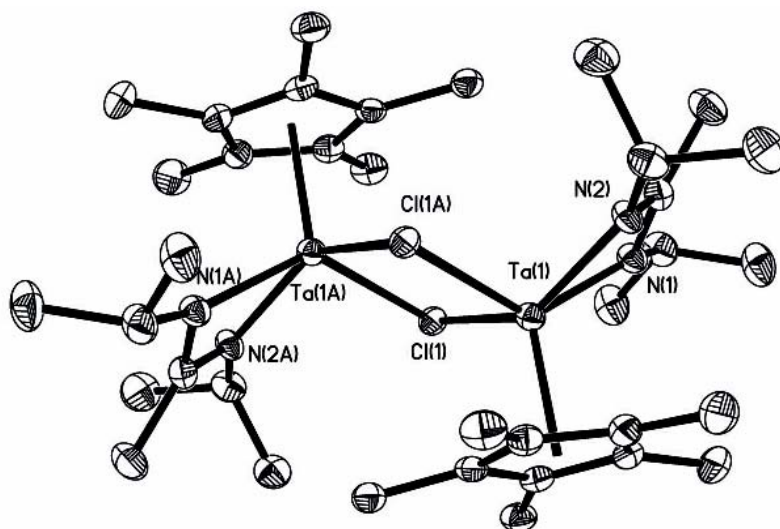


Figure 37 Solid state structure of **41** with 30% probability ellipsoids; hydrogens omitted for clarity

This was true for all attempts to generate the cation in PhCl, without any difference whether $B(C_6F_5)_3$, $[Ph_3C][B(C_6F_5)_4]$ or $[PhN(H)Me_2][B(C_6F_5)_4]$ was used as the cocatalyst. By 1H -NMR, **41** is the only observable species and, in the case of activation with anilinium borate, integrated perfectly against the aniline N,N-dimethyl peak, which suggests that the entirety of the Ta(IV) cationic species decomposed via Cl abstraction from solvent at $-25^\circ C$ immediately as it was generated. This thermal instability is in sharp contrast to the similar decomposition observed for the isostructural cationic Zr(IV) complexes, which also produced a dichloro bridged dication similar to **41**, however, this only occurred at temperatures above $0^\circ C$, and even at RT decomposition was very slow, taking days to go to completion.⁴

This observation of extreme thermal instability is surprising, considering the extreme stability of the Ta(IV) Np cation **40**, which was isolated with relative ease, and later found to be thermally stable to $100^\circ C$ in PhCl solution (vide infra). Presumably, the Np ligand in **40** is just bulky enough, as compared to the *in situ* generated Ta(IV) iBu

cation, to disallow any approach to the metal center, which makes that cation stable against decomposition via the Cl abstraction. This suggests that there is an easier pathway for Cl abstraction for the Ta(IV) cations, as compared to Zr(IV) cations. This instability is surprising considering the steric hindrance of the Ta(IV) species, when compared to Zr(IV), but it may have something to do with the ability of Ta(IV) to one electron chemistry.

5.5.3b Attempts in Toluene

In order to avoid the Cl abstraction from solvent decomposition pathway, and to attempt to isolate the Ta(IV) ⁱBu cation in crystalline form, the same set of activation reactions was carried out in toluene using **38** as the cation precursor and the same three cocatalysts described earlier. When the reaction was tracked by ¹H-NMR, no sharp diamagnetic resonances were found to appear even at room temperature. Only broad resonances attributable to paramagnetic species were visible in the spectrum, however, all attempts to crystallize the cationic complex using pentane diffusion through the toluene solution failed to produce a good crystal of the Ta(IV) cation, and instead only produced an amidinium borate salt, which is presumably a product of the cation decomposition. This suggests that at -25°C, even in toluene, there is decomposition of the cationic Ta(IV) isobutyl complex taking place.

5.5.4 Generation of Ta(V) Dimethyl Cation

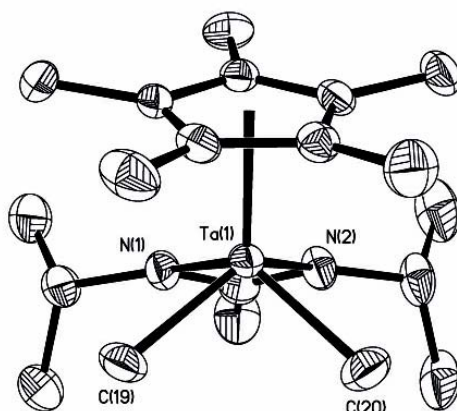


Figure 38 Solid state structure of **42** with 30% probability ellipsoids; hydrogens omitted for clarity

Ta-N_a	2.110(3) Å
Ta-N_b	2.152(4) Å
Ta-C_a	2.144(5) Å
Ta-C_b	2.148(4) Å
Ta - CENT	2.1003(15) Å

Table 15 Selected bond distances for **42**

The original publication by Meyer and coworkers¹⁰⁴ of the synthesis of Ta(V) trimethyl complex **27** also reported attempts to activate **27** with $B(C_6F_5)_3$ or $[Ph_3C][B(C_6F_5)_4]$, which in the presence of ethene were unsuccessful in producing any polymer. Our own attempts at activating **27** with $[PhN(H)Me_2][B(C_6F_5)_4]$ gave no polymer with 1-hexene or ethene in PhCl at 10°C, 0°C, or at RT. Pentane diffusion crystallization produced single crystals that were analyzed via X-ray diffractometry to solve the solid state structure of the Ta(V) dimethyl cation **42** (Figure 38). The Ta-N and Ta-C bond lengths for **42** are shown in Table 15. Ethene and 1-hexene polymerization activity of **42** were tested, only confirming the original findings of the Meyer group that

the Ta(V) dimethyl cation is inactive for olefin polymerization regardless of the counterion.

5.6 Thermolysis of Ta(V) and Ta(IV) Alkyls

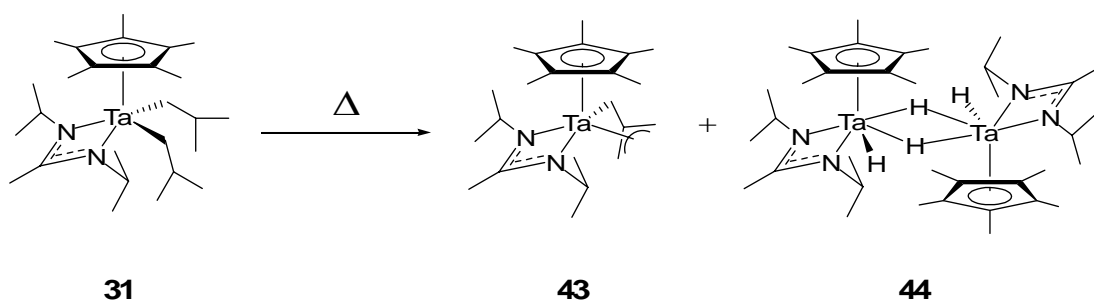
5.6.1 Thermolysis of Ta(V) Ethyl, Ethylidene

It is known that TM alkyl complexes can undergo various modes of decomposition under thermolytic conditions and this reactivity was explored for some of the new Ta alkyl complexes that have been described above. The first compound to be subjected to heating was the Ta(V) ethyl, ethylidene complex **28**. It was found that it is indefinitely stable in benzene at temperatures as high as 80°C, however, in toluene it slowly decomposes at temperatures as low as RT over days, and begins to show decomposition product peaks in just minutes when placed at 50°C. When followed by ¹H-NMR the product mixture could not be de-convoluted, nor were any pure crystals successfully isolated from crystallization attempts.

5.6.2 Thermolysis of Ta(IV) Dialkyls

Considering the ease with which Ta(V) alkylidenes are formed upon reaction of alkylating reagents, such as alkyl lithium or Grignard reagents, with Ta(V) halides, it was thought prudent to try to thermally induce a methyl abstraction of an α hydride from the neighboring alkyl group in **38** or **39** to form a Ta(IV) alkylidene with CH₄ leaving. Surprisingly, both **38** and **39** are remarkably stable at temperatures as high as 80°C in a sealed tube in either benzene or toluene solution for as long as 8 days. The starting material is almost quantitatively recovered by crystallization.

The same stability is not observed for other Ta(IV) dialkyl complexes such as the Ta(IV) diethyl complex **35**, which upon heating in benzene at temperatures above RT decomposes to form unidentifiable diamagnetic products. On the other hand, the Ta(IV) diisobutyl complex **31** decomposes cleanly at even 40°C to form a trimethylenemethane (TMM) Ta(IV) complex **43** and a dimeric Ta(IV) dihydride complex **44** (Scheme 52). Compound **44** is diamagnetic and was observed by ¹H-NMR, however, the existence of **43** was only ascertained upon determination of its solid state structure. Single crystals of both **43** and **44** were produced and their solid state structures determined by single crystal X-ray diffractometry (Figure 39, Table 16 and Table 17).



Scheme 52 Thermolysis of **31** to produce **43** and **44**

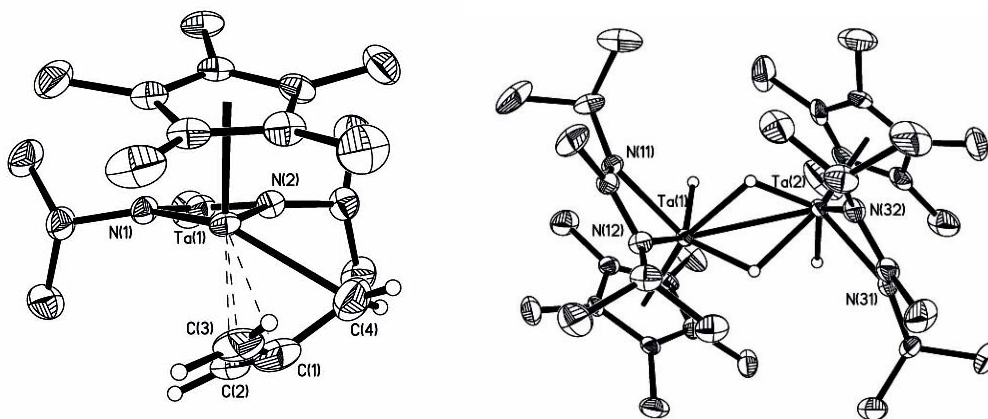
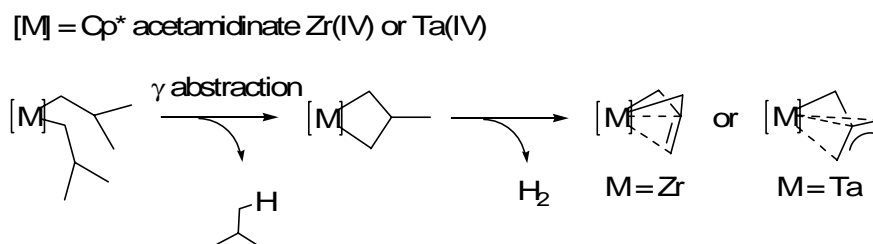


Figure 39 Solid state structures of **43** and **44**, respectively, with 30% probability ellipsoids; Cp* and amidinate hydrogens have been omitted for clarity

Ta(1) – C(1)	2.224(5)	C(1) – C(2)	1.364(8)
Ta(1) – C(2)	2.397(5)	C(1) – C(3)	1.337(9)
Ta(1) – C(3)	2.421(5)	C(1) – C(4)	1.478(9)
Ta(1) – C(4)	2.315(6)		

Table 16 Selected bond distances for **43** in angstroms (Å)

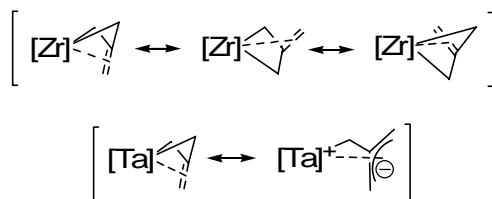
The thermal decomposition of **31** with the evolution of Ta(IV) TMM complex **43** is similar to the thermal decomposition of the Cp*ZA diisobutyl complex reported by Sita in 2002,⁴³ which yields the corresponding Zr(IV)TMM complex. This suggests that the γ -H abstraction mechanism originally suggested for this decomposition process (and discussed in Section 2.5.2) may be ubiquitous for all Cp*MA diisobutyl complexes (Scheme 53).^{43,71}



Scheme 53 Proposed mechanism for the formation of TMM complexes via thermolysis of diisobutyl complexes of Cp* acetamidinate Zr(IV) and Ta(IV)

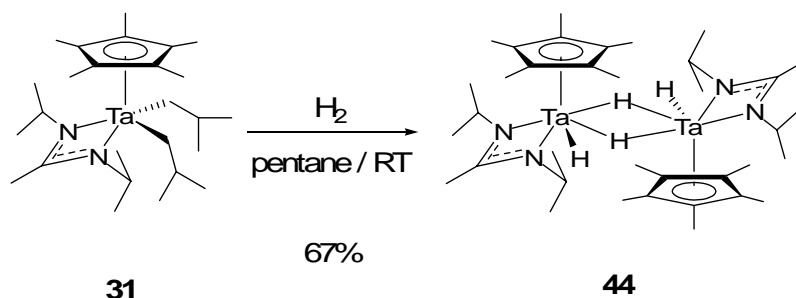
An interesting opportunity presents itself to compare a group 4 d^0 and a group 5 d^1 isostructural and isolobal TMM complexes differing only essentially in their electron counts. Both the Zr(IV) TMM and Ta(IV) TMM (**43**) complexes have a TMM fragment bound to the metal, however, in the solid state they appear to possess very different binding modes. In the solid state the Zr(IV) TMM complex was found to be C₂ symmetric with the TMM fragment in a σ^2, π binding mode, where the TMM ligand would best be described as an η^1, η^1, η^2 -TMM ligand, whereas in the Ta(IV) TMM

complex **43** is C_1 symmetric and the TMM ligand is in a σ,π binding mode where the TMM ligand adopts an η^1,η^3 -TMM conformation.^{43,71,73} This variation in the ligand binding mode is probably due to different resonance forms available to the two complexes, as depicted in Scheme 54.



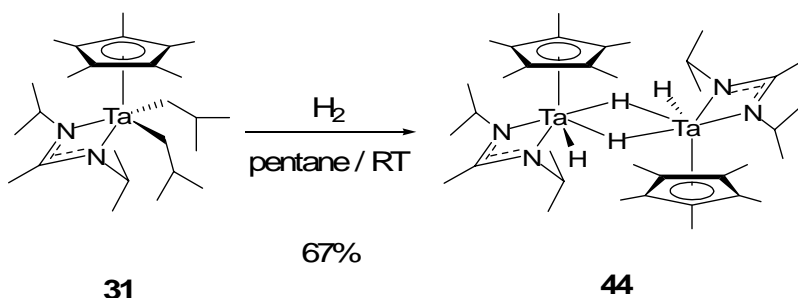
Scheme 54 Zwitterionic η^3 -allyl resonances form of the TMM moiety on **43** is found in the solid state structure of **43** and is different from the structure found for the Cp^*ZA analog.

The Zr(IV) TMM complex was studied via variable temperature NMR to show that at temperatures above 25°C the TMM fragment undergoes free rotation, which can be attributed to the Zr(IV) resonance in Scheme 54.⁷³ Unfortunately, due to the paramagnetic character of **43** it is impossible to carry out a VT NMR experiment to ascertain its barrier to rotation, but in view of the solid state structural data it is possible to predict that **43** should have a significantly higher barrier to rotation as compared to the Zr(IV) TMM complexes. The Cp^*ZA TMM complex was recently described by Sita and coworkers.¹³⁶ as having considerable zwitterionic character, with the TMM fragment possessing nucleophilic character, but in the case of Ta(IV) TMM complex **43**, based on its solid state structure it is in a permanent zwitterionic state.



Scheme 55 Synthesis of $\{\text{Cp}^*\text{ZrH}_2[\text{}^i\text{PrNC}(\text{Me})\text{N}^i\text{Pr}]\}_2$ ⁷⁶

The production of the $\{\text{Cp}^*\text{TaH}_2[\text{}^i\text{PrNC}(\text{Me})\text{N}^i\text{Pr}]\}_2$ compound **44** from the thermal decomposition of **31** was not unprecedented either. A similar $\{\text{Cp}^*\text{ZrH}_2[\text{}^i\text{PrNC}(\text{Me})\text{N}^i\text{Pr}]\}_2$ was produced in our laboratory earlier, through the treatment of Cp^*ZA dichloride **1** with 2 equivalents of EtLi under the atmosphere of H_2 (Scheme 55).⁷⁶ Other Ta(IV) hydride complexes have also been prepared via hydrogenation of Ta(IV) alkyl complexes by the Fryzuk group.^{137,138} The formation of **44** from the thermolysis of **31** is most likely the result of *in situ* formation of H_2 along with an iso-butane for each Ta(IV) TMM complex produced that is formed from the thermolysis of **31**, which must be the source of hydrogen for the formation of **44**. With precedent from Fryzuk's chemistry, the thermolysis of **31**, and the formation of Zr(IV) hydride dimer from earlier work, we felt it would be appropriate to attempt a hydrogenation of **31** to obtain the Ta(IV) dihydride dimer **44** in pure form and high yield. Upon placing **31** in pentane under 40 psi H_2 for 36 h, the expected product **44** was isolated in a 67% crystalline yield (Scheme 56).

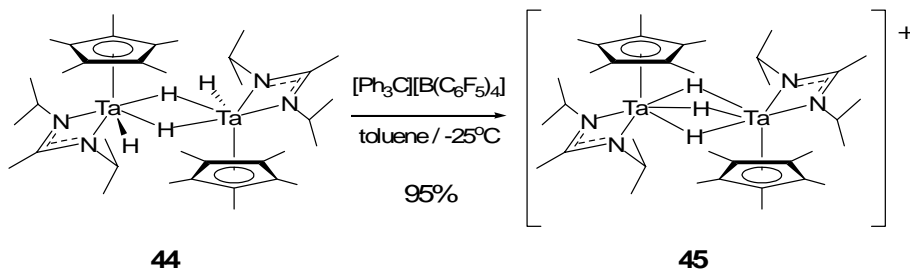


Scheme 56 Direct hydrogenation of **31** to produce **44**

By $^1\text{H-NMR}$, **44** appears as a diamagnetic species suggesting the existence of a Ta-Ta bond, which is consistent with the Ta(IV) hydride reported by Fryzuk.¹³⁷

5.6.2 Generation of a Ditantalum Monocationic μ -Trihydride Complex

To further explore the chemistry of **44**, the Ta(IV) dihydride dimer was dissolved in toluene- d_8 and reacted with 1 equiv. of $[\text{Ph}_3\text{C}][\text{B}(\text{C}_6\text{F}_5)_4]$ at -25°C , producing an immediate color change from the deep brown-red of the dihydride dimer to a light yellow solution of the presumed cation. By $^1\text{H-NMR}$ it was ascertained that the product of the reaction produced much broader resonances, as opposed to the sharp peaks for **44**, and to determine the new cationic species' identity, pentane was layered over the toluene- d_8 solution and the NMR tube and placed at -25°C for 7 days eventually producing a 95% yield of the crystalline monocationic μ -trihydride ditantalum complex **45** (Scheme 57), as determined by single crystal X-ray analysis (Figure 40). The product **45** was also found to be generated regardless whether only one or multiple equivalents of $[\text{Ph}_3\text{C}][\text{B}(\text{C}_6\text{F}_5)_4]$ were added to **44**.



Scheme 57 Generation of the cationic complex **45** from **44**

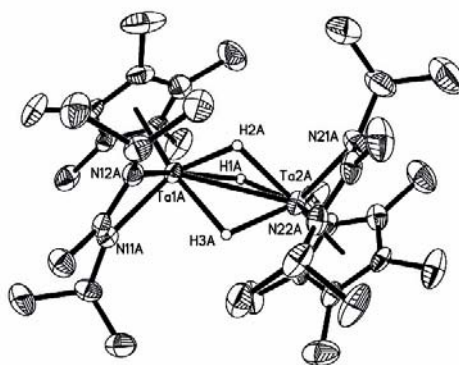


Figure 40 Solid state structure of **45** with 30% probability ellipsoids; all except for metal-bound hydrogens have been omitted for clarity.

	44		20	
Ta - N_a	2.174(3) Å	2.180(3) Å	2.161(4) Å	2.145(4) Å
Ta - N_b	2.241(3) Å	2.234(3) Å	2.225(4) Å	2.171(4) Å
Ta - μ-H	1.67(3) Å	1.68(3) Å	1.78(3) Å	1.78(3) Å
Ta - μ-H	1.65(3) Å	157(3) Å.	1.82(2) Å	1.79(2) Å
Ta - μ-H	N/A	N/A	1.95(3) Å	1.96(3) Å
Ta - H	1.87(3) Å	1.88(3) Å	N/A	N/A
Ta - Ta	2.8387(4) Å		2.9413(3) Å	

Table 17 Selected bond distances for **44** and **45**

Comparing the solid state structure of **45** to the solid state structure of **44** reveals that the neutral μ -dihydride **44** has virtually the same Ta-N bond distances as the cationic **45** (Table 17). Furthermore, in the μ -trihydride cationic **45** the Ta-H bond distances to the

bridging Hs range from 1.78(3) Å to 1.96(3) Å, which significantly longer than the 1.57(3) Å to 1.68(3) Å range observed in the bridging Hs of the neutral **44**. The longer Ta- μ -H bonds force the Ta-Ta bond distance to also be about 0.1 Å longer, with the distance increased for the cationic **45** at 2.9413(3) Å, versus 2.8387(4) Å for the neutral **44**.

5.4 Discussion of Cp* Acetamidinate Ta(V) and Ta(IV) Alkyl Complexes

5.4.1 General Trends in Electron Affinity of Ta Species

An interesting pattern emerges from the comparison of Ta(V) vs. Ta(V)⁺ vs. Ta(IV) vs. Ta(IV)⁺ alkyl species (vide supra). In the solid state structure of **27** the Ta(V)-Me bond distances are found to be 2.216(6) Å and 2.266(5) Å, with the 0.05 Å differential accounted for by two different types of Ta-Me bonds in the molecule, with one type lying in the plane of symmetry, which also includes the Ta and the N-C-N unit of the amidinate, and the other two Me groups exhibiting a different type of Ta-Me bond perpendicular to that plane.¹⁰⁴ Therefore, due to the electron donating trans-influence, the two Me groups lying perpendicularly to the plane of symmetry have the longer 2.266(6) Å bond lengths. These Ta(V)-C bond lengths are comparable to the Ta(V) ethyl, ethylidene **28** Ta(V)-C bond, where the Ta-Et bond distance of 2.236(3) Å is in the same range as the Ta-C distances in **27**.

Ta(IV) dialkyl complexes have shorter Ta-C bond lengths than Ta(V) alkyl complexes, such as the Ta-C bond lengths for the Ta(IV) diethyl complex **35** are 2.171(6) Å and 2.178(6) Å, and the Ta(IV) dibutyl **29** in which they are 2.210(2) Å and 2.233(3) Å. The Ta alkyl species with the next shortest Ta-C bond length is the Ta(V) cationic complex **42**, for which Ta-C bond distances are 2.144(5) Å and 2.148(5) Å, which is shorter than for neutral Ta(IV) complexes, but only by 0.02 Å. When taken into account that in general M-Me bonds tend to be shorter than M bonds to larger alkyl groups, the 0.02 Å difference is almost negligible and suggestive of a similarity in metal electron affinity between Ta(V) cationic and Ta(IV) neutral species.

Finally, to complete the picture, the solid state structure of a Ta(IV) alkyl cation **40** has been obtained showing a Ta-C bond distance of 2.110(4) Å, which is shorter yet as compared to Ta(V) cations and Ta(IV) neutral species. Now it's possible to achieve a better understanding of the stability and relative electron deficiency (affinity) of Ta in its various ionic and oxidations states, with the relationship shown in Figure 41.

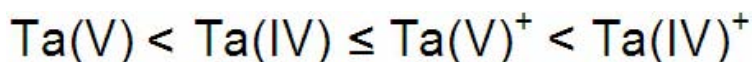


Figure 41 Trend of electrophilicity of Ta species in increasing order

As described in section 5.3.2, it may be possible to also access Cp* acetamidinate Ta(III) chlorides, which would be excellent precursors for further investigations of the properties of Ta in its various ionic and oxidation states.

5.4.2 Comparison of Ta(IV) Alkyls to Hf(IV) Alkyls

	Hf	Hf
Atomic Radius	1.55 Å	1.45 Å
Covalent Radius	1.50 Å	1.38 Å

Table 18 Atomic and covalent radii of Hf and Ta¹³⁹

Based on the consistent observations that the Ta(IV) alkyl compounds have a much tighter ligand sphere than the isostructural Hf(IV) compounds. However, when the differences in atomic and covalent radii between the two metals are taken into account (Table 18), it becomes apparent that the actual differences in the Ta-ligand vs Hf-ligand bond distances are on the same order as the difference in the metals' atomic radii. To compare the electron affinities of these species to each other using the qualitative

approach from crystallographic data is therefore impossible. At best, it is possible to conclude that the electron affinities are approximately the same.

Although the direct comparison of group 4 d^0 versus group 5 d^1 isostructural complexes was achieved, many conclusions remain to be drawn from future reactivity profiles correlated with computational analyses. There are clearly some similarities, such as the thermal decomposition of Ta-diisobutyl complex **31** yielding the Ta-TMM compound **43** and the Ta-hydride **44**, in a similar fashion as was observed for the Zr-diisobutyl complex, as previously reported.⁴³ However, the solid state structure of **43** reveals that there is sufficient difference between the Zr-TMM and the Ta-TMM complexes to warrant further investigations into the nature of the observed bonding modes, in order to better understand these compounds and their potential utility.

Experimental

All manipulations with air and moisture sensitive substances were carried out under an atmosphere of nitrogen (for Zr and Ti work) or argon (for Ta, unless specified otherwise) using standard Schlenk or glovebox techniques. All solvents were dried (Na/benzophenone for Et₂O, THF, and pentane, and Na/K alloy for toluene, CaH for CH₂Cl₂ and chlorobenzene) and distilled under nitrogen prior to use. (η^5 -C₅Me₅)ZrCl₂[RNC(CH₃)NR'] (**1**: R = Et, R' = ^tBu; **1'**: R = R' = ⁱPr), (η^5 -C₅Me₅)ZrCl(SiMe₂Ph)[EtNC(CH₃)NBu^t] (**2**) and (η^5 -C₅Me₅)Zr(η^2 -Styrene)[PrⁱNC(CH₃)NPrⁱ] (**12**) were prepared as previously reported.^{4,44,140} NpMgCl was prepared according to literature.¹⁴¹ ¹H- and ¹³C-NMR spectra were recorded at 400 MHz and 100 MHz respectively, using benzene-*d*₆, toluene-*d*₈, or chlorobenzene-*d*₅ as solvent unless stated otherwise. 2-Butyne was purchased from Lancaster and used as supplied. All other compounds were purchased from Aldrich and used as supplied. Elemental analyses were performed by Midwest Microlab.

Preparation of (η^5 -C₅Me₅)ZrCl[CH₂CH₂(-CH₂CH₂CH₂-)][EtNC(CH₃)NBu^t] (3**).** In a 50-ml Schlenk tube fitted with a gas tight Chemglass teflon valve, 0.30g (0.54mmol) of **2** was dissolved in 10 ml of pentane, to which was then added a 5-fold excess of methylenecyclobutane (precooled to -30°C), and the tube quickly sealed. After removal from the glovebox the tube was pressurized with H₂ (30psi) and sealed once more. The mixture was shaken overnight and volatiles removed *in vacuo*. The yellow solid was then redissolved in pentane. Upon cooling to -30°C overnight, **3** was obtained as yellow crystals (0.20g, 78% yield). For **3**: ¹H NMR: δ 2.84 (dq, J₂=13.9 Hz, J₃=7.2 Hz, 1H), 2.78

(m, 1H), 2.66 (dq, $J_2=14.3$ Hz, $J_3=7.2$ Hz, 1H), 2.52 (m, 1H), 2.30 (m, 1H), 2.05 (m, 1H), 2.00 (s, 15H), 1.98 (m, 2H), 1.71 (s, 3H), 1.70 (m, 1H), 1.32 (s, 9H), 0.88 (dd, $J_2=13.1$ Hz, $J_3=7.8$ Hz, 1H), 0.81 (t, $J=7.2$ Hz, 3H), 0.32 (dd, $J_2=13.1$ Hz, $J_3=5.6$ Hz, 1H). Anal. Calcd. for $C_{23}H_{41}N_2ClZr$: %C 58.50, %H 8.75, %N 5.93; Found %C 58.65, %H 8.72, %N 5.86.

Preparation of $(\eta^5-C_5Me_5)Zr(Cl/Br)(CH_2CH_2CH=CH_2)[EtNC(CH_3)NBu^t]$ (4'**).** 2.12 g (4.8 mmol) of $(\eta^5-C_5Me_5)ZrCl_2[EtNC(CH_3)NBu^t]$ were dissolved in 100 mL of Et_2O in a 250 mL Schlenk flask, and to it 7.6 mL of 3-butenylmagnesium bromide (0.64M in Et_2O , 4.8 mmol) were added drop-wise over a period of 1h. The solution was then allowed to keep stirring at room temperature for another 3h, and upon the completion of this period volatiles were removed *in vacuo*. The yellow product was extracted using 10% toluene in pentane solution, filtered through a pad of Celite, and set at $-30^\circ C$. Recrystallization afforded **4'** as a yellow crystalline material. (1.84g, 79% yield, based on 1.4:1 = Br:Cl product ratio). For **4'**: 1H NMR: δ 6.07 (m, 1H), 5.14 (d, $J=17.1$ Hz, 1H), 4.97 (d, $J=9.9$ Hz, 1H), 2.99 & 2.87 (2 multiplets, 1H), 2.84 (dq, $J_2=13.9$ Hz, $J_3=7.2$ Hz, 1H), 2.63 (dq, $J_2=14.3$ Hz, $J_3=7.2$ Hz, 1H), 2.28 (m, 1H), 1.99 & 1.98 (2 singlets, 15H), 1.68 & 1.67 (2 singlets, 3H), 1.32 & 1.30 (2 singlets, 9H), 0.79 & 0.77 (2 triplets, $J=7.55$ Hz, 3H), 0.74 & 0.65 (2 multiplets, 1H), 0.23 & 0.11 (2 multiplets, 1H).

Preparation of $(\eta^5-C_5Me_5)ZrMe[CH_2CH_2(-CH_2CH_2CH_2-)] [EtNC(CH_3)NBu^t]$ (5**).** To a solution of 0.20 g (0.42 mmol) of **3** in 6 ml of Et_2O at $-30^\circ C$ was added 0.27 ml (0.42 mmol) of MeLi (1.6M in Et_2O). The initially clear yellow solution was allowed to warm up to room temperature over a period of 1h, after which the volatiles were removed *in vacuo*. The crude solid was extracted with pentane, filtered through a pad of Celite, and the filtrate concentrated. Recrystallization at $-30^\circ C$ afforded **5** as pale yellow crystals

(0.12 g, 63% yield). For **5**: $^1\text{H NMR}$: δ 2.90 (m, 3H), 2.71 (m, 1H), 2.46 (m, 1H), 2.37 (m, 1H), 2.22 (m, 1H), 1.97 (s, 15H), 1.96 (m, 1H), 1.80 (s, 3H), 1.78 (m, 1H), 1.19 (s, 9H), 0.88 (t, $J=7.2$ Hz, 3H), 0.60 (m, 1H), 0.13 (s, 3H), 0.04 (m, 1H). Anal. Calcd. for $\text{C}_{24}\text{H}_{44}\text{N}_2\text{Zr}$: %C 63.80, %H 9.81, %N 6.20; Found %C 63.50, %H 9.67, %N 6.26.

Preparation of $(\eta^5\text{-C}_5\text{Me}_5)\text{ZrCl}(\text{CH}_2\text{CH}_2\text{CH}_2\text{CH}=\text{CH}_2)[\text{EtNC}(\text{CH}_3)\text{NBu}^t]^+$ (6**).** In a 50-ml Schlenk tube fitted with a gas tight Kontes teflon valve, 0.10 g (0.21 mmol) of **3** was dissolved in 2 ml of toluene. The tube was then placed in an oil bath at 65°C over 36h, after which the volatiles were removed *in vacuo*. The crude product was an oil (0.10 g, 100% yield) and pure by NMR. For **6**: $^1\text{H NMR}$: δ 6.00 (m, 1H), 5.15 (dt, $J_3=17.1$ Hz, $J_4=1.1$ Hz, 1H), 5.03 (dt, $J_3=10.3$ Hz, $J_4=1.2$ Hz, 1H), 2.80 (dq, $J_2=13.9$ Hz, $J_3=6.8$ Hz, 1H), 2.63 (dq, $J_2=14.0$, $J_3=6.8$ Hz, 1H), 2.31 (m, 1H), 2.19 (m, 1H), 2.01 (s, 15H), 1.69 (s, 3H), 1.57 (m, 1H), 1.32 (s, 9H), 1.24 (m, 1H), 0.80 (t, $J=7.2$ Hz, 3H), 0.55 (ddd, $J_2=13.1$ Hz, $J_3=11.1$ Hz, $J_3=3.6$ Hz, 1H), 0.24 (ddd, $J_2=13.1$ Hz, $J_3=10.7$ Hz, $J_3=5.6$ Hz, 1H).

Preparation of $[(\eta^5\text{-C}_5\text{Me}_5)\text{Zr}(\text{CH}_2\text{CH}_2\text{CH}_2\text{CH}=\text{CH}_2)\{\text{EtNC}(\text{CH}_3)\text{NBu}^t\}]^+[\text{B}(\text{C}_6\text{F}_5)_4]^-$ (7**).** In a 2-ml vial 0.015 g (0.03mmol) of **5** or **8** were dissolved in 0.8 ml $\text{C}_6\text{D}_5\text{Cl}$. In a separate 2-ml vial 0.027 g (0.03 mmol) of $[\text{C}_6\text{H}_5\text{NH}(\text{Me})_2]^+[\text{B}(\text{C}_6\text{F}_5)_4]^-$ were placed, and both vials cooled to -30°C . Upon mixing the solution of **3** or **6** with the anilinium borate salt the solution turns from light to bright yellow and gas is evolved. For **7**: $^1\text{H NMR}$: δ 6.63 (m, 1H), 4.86 (d, $J=17.9$ Hz, 1H), 4.63 (d, $J=9.1$ Hz, 1H), 2.94 (m, 2H), 2.20 (m, 2H), 2.07 (m, 1H), 1.98 (s, 3H), 1.90 (m, 1H), 1.83 (s, 15H), 1.04 (s, 9H), 0.87 (t, $J=7.2$ Hz, 3H), 0.75 (m, 1H), 0.62 (m, 1H).

Preparation of $(\eta^5\text{-C}_5\text{Me}_5)\text{ZrMe}(\text{CH}_2\text{CH}_2\text{CH}_2\text{CH}=\text{CH}_2)[\text{EtNC}(\text{CH}_3)\text{NBu}^t]^+$ (8**).** To a solution of 0.10 g (0.21 mmol) of **5** in 6 ml of Et_2O at -30°C was added 0.13 ml

(0.21mmol) of MeLi (1.6M in Et₂O). The initially clear yellow solution was allowed to warm up to room temperature over a period of 1h, after which the volatiles were removed *in vacuo*. This produced the crude product oil (0.09 g, 94% yield), which was characterized as pure by NMR. For **6**: ¹H NMR: δ 6.03 (m, 1H), 5.16 (d, J=17.1 Hz, 1H), 5.05 (dt, J₃=10.3, J₄=1.2, 1H), 2.90 (m, 2H), 2.72 (m, 1H), 2.24 (m, 2H), 2.07 (m, 1H), 1.99 (s, 15H), 1.74 (s, 3H), 1.17 (s, 9H), 0.88 (t, J=7.2 Hz, 3H), 0.87 (m, 1H), 0.29 (m, 1H), 0.13 (s, 3H).

Preparation of (η⁵-C₅Me₅)ZrMe(CH₂CH₂CH=CH₂)[EtNC(CH₃)NBu^t] (9**).** 0.10g (0.2 mmol) of **4'** were dissolved in 10mL of Et₂O in a 20-mL glass vial, and cooled to -30°C. Thereupon 127 μL of MeLi (1.6M in Et₂O, 0.2 mmol) were added and the vial placed at -30°C overnight. The solution bleached from yellow to clear, and the volatiles were removed *in vacuo*. The product was extracted with pentane and filtered through a pad of Celite. The solution was concentrated and set to recrystallize overnight at -30°C. Recrystallization yielded **9** as white crystals. (0.08 g, 89% yield). For **9**: ¹H NMR: δ 6.12 (m, 1H), 5.17 (d, J=16.7 Hz, 1H), 4.99 (d, J=9.9 Hz, 1H), 2.90 (dq, J₂=21.9 Hz, J₃=7.2 Hz, 1H), 2.70 (m, 2H), 2.53 (bm, 1H), 1.97 (s, 15H), 1.73 (s, 3H), 1.16 (s, 9H), 0.86 (t, J=7.2, 3H), 0.44 (m, 1H), 0.16 (s, 3H), 0.05 (bm, 1H). Anal. Calcd. for C₂₃H₄₂N₂Zr: %C 63.10, %H 9.67, %N 6.40; Found %C 62.85, %H 9.52, %N 6.37.

Preparation of (η⁵-C₅Me₅)Zr(-CH₂CH=CH-CH₂-)[EtNC(CH₃)NBu^t] (10a**).** 0.05 g of **9** in 1 ml of pentane were left at RT overnight, and the solution turned from clear to a deep red. After volatiles were removed *in vacuo*, the crude product was pure by NMR (0.04 g, 98% yield). For **10a**: ¹H NMR: δ 6.17 (dd, J₂=18.1 Hz, J₃=8.3 Hz, 1H), 6.09 (dd, J₂=18.1 Hz, J₃=8.0 Hz, 1H), 2.81 (dq, J₂=2.4 Hz, J₃=7.2 Hz, 2H), 2.05 (s, 15H), 1.96 (dd,

$J_2=9.1$ Hz, $J_3=8.3$ Hz, 1H), 1.57 (dd, $J_2=9.1$ Hz, $J_3=8.0$ Hz, 1H), 1.44 (s, 3H), 1.01 (s, 9H), 0.81 (t, $J=7.2$ Hz, 3H), 0.45 (dd, $J_2=9.1$ Hz, $J_3=8.3$ Hz, 1H), 0.34 ((dd, $J_2=9.1$ Hz, $J_3=8.0$ Hz, 1H). Anal. Calcd. for $C_{22}H_{38}N_2Zr$: %C 62.65, %H 9.08, %N 6.64; Found %C 62.63, %H 8.98, %N 6.56.

Preparation of $(\eta^5-C_5Me_5)Zr(-CH_2CH(Ph)CH_2CH_2-)[Pr^iNC(CH_3)NPr^i]$ (14**).** In a 50 ml Schlenk tube fitted with a gas tight Chemglass Teflon valve, 0.10 g (0.21 mmol) of **12** was dissolved in 5 ml of pentane, and the atmosphere of N_2 evacuated and replaced by 60 psi of ethene. After remaining under the ethene atmosphere for 30 min, the atmosphere was replaced by N_2 , and the solution was then transferred to a 20-ml vial, and volatiles were partially removed *in vacuo* until the solution volume was approximately 2 ml, and the vial was placed at $-30^\circ C$. **14** was isolated as yellow crystals. (0.06 g, 57% yield) Anal. Calcd. for $C_{29}H_{46}N_2Zr$: %C 67.78, %H 9.02, %N 5.45; Found %C 66.81, %H 9.04, %N 5.15.

Preparation of $(\eta^5-C_5Me_5)Zr(-CH_2CH(Me)CH_2CH(Ph)-)[Pr^iNC(CH_3)NPr^i]$ (15a**).** In a 50-ml Schlenk tube fitted with a gas tight Chemglass Teflon valve, 0.20 g (0.42 mmol) of **12** was dissolved in 10 ml of pentane, and the atmosphere of N_2 evacuated and replaced by 45 psi of propene. The tube was then placed at $0^\circ C$ for 2 days (until the color of solution turned from dark green to light yellow). The solution was then transferred to a 20-ml vial, and volatiles were partially removed *in vacuo* until the solution volume was approximately 2 ml, and the vial was placed at $-30^\circ C$. **15a** was isolated as light yellow crystals. (0.11 g, 50% yield) Anal. Calcd. for $C_{29}H_{46}N_2Zr$: %C 67.78, %H 9.02, %N 5.45; Found %C 66.81, %H 9.04, %N 5.15.

Preparation of $(\eta^5\text{-C}_5\text{Me}_5)\text{Zr}(\text{-CH}_2\text{C}(\text{Me})\text{CHCH}(\text{Ph})\text{-})[\text{Pr}^i\text{NC}(\text{CH}_3)\text{NPr}^i]$ (16a**).** In a 20-ml glass vial 0.10 g (0.19mmol) of **15a** was dissolved in 8 ml of pentane and allowed to stand at ambient temperature overnight. The solution turned from light yellow to a dark brown. The volatiles were then removed *in vacuo* and the remaining solids redissolved in a minimal amount of pentane (~1.5 ml) and placed at -30°C . **13** was isolated as a purple crystalline material (0.02 g, 40% yield based on expected 50% yield). Anal. Calcd. for $\text{C}_{29}\text{H}_{44}\text{N}_2\text{Zr}$: %C 68.04, %H 8.66, %N 5.47; Found %C 66.11, %H 8.51, %N 3.65.

Preparation of $(\eta^5\text{-C}_5\text{Me}_5)\text{Zr}(\text{-CH}_2\text{CH}(\text{Ph})\text{CH}_2\text{CH}(\text{Ph})\text{-})[\text{Pr}^i\text{NC}(\text{CH}_3)\text{NPr}^i]$ (15'b**).** In a 50-ml round bottom Schlenk flask, 0.25 g (0.53 mmol) of **12** were dissolved in 4 ml of neat styrene at room temperature, and allowed to react for 1 h (until there was no visible green color in solution). The reaction mixture was then placed under vacuum and the pressure reduced to 0.010 mmHg, where it remained for 12 h, and most of the styrene was removed *in vacuo*. The remaining solids were redissolved in 2 ml of Et_2O , and recrystallized at -30°C , yielding **15'b** as a dark yellow-orange crystalline solid (0.25 g, 82% yield). Anal. Calcd. for $\text{C}_{34}\text{H}_{48}\text{N}_2\text{Zr}$: %C 70.90, %H 8.40, %N 4.86; Found %C 71.18, %H 8.38, %N 4.88.

Preparation of $(\eta^5\text{-C}_5\text{Me}_5)\text{Zr}(\text{-CH}_2\text{C}(\text{TMS})\text{CHCH}(\text{Ph})\text{-})[\text{Pr}^i\text{NC}(\text{CH}_3)\text{NPr}^i]$ (16c**).** In a 50-ml Schlenk tube fitted with a gas tight Chemglass Teflon valve, 0.25 g (0.53 mmol) of **10** was dissolved in 8 ml of pentane, followed by addition of 0.26 g (2.65 mmol) of vinyltrimethylsilane and allowed to stand at ambient temperature for 4 days. Volatiles were then removed *in vacuo* and the remaining residue redissolved in 2 ml of Et_2O , and then placed at -30°C to recrystallize. 0.060 g of the purple crystalline product was isolated

for a 40% yield (based on the expected 50% yield). For **5**: ^1H NMR: δ 7.29 (s, 2H), 7.28 (s, 1H), 6.99 (m, 1H), 6.96 (m, 1H), 3.32 (sept, $J = 6.0$ Hz, 1H), 3.25 (sept, $J = 6.2$ Hz, 1H), 2.19 (d, $J = 8.2$ Hz, 1H), 1.92 (s, 15H), 1.70 (d, $J = 11.2$ Hz, 1H), 1.38 (s, 3H), 1.14 (d, $J = 6.1$ Hz, 3H), 0.93 (d, $J = 6.7$ Hz, 3H), 0.91 (d, $J = 6.5$ Hz, 3H), 0.85 (d, $J = 6.2$ Hz, 3H), 0.37 (s, 9H). Anal. Calcd. for $\text{C}_{31}\text{H}_{50}\text{N}_2\text{SiZr}$: %C 65.32, %H 8.84, %N 4.91; Found %C 65.17, %H 8.81, %N 5.02.

Preparation of $(\eta^5\text{-C}_5\text{Me}_5)\text{Zr}(-\text{CH}(\text{Me})\text{C}(\text{Me})\text{CHCH}(\text{Ph})-)[\text{Pr}^i\text{NC}(\text{CH}_3)\text{NPr}^i]$ (18**).** In a 50-ml Schlenk tube fitted with a gas tight Chemglass Teflon valve, 0.20 g (0.42 mmol) of **10** were dissolved in pentane, to which 0.023 g (0.42 mmol) of 2-butyne were added. The reaction mixture was allowed to stand at ambient temperature overnight, producing a color change from dark green to a deep purple. The volatiles were then removed *in vacuo* and the remaining solids redissolved in Et_2O and placed at -30°C to recrystallize. 0.215 g of purple crystalline material was harvested for a 98% yield. Anal. Calcd. for $\text{C}_{30}\text{H}_{46}\text{N}_2\text{Zr}$: %C 68.51, %H 8.82, %N 5.33; Found %C 69.16, %H 8.75, %N 5.06.

Preparation of $(\eta^5\text{-C}_5\text{Me}_5)\text{Zr}(-\text{CH}_2\text{CH}=\text{CH}-\text{CH}_2-)[\text{Pr}^i\text{NC}(\text{CH}_3)\text{NPr}^i]$ (19a**).** In a 50-ml Schlenk tube fitted with a gas tight Chemglass Teflon valve, 0.20 g (0.42 mmol) of **10** was dissolved in 10 ml of pentane, and the atmosphere of N_2 evacuated and replaced by 10 psi of butadiene. The tube was placed at RT overnight, and the color changed from dark green to burgundy. Volatiles were removed *in vacuo*, and the product recrystallized from pentane at -30°C . **19a** was isolated as burgundy colored crystals. (0.17 g, 94% yield)

Preparation of $(\eta^5\text{-C}_5\text{Me}_5)\text{Zr}(-\text{CH}_2\text{CH}=\text{C}(\text{Me})-\text{CH}_2-)[\text{Pr}^i\text{NC}(\text{CH}_3)\text{NPr}^i]$ (19b**).** In a 20 mL vial 0.15 g (0.32 mmol) of **10** was dissolved in 2mL of pentane, to which was

added 0.05 g of isoprene and left at RT overnight. The color changed from dark green to burgundy. The volatiles were removed *in vacuo*, and the product was recrystallized from pentane at -30°C . (0.13 g, 93%)

Preparation of $(\eta^5\text{-C}_5\text{Me}_5)\text{ZrBr}(\text{CH}=\text{CH}_2)[\text{Pr}^i\text{NC}(\text{CH}_3)\text{NPr}^i]$ (20**).** In a 50-ml Schlenk tube fitted with a gas tight Chemglass Teflon valve, 0.20 g (0.42 mmol) of **12** was dissolved in 10 ml of pentane, and the atmosphere of N_2 evacuated and replaced by 10 psi of vinyl bromide. The tube was placed at -20°C overnight, and the color of solution changed from dark green to pale yellow. The volatiles were removed *in vacuo*, and the crude product was recrystallized from Et_2O yielding pale yellow crystals of **20**. (87 mg, 45% yield)

Preparation of $(\eta^5\text{-C}_5\text{Me}_5)\text{TiCl}_2[\text{Pr}^i\text{NC}(\text{Me})\text{NPr}^i]$ (21**).** To a 150 ml flask charged with 70 ml of Et_2O were added 0.59 g (4.6 mmol) of N,N-diisopropylcarbodiimide and the solution chilled to -30°C . Subsequently 2.91 ml (4.6 mmol) of MeLi (1.6M in Et_2O) were added to the reaction flask and it was allowed to stir for 1h at RT. The reaction was then chilled to -30°C , to it was added 1.35 g of $(\eta^5\text{-C}_5\text{Me}_5)\text{TiCl}_3$ and it was allowed to stir overnight at -30°C . The volatiles were then removed *in vacuo*, and the remaining solids dissolved in toluene and filtered through a pad of Celite. After concentrating the resultant solution to a 10 ml volume, 4 ml of pentane were added to the solution. Upon cooling to -30°C overnight, **21** was obtained as dark crystals (1.48g, 80% yield).

Preparation of $(\eta^5\text{-C}_5\text{Me}_5)\text{TiEt}[\text{Pr}^i\text{NC}(\text{Me})\text{NPr}^i]$ (23**).** In a 150 ml flask, 0.50 g (1.38 mmol) of **21** was suspended in 70 ml of Et_2O and allowed to cool to -30°C . To it was added 5.50 ml (2.76 mmol) of EtLi (0.5M in benzene/cyclohexane 90:10) and the reaction mixture was allowed to stir at RT overnight. All volatiles were removed *in vacuo*

and the remaining solids extracted with pentane and filtered over a pad of Celite. **23** were isolated as dark brownish crystals. (0.30 g, 68% yield) Anal. Calcd. for C₂₀H₃₇N₂Ti: %C 67.98, %H 10.55, %N 7.93; Found %C 68.18, %H 10.27, %N 8.08.

Preparation of (η^5 -C₅Me₅)Ti[BuⁱNCEt][PrⁱNC(Me)NPrⁱ] (24**).** In a 20 ml vial, 0.10 g (0.31 mmol) of **23** were dissolved in 4 ml of pentane, and to it was added 40 mg (0.48 mmol) of BuⁱNC. The reaction mixture was allowed to stand at RT overnight, producing crystals. Upon cooling to -30°C overnight, **4** was obtained as dark crystals with a blue hue (0.12 g, 96% yield). Anal. Calcd. for C₂₅H₄₆N₃Ta: %C 68.79, %H 10.62, %N 9.63; Found %C 69.01, %H 10.59, %N 9.87.

Preparation of (η^5 -C₅Me₅)TaEt[CHCH₃][ⁱPrNC(Me)NⁱPr] (28**).** In a 150 ml flask, 305 mg (0.55 mmol) of **1** was suspended in 50 ml of Et₂O and cooled to -25°C. To it was added 3.28 ml (1.64 mmol) of EtLi (0.5M in benzene/cyclohexane 90:10) and the reaction was allowed to stir at RT overnight. All volatiles were removed *in vacuo* and the remaining solids extracted with pentane and filtered over a pad of Celite. After concentrating the resultant solution to a 1 ml volume, the vial was allowed to stand at -25°C overnight, and **2** was obtained as brown crystals (236 mg, 84% yield). For **2**: ¹H NMR (C₆D₆, 25°C): δ 0.61 (q, 2 H, J = 6.4 Hz, CH₂CH₃); 1.05 (d, 3H, J = 6.8 Hz, CHMe₂); 1.07 (d, 3H, J = 7.2 Hz, CHMe₂); 1.08 (d, 3H, J = 6.4 Hz, CHMe₂); 1.19 (d, 3H, J = 6.8 Hz, CHMe₂); 1.58 (s, 3H, CCH₃); 1.95 (s, 15H, C₅Me₅); 2.22 (t, 3H, J = 7.4 Hz, CH₂CH₃); 2.80 (d, 3H, J = 6.4 Hz, CHCH₃); 3.43 (qq, 1H, J = 6.4, J = 6.8 Hz, CHMe₂); 3.64 (qq, 1H, J = 6.8, J = 7.2 Hz, CHMe₂); 4.16 (q, 1H, J = 6.4 Hz, CHCH₃). ¹³C {¹H} NMR (C₆D₆, 25°C): δ 11.4 (C₅Me₅); 17.9 (CCH₃); 24.0 (CH₂CH₃), 24.52, 24.77, 24.82, 24.99 (CHMe₂); 27.8 (CHCH₃); 43.5 (CH₂CH₃); 45.5, 49.6 (CHMe₂); 109.9 (C₅Me₅);

173.4 (CCH_2); 236.9 ($CHCH_3$). Anal. Calcd. for $C_{22}H_{41}N_2Ta$: %C 51.36, %H 8.03, %N 5.44; Found %C 50.98, %H 7.85, %N 5.19. **Preparation of $(\eta^5-C_5Me_5)Ta^iBu_2[{}^iPrNC(Me)N^iPr]$ (29).** In a 100 ml flask, 100 mg (0.18 mmol) of **1** was suspended in 40 ml of Et_2O and stirred. 266 μ l (0.54 mmol) of nBuLi (2.0M in hexane) were diluted with 15 ml of Et_2O in an addition funnel, and added dropwise to the suspension of **1** over a period of 3 h at RT. The reaction mixture was allowed to stir for 4 h, followed by the removal of all volatiles *in vacuo*. A pentane extraction and filtration through a pad of Celite yielded a dark red-brown solution, which upon concentration was allowed to stand at $-25^\circ C$ overnight producing **4** as orange-brown crystals (86 mg, 85% yield). For **4**: Anal. Calcd. for $C_{26}H_{50}N_2Ta$: %C 54.63, %H 8.82, %N 4.90; Found %C 52.91, %H 8.30, %N 5.14.

Preparation of $(\eta^5-C_5Me_5)Ta^iBu_2[{}^iPrNC(Me)N^iPr]$ (31). In a 150 ml flask, 259 mg (0.46 mmol) of **1** was suspended in 30 ml of pentane and cooled to $-25^\circ C$. To it was added 2.38 ml (1.38 mmol) of Bu^iLi (0.58M in pentane) and the reaction was allowed to stir at RT overnight. The reaction was then twice filtered over a pad of Celite. After concentrating the resultant solution to a 1 ml volume, the vial was allowed to stand at $-25^\circ C$ overnight, and **3** was obtained as brown crystals (230 mg, 89% yield). For **3**: Anal. Calcd. for $C_{26}H_{50}N_2Ta$: %C 54.63, %H 8.82, %N 4.90; Found %C 54.17, %H 8.42, %N 5.08.

Preparation of $(\eta^5-C_5Me_5)Ta^iNp[{}^iPrNC(CH_2)N^iPr]$ (32). In a 150 ml flask, 0.60 g (1.0 mmol) of **1** was suspended in 30 ml of pentane and cooled to $-25^\circ C$. To it was added 0.34 g (3.19 mmol) of $NpLi$ (Schrock prep) and the reaction was allowed to stir at RT for 4h. The reaction was then twice filtered over a pad of Celite. After concentrating the resultant

solution to a 1 ml volume, the vial was allowed to stand at -25°C overnight, and **5** was obtained as bright green crystals (402 mg, 72% yield). For **5**: Anal. Calcd. for $\text{C}_{23}\text{H}_{42}\text{N}_2\text{Ta}$: %C 52.36, %H 8.02, %N 5.31; Found %C 52.18, %H 7.89, %N 5.30.

Preparation of $(\eta^5\text{-C}_5\text{Me}_5)\text{TaCl}_2[\text{Pr}^i\text{NC}(\text{Me})\text{N}^i\text{Pr}]$ (33**)**. To a 100 ml flask charged with 50 ml of Et_2O were added 1.18 g (2.1 mmol) of **1** and the solution chilled to -25°C . Subsequently 6.5 g (2.3 mmol of Na) of Na/Hg were added to the reaction flask and it was allowed to stir for 36h at RT. The volatiles were then removed *in vacuo*, and the remaining solids dissolved in toluene and filtered through a pad of Celite. After subsequent removal of volatiles *in vacuo*, **6** was obtained as red-orange crystals (1.09 g, 98% yield). For **6**: Anal. Calcd. for $\text{C}_{18}\text{H}_{32}\text{N}_2\text{Cl}_2\text{Ta}$: %C 40.92, %H 6.10, %N 5.30; Found %C 40.66, %H 6.00, %N 5.50.

Preparation of $(\eta^5\text{-C}_5\text{Me}_5)\text{TaEt}_2[\text{Pr}^i\text{NC}(\text{Me})\text{N}^i\text{Pr}]$ (35**)**. In a 100 ml flask, 105mg (0.20mmol) of **6** was suspended in 30 ml of Et_2O and allowed to cool to -25°C . To it was added 0.80 ml (0.40 mmol) of EtLi (0.5M in benzene/cyclohexane 90:10) and the reaction mixture was allowed to stir at RT overnight. All volatiles were removed *in vacuo* and the remaining solids extracted with pentane and filtered over a pad of Celite. After concentrating the resultant solution to a 2 ml volume, the vial was allowed to stand at -25°C overnight, and **7** was obtained as brown crystals (97 mg, 95% yield). For **7**: Anal. Calcd. for $\text{C}_{22}\text{H}_{42}\text{N}_2\text{Ta}$: %C 51.26, %H 8.21, %N 5.43; Found %C 50.94, %H 7.90, %N 5.64.

Preparation of $(\eta^5\text{-C}_5\text{Me}_5)\text{TaCl}^i\text{Bu}[\text{Pr}^i\text{NC}(\text{Me})\text{N}^i\text{Pr}]$ (36**)**. In a 100 ml flask, 285 mg (0.54 mmol) of **5** was suspended in 30 ml of Et_2O and allowed to cool to -25°C . To it was added 245 μl (0.54 mmol) of Bu^iMgCl (2.2M in Et_2O) and the reaction mixture was

allowed to stir at RT overnight. All volatiles were removed *in vacuo* and the remaining solids extracted with pentane and filtered over a pad of Celite. After concentrating the resultant solution to a 3 ml volume, the vial was allowed to stand at -25°C overnight, and **8a** was obtained as red-orange crystals (275 mg, 93% yield). For **8a**: Anal. Calcd. for C₂₂H₄₁N₂ClTa: %C 48.04, %H 7.51, %N 5.09; Found %C 47.73, %H 7.41, %N 5.08.

Preparation of (η⁵-C₅Me₅)TaClNp[PrⁱNC(Me)NPrⁱ] (37). In a 100 ml flask, 300 mg (0.57 mmol) of **5** was suspended in 45 ml of Et₂O and allowed to cool to -25°C. To it was added 2.0 ml (0.57 mmol) of BuⁱMgCl (0.26M in Et₂O) and the reaction mixture was allowed to stir at RT overnight. All volatiles were removed *in vacuo* and the remaining solids extracted with toluene and filtered over a pad of Celite. After concentrating the resultant solution to a 0.5 ml volume, 0.5 ml of pentane were added and the vial was allowed to stand at -25°C overnight, and **8b** was obtained as red-brown crystals (275 mg, 93% yield). For **8b**: Anal. Calcd. for C₂₃H₄₃N₂ClTa: %C 48.98, %H 7.68, %N 4.97; Found %C 48.62, %H 7.34, %N 5.04.

Preparation of (η⁵-C₅Me₅)TaMeⁱBu[PrⁱNC(Me)NPrⁱ] (38). In a 50 ml flask, 199 mg (0.36 mmol) of **8a** was suspended in 10 ml of Et₂O and allowed to cool to -25°C. To it was added 226 μl (0.36 mmol) of MeLi (1.6M in Et₂O) and the reaction mixture was allowed to stir at RT overnight. All volatiles were removed *in vacuo* and the remaining solids extracted with pentane and filtered over a pad of Celite. After concentrating the resultant solution to a <0.5 ml volume, the vial was allowed to stand at -25°C overnight, and **9a** was obtained as red-orange crystals (147 mg, 76% yield). For **9b**: Anal. Calcd. for C₂₃H₄₄N₂Ta: %C 54.54, %H 8.39, %N 5.30; Found %C 50.89, %H 7.98, %N 5.58.

Preparation of $(\eta^5\text{-C}_5\text{Me}_5)\text{TaMeNp}[\text{Pr}^i\text{NC}(\text{Me})\text{NPr}^i]$ (39**).** In a 50 ml flask, 264 mg (0.47 mmol) of **8b** was suspended in 20 ml of Et₂O and allowed to cool to -25°C. To it was added 293 μl (0.47 mmol) of MeLi (1.6M in Et₂O) and the reaction mixture was allowed to stir at RT overnight. All volatiles were removed *in vacuo* and the remaining solids extracted with pentane and filtered over a pad of Celite. After concentrating the resultant solution to a <0.5 ml volume, the vial was allowed to stand at -25°C overnight, and **9b** was obtained as red crystals (230 mg, 91% yield). For **9b**: Anal. Calcd. for C₂₄H₄₆N₂Ta: %C 53.13, %H 8.55, %N 5.16; Found %C 50.75, %H 8.16, %N 5.01.

Preparation of $[(\eta^5\text{-C}_5\text{Me}_5)\text{TaNp}\{\text{Pr}^i\text{NC}(\text{Me})\text{NPr}^i\}][\text{B}(\text{C}_6\text{F}_5)_4]$ (40**).** In a 2.5 ml vial 8 mg of **5** was dissolved in 0.5 ml of PhCl. In a separate 2.5 ml vial, 12 mg of [PhN(H)Me₂][B(C₆F₅)₄] was dissolved in 0.2 ml of PhCl. Both vials were allowed to cool to -25°C, and their contents were then mixed producing a color change from dark green to a light yellow solution. 1.5 ml of pentane was then layered on top of the PhCl phase and the vial was allowed to stand at -25°C overnight, producing pale yellow crystals of **10b** (18 mg, 96% yield).

Preparation of $[(\eta^5\text{-C}_5\text{Me}_5)\text{Ta}(\text{TMM})\{\text{Pr}^i\text{NC}(\text{Me})\text{NPr}^i\}]$ (43**).** In a 50 ml Schlenk tube fitted with a teflon valve, 100 mg of **3** was dissolved in 5 ml of toluene and heated to 80°C over 24 h. Upon removal of volatiles *in vacuo*, the remaining solids were redissolved in pentane. Upon cooling to -30°C overnight, colorless clear crystals of **11** were isolated (38 mg, 50% yield).

References

1. Jayaratne, K. C.; Sita, L. R. *J. Am. Chem. Soc.* **2000**, 122, 958-959.
2. Resconi, L.; Cavallo, L.; Fait, A.; Piemontesi, F. *Chem. Rev.* **2000**, 100, 1253-1345.
3. Jayaratne, K. C.; Keaton, R. J.; Henningsen, D. A.; Sita, L. R. *J. Am. Chem. Soc.* **2000**, 122, 10490-10491.
4. Keaton, R. J.; Jayaratne, K. C.; Fettinger, J. C.; Sita, L. R. *J. Am. Chem. Soc.* **2000**, 122, 12909-12910.
5. Jayaratne, K. C.; Sita, L. R. *J. Am. Chem. Soc.* **2001**, 123, 10754-10755.
6. Zhang, Y.; Keaton, R. J.; Sita, L. R. *J. Am. Chem. Soc.* **2003**, 125, 9062-9069.
7. Zhang, Y.; Sita, L. R. *Chem. Commun.* **2003**, 2358-2359.
8. Zhang, Y.; Reeder, E. K.; Keaton, R. J.; Sita, L. R. *Organometallics* **2004**, 23, 3512-3520.
9. Zhang, Y.; Sita, L. R. *J. Am. Chem. Soc.* **2004**, 126, 7776-7777.
10. Zhang, Y. Degenerative Transfer Living Ziegler-Natta Polymerization of alpha-Olefins. University of Maryland, College Park, 2005.
11. Harney, M. B.; Keaton, R. J.; Fettinger, J. C.; Sita, L. R. *J. Am. Chem. Soc.* **2006**, 128, 3420-3432.
12. Harney, M. B.; Zhang, Y.; Sita, L. R. *Angew. Chem., Int. Ed.* **2006**, 45, 2400-2404.
13. McLain, S. J.; Schrock, R. R. *J. Am. Chem. Soc.* **1978**, 100, 1315-17.
14. McLain, S. J.; Wood, C. D.; Schrock, R. R. *J. Am. Chem. Soc.* **1979**, 101, 4558-70.
15. Eshuis, J. J. W.; Tan, Y. Y.; Teuben, J. H.; Renkema, J. J. *Mol. Catal.* **1990**, 62, 277-87.
16. Coates Geoffrey, W.; Hustad Phillip, D.; Reinartz, S. *Angew. Chem., Int. Ed. Eng.* **2002**, 41, 2237-57.
17. Chirik, P. J.; Zubris, D. L.; Ackerman, L. J.; Henling, L. M.; Day, M. W.; Bercaw, J. E. *Organometallics* **2003**, 22, 172-187.
18. Chirik, P. J.; Bercaw, J. E. *Organometallics* **2005**, 24, 5407-5423.
19. Negishi, E.; Cederbaum, F. E.; Takahashi, T. *Tetrahedron Lett.* **1986**, 27, 2829-32.
20. Negishi, E.; Swanson, D. R.; Cederbaum, F. E.; Takahashi, T. *Tetrahedron Lett.* **1987**, 28, 917-20.
21. Takahashi, T.; Swanson, D. R.; Negishi, E. *Chem. Lett.* **1987**, 623-6.
22. Elschenbroich, C., *Organometallics*. 3 ed.; WILEY-VCH: Weinheim, 2006;
23. Wilkinson, G.; Pauson, P. L.; Birmingham, J. M.; Cotton, F. A. *J. Am. Chem. Soc.* **1953**, 75, 1011-12.
24. Schwartz, J.; Labinger, J. A. *Angew. Chem., Int. Ed. Eng.* **1976**, 15, 333-340.
25. Wipf, P.; Jahn, H. *Tetrahedron* **1996**, 52, 12853-12910.
26. Ziegler, K.; Holzkamp, E.; Breil, H.; Martin, H. *Angew. Chem.* **1955**, 67, 426.
27. Natta, G.; Pino, P.; Mazzanti, G.; Giannini, U. *J. Am. Chem. Soc.* **1957**, 79, 2975-6.
28. Natta, G. *Angew. Chem.* **1956**, 68, 393-403.
29. Natta, G. *J. Polym. Sci.* **1955**, 16, 143-54.

30. Severn, J. R.; Chadwick, J. C.; Duchateau, R.; Friederichs, N. *Chem. Rev.* **2005**, 105, 4073-4147.
31. Cossee, P. *Tetrahedron Lett.* **1960**, 17-21.
32. Cossee, P. *Tetrahedron Lett.* **1960**, 12-16.
33. Arlman, E. J. *J. Catal.* **1964**, 3, 89-98.
34. Natta, G.; Pino, P.; Mazzanti, G.; Giannini, U. *J. Inorg. Nuc. Chem.* **1958**, 8, 612-19.
35. Long, W. P.; Breslow, D. S. *J. Am. Chem. Soc.* **1960**, 82, 1953-7.
36. Sinn, H.; Kaminsky, W.; Vollmer, H. J.; Woldt, R. *Angew. Chem.* **1980**, 92, 396-402.
37. Kaminsky, W.; Kuelper, K.; Brintzinger, H. H.; Wild, F. R. W. P. *Angew. Chem.* **1985**, 97, 507-8.
38. Arlman, E. J.; Cossee, P. *J. Catal.* **1964**, 3, 99-104.
39. Cossee, P. *J. Catal.* **1964**, 3, 80-8.
40. Keaton, R. J.; Sita, L. R. *J. Am. Chem. Soc.* **2002**, 124, 9070-9071.
41. Harney, M. B.; Keaton, R. J.; Sita, L. R. *J. Am. Chem. Soc.* **2004**, 126, 4536-4537.
42. Wipf, P.; Kendall, C. *Chem. Euro. J.* **2002**, 8, 1778-1784.
43. Keaton, R. J.; Koterwas, L. A.; Fettinger, J. C.; Sita, L. R. *J. Am. Chem. Soc.* **2002**, 124, 5932-5933.
44. Zhang, Y.; Keaton, R. J.; Sita, L. R. *J. Am. Chem. Soc.* **2003**, 125, 8746-8747.
45. Negishi, E.-i. *Dalton Trans.* **2005**, 827-848.
46. Dioumaev, V. K.; Harrod, J. F. *Organometallics* **1997**, 16, 1452-1464.
47. McLain, S. J.; Sancho, J.; Schrock, R. R. *J. Am. Chem. Soc.* **1979**, 101, 5451-3.
48. Fellmann, J. D.; Schrock, R. R.; Rupprecht, G. A. *J. Am. Chem. Soc.* **1981**, 103, 5752-8.
49. Wielstra, Y.; Gambarotta, S.; Chiang, M. Y. *Organometallics* **1988**, 7, 1866-7.
50. Gibson, V. C.; Kee, T. P.; Poole, A. D. *J. Chem. Soc., Chem. Commun.* **1990**, 1720-2.
51. Briggs, J. R. *J. Chem. Soc., Chem. Commun.* **1989**, 674-5.
52. Andes, C.; Harkins, S. B.; Murtuza, S.; Oyler, K.; Sen, A. *J. Am. Chem. Soc.* **2001**, 123, 7423-7424.
53. Deckers, P. J. W.; Hessen, B.; Teuben, J. H. *Angew. Chem., Int. Ed.* **2001**, 40, 2516-2519.
54. Carter, A.; Cohen, S. A.; Cooley, N. A.; Murphy, A.; Scutt, J.; Wass, D. F. *Chem. Commun.* **2002**, 858-859.
55. Deckers, P. J. W.; Hessen, B.; Teuben, J. H. *Organometallics* **2002**, 21, 5122-5135.
56. McGuinness, D. S.; Wasserscheid, P.; Keim, W.; Hu, C.; Englert, U.; Dixon, J. T.; Grove, C. *Chem. Commun.* **2003**, 334-335.
57. McGuinness, D. S.; Wasserscheid, P.; Keim, W.; Morgan, D.; Dixon, J. T.; Bollmann, A.; Maumela, H.; Hess, F.; Englert, U. *J. Am. Chem. Soc.* **2003**, 125, 5272-5273.
58. Agapie, T.; Schofer Susan, J.; Labinger Jay, A.; Bercaw John, E. *J. Am. Chem. Soc.* **2004**, 126, 1304-5.
59. Hessen, B. *J. Mol. Cat. A: Chem.* **2004**, 213, 129-135.
60. Yang, S.-Y.; Ziegler, T. *Organometallics* **2006**, 25, 887-900.

61. Burger, B. J.; Thompson, M. E.; Cotter, W. D.; Bercaw, J. E. *J. Am. Chem. Soc.* **1990**, 112, 1566-77.
62. Casey, C. P.; Hallenbeck, S. L.; Wright, J. M.; Landis, C. R. *J. Am. Chem. Soc.* **1997**, 119, 9680-9690.
63. Casey, C. P.; Hallenbeck, S. L.; Pollock, D. W.; Landis, C. R. *J. Am. Chem. Soc.* **1995**, 117, 9770-1.
64. Sita, L. R.; Babcock, J. R. *Organometallics* **1998**, 17, 5228-5230.
65. Koterwas, L. A.; Fettinger, J. C.; Sita, L. R. *Organometallics* **1999**, 18, 4183-4190.
66. Zhang, Y., Unpublished results.
67. Casey, C. P.; Fagan, M. A.; Hallenbeck, S. L. *Organometallics* **1998**, 17, 287-289.
68. Casey, C. P.; Fisher, J. J. *Inorg. Chim. Acta* **1998**, 270, 5-7.
69. Baldwin, J. E. *J. Chem. Soc., Chem. Commun.* **1976**, 734-6.
70. Jemmis, E. D.; Phukan, A. K.; Jiao, H.; Rosenthal, U. *Organometallics* **2003**, 22, 4958-4965.
71. Dioumaev, V. K.; Harrod, J. F. *Organometallics* **1997**, 16, 1452-1464.
72. McDermott, J. X.; Wilson, M. E.; Whitesides, G. M. *J. Am. Chem. Soc.* **1976**, 98, 6529-36.
73. Kissounko, D. A.; Fettinger, J. C.; Sita, L. R. *J. Organomet. Chem.* **2003**, 683, 29-38.
74. Negishi, E.; Takahashi, T. *Reviews on Heteroatom Chemistry* **1992**, 6, 177-201.
75. Negishi, E. I.; Takahashi, T. *Sci. Synth.* **2003**, 2, 681-848.
76. Kissounko, D. A., Unpublished results.
77. Kissounko, D. A.; Epshteyn, A.; Sita, L. R. *Organometallics* **2006**, in press.
78. Negishi, E.-i.; Takahashi, T. *Bul. Chem. Soc. Jpn.* **1998**, 71, 755-769.
79. Takahashi, T.; Fischer, R.; Xi, Z.; Nakajima, K. *Chem. Lett.* **1996**, 357-358.
80. Knight, K. S.; Wang, D.; Waymouth, R. M.; Ziller, J. *J. Am. Chem. Soc.* **1994**, 116, 1845-54.
81. Hagadorn, J. R.; Arnold, J. *J. Chem. Soc., Dalton Trans.: Inorg. Chem.* **1997**, 3087-3096.
82. Mansel, S.; Thomas, D.; Lefebvre, C.; Heller, D.; Kempe, R.; Baumann, W.; Rosenthal, U. *Organometallics* **1997**, 16, 2886-2890.
83. Warren, T. H.; Erker, G.; Froehlich, R.; Wibbeling, B. *Organometallics* **2000**, 19, 127-134.
84. Sun, H.; Burlakov, V. V.; Spannenberg, A.; Baumann, W.; Arndt, P.; Rosenthal, U. *Organometallics* **2001**, 20, 5472-5477.
85. Takahashi, T.; Fujimori, T.; Seki, T.; Saburi, M.; Uchida, Y.; Rousset, C. J.; Negishi, E. I. *J. Chem. Soc., Chem. Commun.* **1990**, 182-3.
86. Takahashi, T.; Kageyama, M.; Denisov, V.; Hara, R.; Negishi, E. *Tetrahedron Lett.* **1993**, 34, 687-90.
87. Takahashi, T.; Seki, T.; Nitto, Y.; Saburi, M.; Rousset, C. J.; Negishi, E. *J. Am. Chem. Soc.* **1991**, 113, 6266-8.
88. Takahashi, T.; Kotora, M.; Fischer, R.; Nishihara, Y.; Nakajima, K. *J. Am. Chem. Soc.* **1995**, 117, 11039-40.
89. Yu, Z.-X.; Houk, K. N. *Angew. Chem., Int. Ed.* **2003**, 42, 808-811.
90. Huang, X.; Zhu, J.; Lin, Z. *Organometallics* **2004**, 23, 4154-4159.

91. Freeman, P. K. *J. Org. Chem.* **2005**, 70, 1998-2001.
92. Luinstra, G. A.; Teuben, J. H. *J. Am. Chem. Soc.* **1992**, 114, 3361-7.
93. Manzer, L. E. *Inorg. Chem.* **1976**, 15, 2567-9.
94. De Boer, E. J. M.; Teuben, J. H. *J. Organomet. Chem.* **1978**, 153, 53-7.
95. Nieman, J.; Pattiasina, J. W.; Teuben, J. H. *J. Organomet. Chem.* **1984**, 262, 157-69.
96. Luinstra, G. A.; Teuben, J. H. *J. Chem. Soc., Chem. Commun.* **1987**, 849-50.
97. Pattiasina, J. W.; Heeres, H. J.; Van Bolhuis, F.; Meetsma, A.; Teuben, J. H.; Spek, A. L. *Organometallics* **1987**, 6, 1004-10.
98. Jensen, J. A.; Wilson, S. R.; Girolami, G. S. *J. Am. Chem. Soc.* **1988**, 110, 4977-82.
99. Cano, A.; Cuenca, T.; Rodriguez, G.; Royo, P.; Cardin, C.; Wilcock, D. J. *J. Organomet. Chem.* **1993**, 447, 51-7.
100. Jeske, P.; Wiegardt, K.; Nuber, B. *Inorg. Chem.* **1994**, 33, 47-53.
101. de Wolf, J. M.; Meetsma, A.; Teuben, J. H. *Organometallics* **1995**, 14, 5466-8.
102. Love, J. B.; Clark, H. C. S.; Cloke, F. G. N.; Green, J. C.; Hitchcock, P. B. *J. Am. Chem. Soc.* **1999**, 121, 6843-6849.
103. Greidanus, G.; McDonald, R.; Stryker, J. M. *Organometallics* **2001**, 20, 2492-2504.
104. Decker, J. M.; Geib, S. J.; Meyer, T. Y. *Organometallics* **1999**, 18, 4417-4420.
105. Murtuza, S.; Harkins, S. B.; Long, G. S.; Sen, A. *J. Am. Chem. Soc.* **2000**, 122, 1867-1872.
106. Mashima, K.; Nakayama, Y.; Ikushima, N.; Kaidzu, M.; Nakamura, A. *J. Organomet. Chem.* **1998**, 566, 111-116.
107. Hakala, K.; Lofgren, B.; Polamo, M.; Leskela, M. *Macromol. Rapid Commun.* **1997**, 18, 635-638.
108. Mashima, K.; Fujikawa, S.; Tanaka, Y.; Urata, H.; Oshiki, T.; Tanaka, E.; Nakamura, A. *Organometallics* **1995**, 14, 2633-40.
109. Mashima, K.; Fujikawa, S.; Nakamura, A. *J. Am. Chem. Soc.* **1993**, 115, 10990-1.
110. Antonelli, D. M.; Leins, A.; Stryker, J. M. *Organometallics* **1997**, 16, 2500-2502.
111. Keaton, R. J.; Jayaratne, K. C.; Henningsen, D. A.; Koterwas, L. A.; Sita, L. R. *J. Am. Chem. Soc.* **2001**, 123, 6197-6198.
112. Keaton, R. J.; Sita, L. R. *Organometallics* **2002**, 21, 4315-4317.
113. Kissounko, D. A.; Fettingner, J. C.; Sita, L. R. *Inorg. Chim. Acta* **2003**, 345, 121-129.
114. Zhang, Y.; Kissounko, D. A.; Fettingner, J. C.; Sita, L. R. *Organometallics* **2003**, 22, 21-23.
115. Zhang, Y. H.; Kissounko, D. A.; Fettingner, J. C.; Sita, L. R. *Organometallics* **2003**, 22, 21-23.
116. Kissounko, D. A.; Zhang, Y.; Harney, M. B.; Sita, L. R. *Adv. Synth. Catal.* **2005**, 347, 426-432.
117. Schrock, R. R. *Chem. Rev.* **2002**, 102, 145-179.
118. Keaton, R. J.; Koterwas, L. A.; Fettingner, J. C.; Sita, L. R. *J. Am. Chem. Soc.* **2002**, 124, 5932-5933.
119. Atwood, J. L.; Hunter, W. E.; Hrcir, D. C.; Samuel, E.; Alt, H.; Rausch, M. D. *Inorg. Chem.* **1975**, 14, 1757-62.

120. Dewar, M. J. S. *Bull. Soc. Chim. Fr.* **1951**, C71-9.
121. Chatt, J.; Duncanson, L. A. *J. Chem. Soc., Abstracts* **1953**, 2939-47.
122. Keaton, R. J., Unpublished results.
123. Keaton, R. J.; Jayaratne, K. C.; Henningsen, D. A.; Koterwas, L. A.; Sita, L. R. *J. Am. Chem. Soc.* **2001**, 123, 6197-6198.
124. Keaton, R. J.; Sita, L. R. *Organometallics* **2002**, 21, 4315-4317.
125. Fryzuk, M. D.; Johnson, S. A. *Coord. Chem. Rev.* **2000**, 200-202, 379-409.
126. Gambarotta, S.; Scott, J. *Angew. Chem., Int. Ed.* **2004**, 43, 5298-5308.
127. Kozak, C. M.; Mountford, P. *Angew. Chem., Int. Ed.* **2004**, 43, 1186-1189.
128. MacKay, B. A.; Fryzuk, M. D. *Chem. Rev.* **2004**, 104, 385-401.
129. Lee, T.-Y.; Wooten, A. J.; Luci, J. J.; Swenson, D. C.; Messerle, L. *Chem. Commun.* **2005**, 5444-5446.
130. Yang, X.; Stern, C. L.; Marks, T. J. *J. Am. Chem. Soc.* **1991**, 113, 3623-5.
131. Yang, X.; Stern, C.; Marks, T. J. *Organometallics* **1991**, 10, 840-2.
132. Luo, L.; Marks, T. J. *Top. Catal.* **1999**, 7, 97-106.
133. Deck, P. A.; Beswick, C. L.; Marks, T. J. *J. Am. Chem. Soc.* **1998**, 120, 1772-1784.
134. Chien, J. C. W.; Tsai, W. M.; Rausch, M. D. *J. Am. Chem. Soc.* **1991**, 113, 8570-1.
135. Anderson, L. L.; Schmidt, J. A. R.; Arnold, J.; Bergman, R. G. *Organometallics* **2006**, 25, 3394-3406.
136. Kissounko, D. A.; Sita, L. R. *J. Am. Chem. Soc.* **2004**, 126, 5946-5947.
137. Fryzuk, M. D.; Johnson, S. A.; Rettig, S. J. *J. Am. Chem. Soc.* **1998**, 120, 11024-11025.
138. Fryzuk, M. D.; Johnson, S. A.; Patrick, B. O.; Albinati, A.; Mason, S. A.; Koetzle, T. F. *J. Am. Chem. Soc.* **2001**, 123, 3960-3973.
139. Suresh, C. H.; Koga, N. *J. Phys. Chem. A* **2001**, 105, 5940-5944.
140. Kissounko, D.; Epshteyn, A.; Fettinger, J. C.; Sita, L. R. *Organometallics* **2006**, 25, 531-535.
141. Blomberg, C.; Salinger, R. M.; Mosher, H. S. *J. Org. Chem.* **1969**, 34, 2385-8.